UNIVERSITÉ DE SHERBROOKE
Faculté de génie
Département de génie mécanique

Simulation CFD et analyse des flux exergétiques de dispositifs pour l'expansion de CO_2 supercritique afin d'améliorer la performance énergétique du système de pompe à chaleur

CFD simulation and exergy flow analysis inside devices for expansion of supercritical CO_2 streams to improve the energy performance of a heat pump system

Thèse de doctorat
Spécialité : Génie Mécanique

ABBAS AGHAGOLI

Sherbrooke (Québec) Canada

November 2020

Jury: Prof. Mikhail Sorin (directeur)

Prof. Dahai Qi (rapporteur)

Prof. Hachimi Fellouah (examinateur)

Dr. Étienne Saloux (examinateur)

RÉSUMÉ

Les cycles de pompes à chaleur sont largement utilisés dans des applications résidentielles et commerciales dans le monde entier grâce à ses avantages attrayants d'une efficacité énergétique élevée, de sa fiabilité et ses impacts environnementaux. Le souci d'économie d'énergie continue d'augmenter en raison du coût de l'énergie et de la réduction des sources de combustibles fossiles. En outre, les pompes à chaleur sont capables de fonctionner une multitude des sources de chaleur. Le grand potentiel d'économie d'énergie d'une pompe à chaleur a attiré beaucoup d'attention et de nombreux chercheurs ont tenté d'améliorer son efficacité globale. Malgré le rendement énergétique élevé de pompe à chaleur, il y a un problème concernant les énormes pertes d'exergie ou l'irréversibilité lors du processus isenthalpique d'expansion dans la vanne de détente. Il y a plusieurs équipements destinés à la diminution de ces pertes d'exergie, tels que : des éjecteurs, des tubes vortex, etc.; Cependant, le problème réside dans l'intégration et le dimensionnement optimals de ces équipements à l'intérieur des pompes à chaleur.

L'objectif principal du présent projet est d'introduire une nouvelle configuration de pompe à chaleur au CO_2 supercritique afin de maximiser l'efficacité thermique du cycle due à la réduction des irréversibilités à l'intérieur du dispositif de détente. L'énergie est une quantité conservée, ce qui signifie qu'elle ne peut pas être détruite ou créée, mais l'exergie est la caractéristique de la qualité d'énergie qui n'est pas conservée. La présente recherche propose deux dispositifs d'expansion différents à savoir, le Tube à vortex et la turbine Tesla qui sont employés sur le système de pompe à chaleur qui permettent de réduire les pertes d'exergie comparées au processus de détente isenthalpique. Les principaux composants de ces pompes à chaleur au CO_2 sont: le compresseur, le refroidisseur de gaz, l'évaporateur, le tube vortex ou la turbine Tesla. La première étape de travail est la simulation de la dynamique des fluides par calcul (CFD) du tube vortex et de la turbine Tesla en basant sur des différentes conditions aux limites d'entrée et de sortie qui sont les conditions de sortie du refroidisseur de gaz et les conditions d'entrée de l'évaporateur respectivement. L'étape suivante consiste à extraire les résultats CFD et à les importer comme les données initiales à la modélisation du cycle de la pompe à chaleur. La troisième étape consiste à appliquer la première et la deuxième loi de thermodynamique et maximiser le coefficient de performance (COP) et l'efficacité exergétique du cycle via la réduction des irréversibilités de détente.

L'approche a été tout d'abord appliquée au tube vortex CO_2 basse pression dans lequel la pression d'entrée a été choisie de 1,3 MPa. Les résultats ont démontré que le tube vortex à CO_2 est capable de produire deux flux dans lesquels un flux qui est évacué au centre du tube vortex à une température inférieure à la température d'entrée et un second flux qui se déplace en périphérie et extrait loin de l'entrée à une température plus élevée. Il a été démontré qu'une

pression d'entrée plus élevée produit une différence de température plus élevée. Ensuite, l'approche utilisait le tube vortex de CO_2 haute pression dans lequel la pression d'entrée était supérieure à la pression critique de CO_2 (7,37 MPa). Les résultats ont montré qu'en raison de la faible vitesse d'entrée dans le tube vortex, il ne fonctionne pas dans une situation idéale et en raison de la présence de la phase liquide dans le tube vortex. En conséquence, la séparation d'énergie diminue rapidement à mesure que la qualité de la vapeur diminue. La troisième approche consistait à intégrer la turbine Tesla dans la pompe à chaleur en tant que dispositif d'expansion. L'analyse numérique de la turbine Tesla aux différentes pressions d'entrée et de sortie a été conduite pour évaluer l'impact sur l'efficacité exergétique transitoire et la perte exergétique de la turbine Tesla et sur l'efficacité globale du cycle de la pompe à chaleur. Les résultats ont montré que la turbine Tesla peut améliorer le COP du système de pompe à chaleur jusqu'à 16,3%.

Mots clés: CO_2, tube Vortex, turbine Tesla, système de pompe à chaleur, CFD

ABSTRACT

The heat pumps cycles have been used in residential and commercial application throughout the world due to the attractive advantages of high energy efficiency, reliability, and environmental impacts. The concern on energy-saving continues to rise due to the cost of energy and reducing the sources of fossil fuel. Besides, the heat pump systems are capable of working under various heat sources. The great potential of energy saving of the heat pump system has attracted much attention and many researchers have been attempting to improve its overall efficiency. Despite the high energy efficiency, there is an issue regarding the enormous exergy losses or irreversibility during the isenthalpic process in the expansion valve. There are several pieces of equipment intended to reduce these exergy losses, such as: ejectors, vortex tubes, etc.; however, the problem lies in the optimal integration and sizing of this equipment inside the heat pumps.

The main objective of this project is to introduce a new configuration of supercritical CO_2 heat pump system in order to maximize the thermal efficiency of the cycle due to the reduction of irreversibilities inside the expansion device. Energy is a conserved quantity, which means that it cannot be destroyed or created, but exergy is the characteristic of the quality of energy that is not consumed. The present research proposes to investigate the use, in the heat pump system, of two different expansion devices namely, the vortex tube and the Tesla turbine The main components of these CO_2 heat pumps are: the compressor, gas cooler, evaporator, vortex tube, or Tesla turbine. The first step is the simulation of computational fluid dynamic (CFD) of the vortex tube and Tesla turbine based on different inlet and outlet boundary conditions which are the outlet conditions of the gas cooler and the entry conditions of the evaporator, respectively. The next step is to extract the CFD results and import them as the initial data for modeling the heat pump cycle. The results of the CFD modeling of the second step will be imported into the heat pump system as inputs. The third step is applying the first and second laws of thermodynamics and analyzing the coefficient of performance (COP), exergy efficiency, and irreversibilities.

Applying the numercial analysis for the proposed expansion device was, first, applied to the low-pressure CO_2 vortex tube in which the inlet pressure was chosen 1.3 MPa. The results indicates that the CO_2 vortex splits the inlet stream into two main streams. One stream is discharged at the center of the vortex tube has a temperature lower than the inlet temperature and second flow that moves peripherally and extracts far from the inlet has the higher temperature. It was depicted that higher inlet pressure produces a higher temperature difference. Afterward, the approach was employing the high-pressure CO_2 vortex tube in which the inlet pressure was higher than the critical pressure of CO_2 (7.37 MPa). The results showed that due to low inlet velocity in the vortex tube, the vortex tube doesn't work in an ideal situation and due to the presence of the liquid phase in the vortex tube. Therefore, the energy separation diminishes rapidly as the quality of the vapor decreases. The third approach was integrating the Tesla turbine in the heat pump system as an expansion device. The numerical analysis of the Tesla turbine at different inlet and outlet pressures is investigated on the transiting exergy efficiency and exergy loss of the Tesla turbine and overall efficiency of the heat pump cycle. The results showed that the Tesla turbine can improve the COP of the heat pump system by up to 16.3%.

Keywords: CO_2, Vortex tube, Tesla turbine, Heat pump system, CFD

ACKNOWLEDGMENTS

Throughout the writing of this dissertation I have received a great deal of support and assistance.

I would first like to thank my supervisor, Professor Mikhail Sorin for providing guidance and feedback throughout this project

I would like to extend my sincere thanks to my committee member, Dr. Etienne Saloux, Prof. Dahai Qi and Prof. Hachimi Fellouah.

I take this opportunity to express gratitude to all of my colleagues and friends.

In addition, I would like to thank my parents and my brother for supporting me spiritually throughout my life. You are always there for me.

Finally, I could not have completed this dissertation without the support of my beloved wife, Forouzan Kazemi.

TABLE OF CONTENTS

LIST OF FIGURES

LIST OF TABLES

Chapter 1

INTRODUCTION

1-1 Motivation

The high energy consumption and serious pollution from the fuels burning for buildings heating have drawn increasing attention, with the goal of alleviating these problems. In addition, the Montreal Protocol is widely considered as the most successful environment protection agreement, banned the usage of the CFC (chlorofluorocarbon) and HCFC (hydrochlorofluorocarbon) refrigerants which are harmful to the environment. The global warming potential (GWP) of the HFC gases are high [1]. Typically, a release of one kilogram of an HFC gas contributes 1000–3000 times more to global warming, than the release of one kilogram CO_2 [2]. Consequently, there has been a noticeable increase in interest in the applications of the transcritical CO_2 heat pump system.

In a transcritical heat pump, heat rejection is not limited by the critical temperature, which leads to higher performance. However, the most important cause of the thermodynamic imperfection of a transcritical heat pump cycle is the large exergy destruction within a throttling valve due to the refrigerant passing from the supercritical state (80–120 bar) to the subcritical state (30–40 bar). In other words, the greater pressure difference between the gas cooler and the evaporator causes important exergy losses due to expansion. One key approach to improve the performance of a heat pump cycle is to recover part of these throttling losses by producing useful work.

1-2 Objectives

So far, the ejector has been introduced as an expansion device for the heat pump system. However, due to presence of second phase inside the ejector, the performance of the ejector drops rapidly. The main objective of the project is to introduce a new expansion device to

replace an expansion valve in order to reduce the throttling loss within a heat pump system. This general objective includes the following specific points:

- Find an alternative to partially recover the throttling losses
- Conduct CFD simulations of the expansion devices
- Conduct of thermodynamic analysis of the expansion devices and their comparison in terms of exergy based metrics
- Integrating the Tesla turbine and vortex tube into the heat pump system and analyzing the conditions to maximize the COP of a novel heat pump system

This study proposes a novel transcritical heat pump system which focuses on the exergy loss during the expansion process. The approach is accomplished with two steps: finding a new expansion device and analyzing the heat pump system with the integration of a new expansion device. In the first step, two new expansion devices are proposed which are the vortex tube and the Tesla turbine. The CFD simulation analysis was carried out based on the proper turbulence model. The boundary conditions of the proposed expansion devices were fixed based on the gas cooler and evaporator pressures. The second law of thermodynamics was applied to find the expansion device with lower exergy losses or higher exergy efficiency. Then the chosen expansion device was integrated with the heat pump system to evaluate the performance of the candidate expansion device of the heat pump system based on the exergy efficiency and COP. The approach is, first, applied to the vortex tube as a first candidate and the energy separation of the vortex tube is illustrated. Afterward, the approach is developed on the Tesla turbine. In this study, the performance of the expansion devices is evaluated based on the first and second laws of Thermodynamics.

1-3 Thesis outline

The present thesis contains seven chapters. In Chapter 2, an extensive literature review on the development of the heat pump system is provided. Chapter 3 is devoted to the CFD simulation of the low-pressure vortex using CO_2 as a real gas. The effect of inlet pressure is investigated on the temperature separation inside the vortex tube. Chapter 4 investigates the CFD simulation of the high-pressure vortex tube with two-phase CO_2 where the inlet pressure

is chosen based on the gas cooler pressure. The effect of inlet pressure is investigated on the exergy loss of the vortex tube. Chapter 5 analyzes the heat pump system integrated with the vortex tube to partially recover the throttling losses. Moreover, the effect of gas cooler pressure on the COP of the transcritical vortex tube heat pump system is investigated. Chapter 6 illustrates the CFD simulation of the Tesla turbine, working with CO_2 as real working fluid. Moreover, the effect of inlet and outlet pressures are investigated on the transiting exergy efficiency of the Tesla turbine and COP of the heat pump system integrated with the Tesla turbine. Finally, conclusions are presented in Chapter 7.

Chapter 2

STATE OF THE ART

This chapter is devoted to an extensive review of studies conducted by previous researchers on the expansion device and heat pump system analysis.

2-1 Heat pump system

The increasing worldwide energy consumption, global warming effect, and the cost of fossil fuel at the forefront of world attention, the heat pump systems have gained much attention in the past decades [3,4]. The heat pump is able to reuse the waste heat back into a heat production process and the application of heat pump in domestic and commercial buildings are drastically popularized [1]. The schematic of the heat pump is illustrated in Figure 2-1.

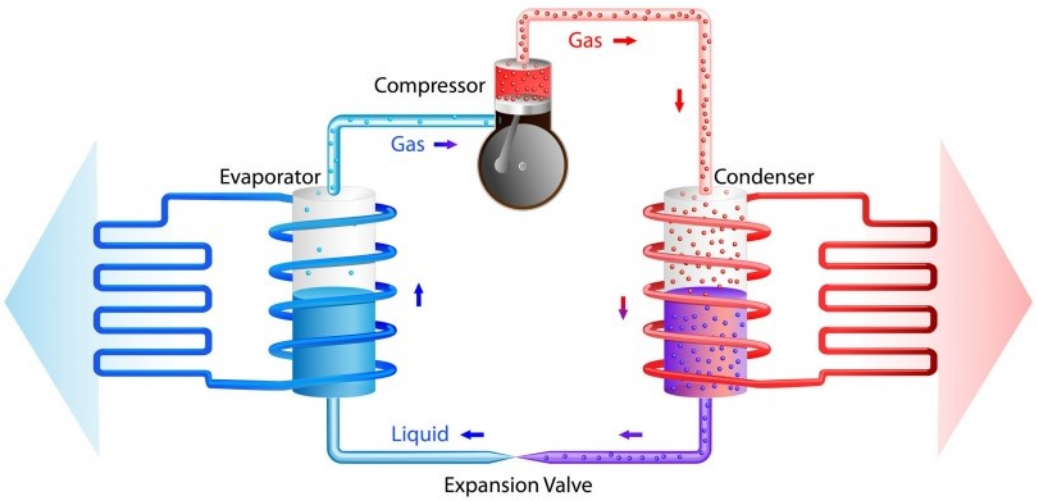

Figure 2-1. The schematic of heat pump [5].

In a heat pump cycle either subcritical or transcritical cycle, the heat absorption takes place in the evaporator and the saturated vapor of refrigerant leaves the evaporator and enters the compressor. During the isentropic process in the compressor, the temperature and pressure of the refrigerant increase. In a traditional heat pump, the cycle works under the critical point of

the used refrigerant. The heat rejection occurs in the condenser and the refrigerant isobarically cools as it passes through the condenser when the hydraulic losses are neglected. However, in a transcritical heat pump, the heat rejection takes place in a gas cooler by single-phase sensible cooling and the refrigerant isobarically cools as it passes through the gas cooler [6]. Finally, during the isenthalpic process, the pressure and temperature of the cooled refrigerant decrease in the expansion valve. Figure 2-2 presents the P-h diagrams of the subcritical and transcritical heat pump system.

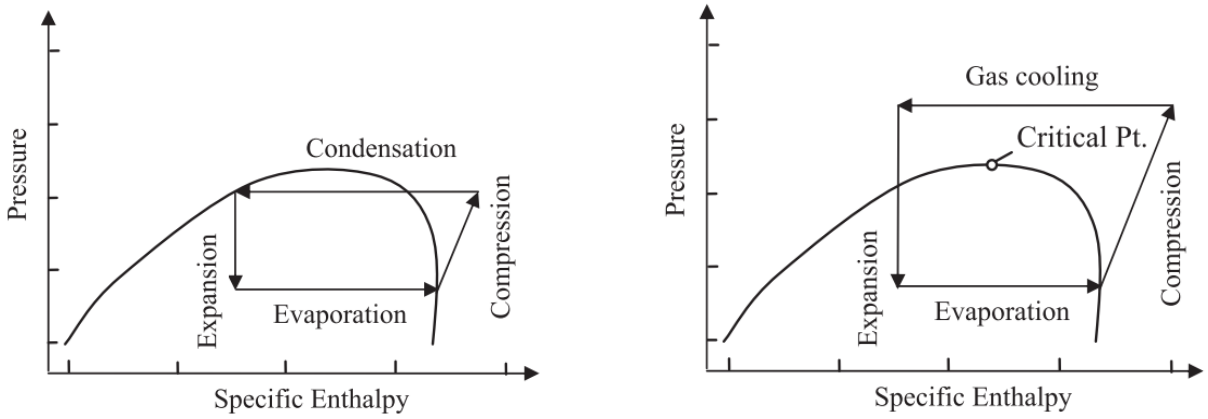

(a) (b)

Figure 2-2. P–h diagrams showing: (a) subcritical cycle and (b) transcritical cycle.

The heat rejections in the gas cooler and condenser are by sensible cooling and condensing process so the temperature difference in the gas cooler is greater than the condenser. Hence, the transcritical heat pump is more efficient than the subcritical heat pump.

2-2 Heat pump system modification

The heat pump system has become the main energy-efficient system in many industrial and domicile applications so many researches have been carried out to improve the overall efficiency of the heat pump system. The throttling loss in the heat pump system during the isenthalpic process reduces the efficiency of the heat pump because no useful power can be produced in the expansion process. This loss is small in the subcritical heat pump due to lower pressure difference however, the pressure difference in the transcritical cycle is high which leads to higher loss .

Several types of expansion process modifications have been proposed to improve the heat pump system efficiency.

2-2-1 Ejector expansion device

The ejector, which is the heart of the jet refrigeration system was invented by Sir Charles Parsons around 1901 for removing air from a steam engine's condenser [7]. The ejector has been used in different applications, such as expansion work recovery and utilization of low-grade energy. The ejector has received much attention as expansion due to its simple construction, low maintenance cost, and no moving parts. Figure 2-3 shows a schematic of an ejector that consists of a motive nozzle, suction nozzle, mixing section, and diffuser. High pressure working gas enters the primary nozzle of the ejector where its pressure decreases and the velocity increases. The secondary working fluid enters the suction nozzle and the primary and secondary fluids combine in the mixing chamber of the ejector. Finally, at the diffuser, the velocity of working gas reduces, and the pressure increases.

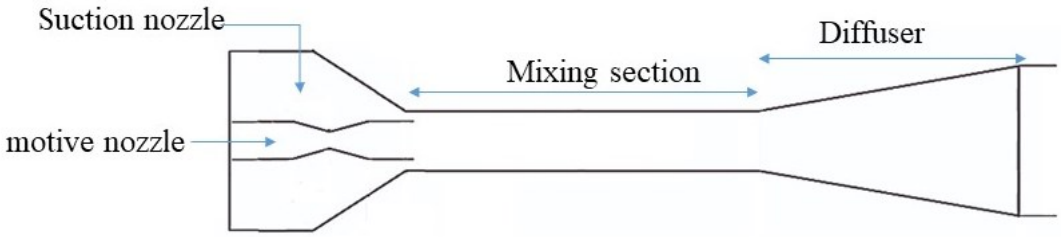

Figure 2-3. Schematic of an ejector.

The ejector was proposed to recover the expansion work in the vapor compression refrigeration system in 1931 [8] and since then it has gained increasing attention on the ejector transcritical CO_2 heat pump cycle. The schematic and P-h diagram of the transcritical CO_2 ejector heat pump system is shown in Figure 2-4 [9].

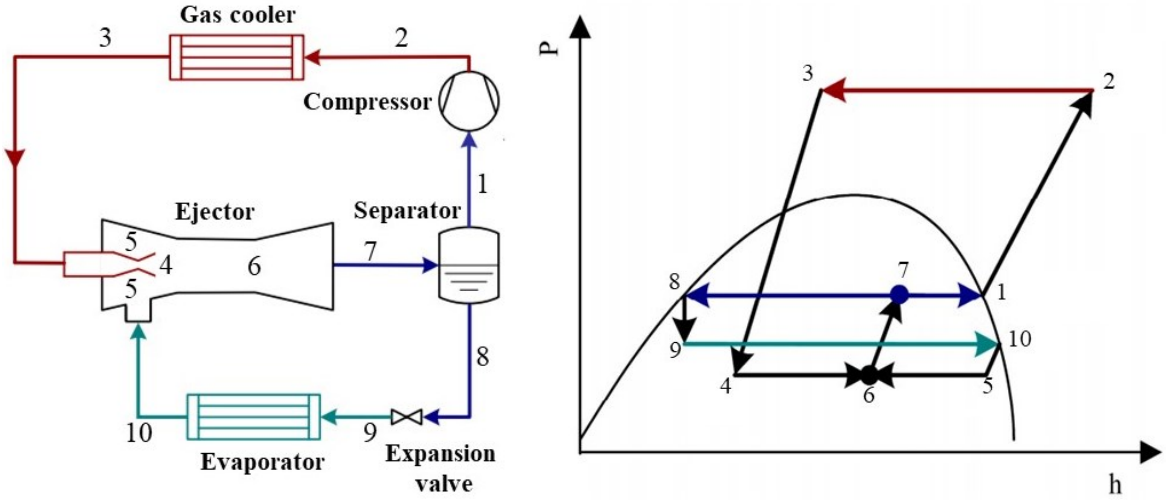

(a) (b)

Figure 2-4. (a) The schematic and (b) P-h diagram of transcritical CO_2 ejector heat pump system.

Li and Groll [10] studied the effect of the ejector on the COP of the transcritical heat pump system and compared it with the basic heat pump system at different operating conditions. Their results showed that the ejector can improve the COP of the heat pump up to 16%. Taslimi taleghani and et al. [11] analyzed the ejector geometrical parameters on the COP of the heat pump system. Their findings indicated that the primary nozzle throat diameter has a significant impact on the performance of the heat pump system. In addition, they concluded that the highest ejector efficiency occurred at a pressure lower than the optimum gas cooler pressure.

The ejector decreases the expansion losses and also increases the pressure at the inlet of the compressor, so the compressor required power decrease. However, the two-phase ejector cycles have not experienced large-scale commercialization [12]. In addition, due to presence of second phase inside the ejector, the performance of the ejector drops rapidly. Also, when the pressure of the primary flow is high, the ejector efficiency and entrainment ratio are lower.

2-2-2 Vortex tube expansion device

The vortex tube, also known as the Ranque-Hilsch vortex tube is a device that can produce both hot and cold streams, simultaneously. The schematic of the vortex tube is illustrated in Figure 2-5. The vortex tube was discovered in 1931 by a French physicist Georges J. Ranque. Even though there have been many studies regarding the understanding of the energy separation

inside the vortex tube but this phenomenon is still unknown. Vortex Tubes can be used in a variety of industrial processes such as the cooling system for a drill bit, air suit, gas separation, etc. [13]. Majority of studies focused on the energy separation in the vortex tube and attempted to raise the temperature difference numerically and experimentally [14–16]. Lagrandeur et al [17] analysed the exergy efficiency of the vortex tube using air as a working gas. Their results showed that the friction is the main cause of the exergy loss and by employing the second vortex tube, the exergy efficiency increases up to 4.4%. Moreover, it was introduced as an expansion device in a heat pump system to reduce expansion losses [18]. In contrast to the vortex tube, ejector-expansion devices have been successfully commercialized. In addition, all studies,regarding the integration of the vortex tube with the heat pump system, have been done based on one dimensional thermodynamic analysis of vortex tube which the energy separation hasn't been analyzed. The schematic and P-h diagram of the transcritical CO_2 vortex tube heat pump system is shown in Figure 2-5.

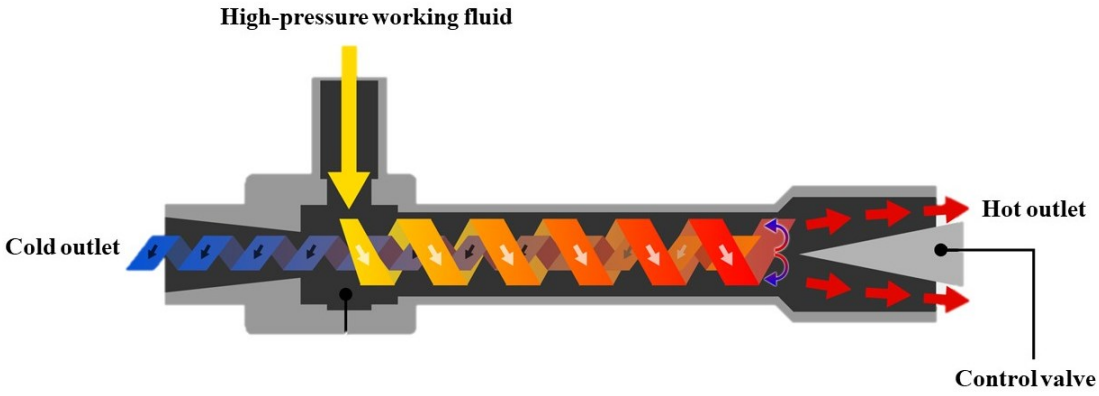

Figure 2-5. The schematic of vortex tube.

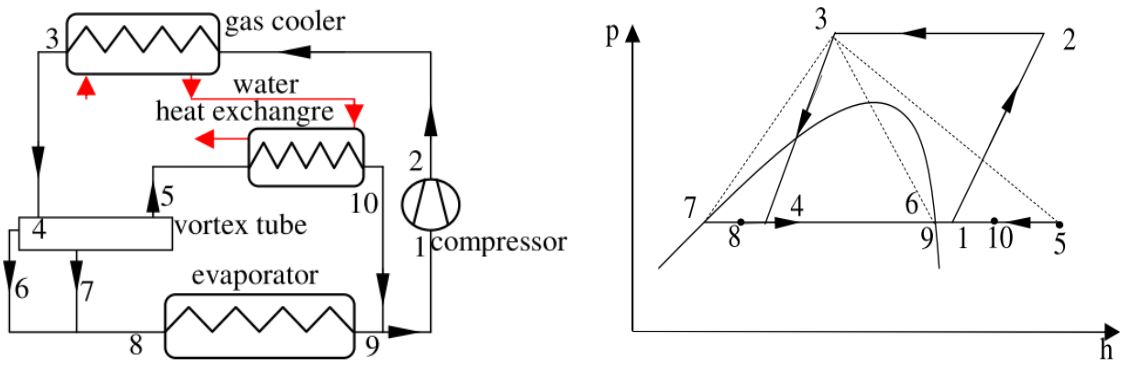

Figure 2-6. (a) The schematic and (b) P-h diagram of transcritical CO_2 vortex tube heat pump system.

2-2-3 Work Recovery Expansion device

The performance of the basic heat pump system can be improved by reducing the expansion losses of the transcritical heat pump system during the isenthalpic process. In a transcritical CO_2 cycle, the higher pressure difference leads to higher expansion losses, thus making work recovery beneficial. There are many devices that can potentially be used as a work recovery expansion device in a transcritical heat pump system such as piston expander, Scroll expander, etc. The researchers estimate the potential improvement of energy efficiency to be 20% to 50% [19,20]. Nevertheless, in recent years, many researchers have attempted to reduce the expansion losses of transcritical CO_2 by using work recovery but none of these designs have been commercialized due to the presence of two-phase flow and technically it is difficult and also costly to design the two-phase expander. Besides, the one dimensional thermodynamic analysis of the expander has been investigated which the effect of rotor speed on the torque production hasn't been analysed.. Thus, the Tesla turbine which is known as a bladeless turbine could be an interesting expansion device. The schematic of the Tesla turbine is presented in Figure 2-7.

Figure 2-7. The schematic of Tesla turbine.

The Tesla turbine was patented in 1913 by Tesla [21] but due to its low efficiency in comparison with traditional turbine, it was abandoned. However, manufacturing the Tesla turbine is easier and production costs for disks are much lower than for blades. In addition, the Tesla turbine is capable to work with wide range of fluids such as two-phase, very viscous fluid or non-Newtonian fluid and etc. however it was abandoned due to its low efficiency and performance in comparison to traditional turbomachinery. Song et al. [22] introduced the Tesla turbine as a small expander due to its simplicity and low capital cost. There are few numerical and experimental studies which focused on the flow analysis in the Tesla turbine [23–25].

2-3 Refrigerant

Refrigerants play an important role in human life and they have been widely used in many industrial and residential applications such as refrigerator, air conditioner, etc. Since the invention of the vapor-compression in 1834 by Evans and Perkins, CO_2 has been a candidate for a refrigerant and due to its interesting future such as no flammability and low toxicity CO_2 was widely used in marine systems in the twentieth century [6]. However, CO_2 phased out due to the arrival of synthetic refrigerants, high cost of the component, sealing difficulty due to high pressure [1,26] and the synthetic refrigerants such as R22 and R12 have unique properties such

as low critical pressure with no toxicity and no flammability but have adverse effects on the environment. The studies indicated that some refrigerants are harmful to the environment and have a great impact on damaging the Ozone layer. Therefore, in 1987, the Montreal Protocol was adopted to reduce and phase-out of ozone-depleting substances. As Table 2-1 indicates, taking into account the Global Warming potential (GWP), the Ozone Depletion potential (ODP) and other environmental data, CO_2 could be an alternative [27].

Table 2-1. Environmental data of some refrigerants.

Refrigerant	R12	R600a	R410A	R134a	R22	CO_2
Natural fluid	No	No	No	No	No	Yes
ODP	0.82	0	0	0	0.04	0
Critical temperature (°C)	112.0	134.7	71.4	101.2	96.2	31.1
GWP (100 years)	8100	~20	2100	1300	1500	1
Flammability	No	Yes	No	No	No	No
Toxicity	No	No	No	No	No	No

CO_2 is a natural refrigerant that is non-toxic, non-flammable with an ozone depletion potential of zero, and a GWP of 1. The critical temperature of CO_2 is 31.1 °C which cannot be used effectively in a subcritical cycle however, it can be effective in a transcritical cycle. In addition, due to the low viscosity of CO_2, the Reynolds number is relatively high which means the flow is turbulence and causes a good heat transfer rate.

So far, the ejector has been introduced as an expansion device for the heat pump system. However, due to presence of second phase inside the ejector, the performance of the ejector drops rapidly. Also, when the pressure of the primary flow is high, the ejector efficiency and entrainment ratio are lower. The main objective of this study is to find the proper expansion device in order to reduce the losses due to the expansion. Two expansion devices are chosen namely; vortex tube and Tesla turbine. The numerical simulation was carried out on both expansion machines and the data was extracted from the CFD simulation. For the next step, the device was implemented into the heat pump system to evaluate each device capability to reduce

the throttling losses. Finally, the performance of the heat pump system was evaluated in term of COP.

Chapter 3

Thermodynamic Performance of a CO_2 Vortex tube based on 3D CFD flow analysis

Avant-propos

Auteurs et affiliation:

Abbas Aghagoli: étudiant au doctorat, faculté de génie, département de génie mécanique, Université de Sherbrooke.

Mikhail Sorin: professeur, faculté de génie, département de génie mécanique, Université de Sherbrooke.

Date d'acception: 18 août 2019

État de l'acceptation: version finale publiée, Vol 108, pages 124-137

Revue: International Journal of Refrigeration

Titre français: Performance thermodynamique d'un tube vortex de CO_2 basée sur l'analyse de flux CFD 3D

Contribution au document:

Cet article contribue à la thèse en appliquant le CO_2 basse pression dans le tube vortex.

Résumé français:

Le tube vortex (VT) est un dispositif mécanique qui peut fournir simultanément chauffage et refroidissement. Dans ce travail, un modèle CFD 3D a été tout d'abord développé pour simuler l'écoulement de CO_2 dans un tube vortex, puis il est validé avec des données

expérimentales déjà publiées. Le modèle de turbulence supposé k-ε utilise des nœuds hexaédriques structurés générés dans le maillage ANSYS. Seulement 1/6 de la géométrie est nécessaire en raison de la symétrie du VT. Le modèle CFD validé est combiné à un modèle thermodynamique du VT pour compléter une étude paramétrique, où la pression d'entrée (550kPa à 1300kPa) et la fraction massique froide (0,2 à 0,9) sont les paramètres choisis. Les effets sur la séparation d'énergie et les performances du VT ont été présentés. La séparation de flux d'énergie est examinée en termes de différences de température de sortie chaude et de sortie froide, toutes deux en ce qui concerne la température d'entrée du VT. Les performances sont caractérisées par la puissance de refroidissement, la puissance de chauffage et les coefficients de performance énergétique et exergétique. Les résultats numériques montrent que la variation de la fraction massique froide de 0,2 à 0,9, pour une pression d'entrée fixe de 1300 kPa, fait passer la différence de température de sortie chaude de 10 ˚C à 78,9 ˚C, tandis que la différence de température de sortie froide diminue de 44,2 ˚C à 9,7 ˚C.

3-1 Abstract

The vortex tube (VT) is a mechanical device that can simultaneously provide heating and cooling. In this work, a 3D CFD model is first developed to simulate the flow of CO_2 within a vortex tube, and then it is validated with published experimental data. The assumed k-ε turbulence model uses Structured Hexahedral nodes generated in ANSYS Meshing. Only 1/6 of the geometry is required due to the symmetry of the VT. The validated CFD model is combined with a thermodynamic model of the VT to complete a parametric study, where the inlet pressure (550kPa to 1300kPa) and cold mass fraction (0.2 to 0.9) are the chosen parameters. The effects on the VT energy separation and performance are presented. Energy separation is discussed in terms of the hot exit and cold exit temperature differences, both with respect to the VT inlet temperature. Performance is characterized by cooling power, heating power, and both energy and exergy metrics. The numerical results show that the variation of the cold mass fraction from 0.2 to 0.9, for a fixed inlet pressure of 1300 kPa, causes the hot exit temperature difference to rise from 10 ˚C to 78.9 ˚C, while the cold exit temperature difference falls from 44.2 ˚C to 9.7 ˚C.

Keywords: Vortex tube, CO_2, CFD, exergy efficiency

3-2 Introduction

Since the negative effects of chlorofluorocarbons (CFCs) on global warming and Ozone depletion have been recognized, the use of CFCs has been decreasing and scientists have been attempting to find promising substitute refrigerants in order to preserve the environment. Carbon dioxide is considered as a very attractive refrigerant due to its zero ozone depletion potential and low global warming potential [6]. Carbon dioxide has been a potential candidate for refrigeration since the invention of the vapor compression cycle.

Refrigeration plays an important role in industry, hence researchers are looking for new techniques to enhance the efficiency of the systems that require refrigeration. With the rise in global population, industrialisation, and growing worldwide energy consumption, there is a growing interest in the reuse of waste energy. Likewise, there is continuing interest in energy efficiency, as small change in efficiency can have a great impact on energy saving, particularly in devices that are not considered very efficient, such as the vortex tube (VT). The vortex tube was discovered by the French scientist Ranque in 1931 and since then there have been many research works on the performance of vortex tubes [28]. A vortex tube is a device, which simultaneously produces both hot and cold streams from highly compressed gas. Figure 3-1 shows the main parts of the vortex tube which are: a cylinder, inlet nozzle(s), cone valve and cold diaphragm [29]. Compressed air or other fluids is injected through the inlet nozzle(s) tangentially and starts to swirl along the vortex tube. Two streams separately exit the vortex tube. The hot stream, which has a temperature higher than the inlet fluid, swirls peripherally and exits through a cone valve. The cold stream, which has a temperature lower than the inlet fluid, swirls in the centre of the vortex tube and exits through a cold diaphragm.

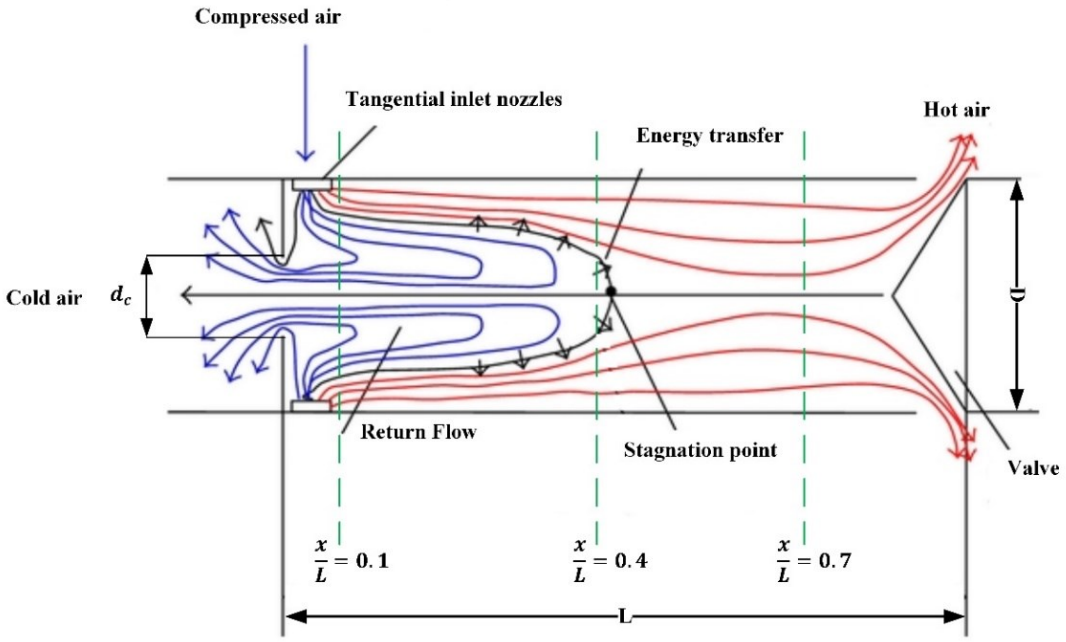

Figure 3-1. Flow pattern and schematic diagram of vortex tube (Dutta et al. 2013).

Even though, it has been nine decades since the invention of the vortex tube, the concept of energy separation phenomena in the vortex tube is not well understood. Published papers in both experiment and numerical studies have considered a variety of parameters while investigating the energy separation in the vortex tube. Hilsch [30] observed that compressed air at 6 atm and 20 ˚C produce 82 ˚C a temperature difference between the cold and hot exits ($\Delta T_{hc} = \Delta T_h - \Delta T_c$) due to internal friction between stream layers, and established a constant angular velocity between layers. Ahlborn and Groves [31] carried out an experiment to measure the axial and angular velocities in the vortex tube. They observed that the amount of mass flow rate, which escapes at the cold exit, is less than amount of mass flow rate, which moves back toward the cold exit, which suggested that there is a secondary flow inside the vortex tube. Later, Ahlborn et al. [32] proposed a new idea, whereby the secondary circulation acts as a heat pump which transfers energy from inner layer (near the core) to the outer layer (near the wall). Some numerical research [33] illustrated that the secondary circulation depends on the ratio of cold the part diameter to tube diameter ($\frac{d_c}{D}$). Hundreds of experimental papers used air as a working gas and investigated different initial condition such as an inlet pressure, cold mass fraction and different vortex tube geometry. Hamdan et al. [34] evaluated the effect of inlet

pressure on the temperature difference of the vortex tube for different lengths and diameters. According to their results, with the increasing length of the vortex tube, as long as the stagnation point (a point where inner stream velocity becomes zero) occurs inside the tube, temperature difference increases. An increase in the tube diameter (D) has both an advantage and a disadvantage. On one hand, the angular velocity decreases and leads to lower centrifugal force and finally lower energy separation. On the other hand, the residence time inside the tube is higher, and as a result the energy transfer between layers is improved, what leads to higher energy separation. Gutak [35] carried out an experiment with high pressure air (78 and 88 bar). Based on their experiment, it was concluded that increasing the inlet pressure induces a higher velocity inside the tube, leading in turn to higher energy separation. Xue et al. [36] used a large vortex tube, with a 2000 mm length and 60 mm diameter. They observed the transferring the forced vortex (swirl velocity is directly proportional to the radius ($V \propto r$)) near centerline to free vortex (swirl velocity is inversely proportional to the radius ($V \propto \frac{1}{r}$)) at the hot exit near the wall because of decreasing the swirling velocity.

Han et al. [37] used R728, R744, R32, R22, R161, R134a as working gases. The initial parameters were an inlet pressure from 0.2 MPa to 1.3 MPa and temperature was 12℃. They proposed that specific heat ratio, kinematic viscosity and thermal conductivity have an important influence on energy separation of the vortex tube; they also illustrated that the isentropic throttling effect on the cold exit of the working gas has a major impact on temperature difference between inlet and cold exit (ΔT_c). Agrawal et al. [38] experimentally studied the influence of three working fluids (air, nitrogen, and carbon dioxide) on a vortex tube under different inlet pressures (3, 4 and 5 bar) and different length to diameter ratios (12.5, 17.5 and 22.5). Their results showed that carbon dioxide has the highest temperature difference in compare to air and nitrogen. A disadvantage of the experimental approach is the fact that applying some tools, such as a pitot tube to measure the velocity and other turbulent flow characteristics, might interrupt the highly turbulent flow pattern inside the vortex tube. This is why computational fluid dynamic (CFD) modeling helps to understand the flow characteristics. Thakare and Parekh [39] employed the 2D CFD modeling with the standard $k-\varepsilon$ turbulence model for a range of inlet pressures (2-5 bar) in both non-isolated and isolated vortex tube.

Their results showed that temperature difference is higher for isolated than non-isolated vortex tube. Also, they [40] analyzed the temperature difference for four different working gases (air, N_2, CO_2 and O_2) and their results showed that N_2has the highest and CO_2 has the lowest energy separation. No validation with experimental data for N_2, CO_2 and O_2 was presented. Rafiee and Sadeghiazad [41] used 3D modeling of a vortex tube with 6 inlet nozzles, using the standard $k-\varepsilon$ turbulence model. Pourmahmoud et al [42], and Thakare and Parekh [40] studied the vortex tube with CO_2 as the working gas, where the inlet temperature and total mass flow were fixed at 294.2 K and 8.35 $g.s^{-1}$. The achieved results, however, are in contrast with each other for instance where $\varepsilon = 0.3$, with calculated cold exit temperatures of 246.48 K and 264.2 K, respectively. So far, the ideal gas equation of state has been assumed for the numerical simulation of the vortex tube which the Cp was considered as constant. However, for this study the NIST real gas models in an ANSYS FLUENT session.The REFPROP v7.0 database employs accurate pure-fluid equations of state that are available from NIST.

In the present study, a 3D simulation of the vortex tube is carried out using ANSYS FLUENT 19, and CO_2 is chosen as a working gas. The modeling results are validated against the experimental data of Han et al. [37]. Energy separation is discussed in terms of the hot exit and cold exit temperature differences, both with respect to the VT inlet temperature. Performance is characterized by cooling power, heating power, and both energy and exergy metrics.

3-3 Mathematical modeling

3-3-1 Governing equations of CFD modeling

In this study, a three-dimensional numerical model of the vortex tube has been developed using the standard $k-\varepsilon$ turbulence model and flow pattern in the vortex tube can be regarded as in steady state. The mass, momentum and energy equations for compressible turbulent flow in the vortex tube are:

$$\frac{\partial}{\partial x_j}\left(\rho u_j\right) = 0 \qquad (3\text{-}1)$$

$$\frac{\partial}{\partial x_j}(\rho u_i u_j) = -\frac{\partial p}{\partial x_i} + \frac{\partial}{\partial x_j}\left[\mu\left(\frac{\partial u_i}{\partial x_j} + \frac{\partial u_j}{\partial x_i} - \frac{2}{3}\delta_{ij}\frac{\partial u_k}{\partial x_k}\right)\right] + \frac{\partial}{\partial x_j}\left(-\rho\bar{\acute{u}}_i\bar{\acute{u}}_j\right) \tag{3-2}$$

$$\frac{\partial}{\partial x_j}\left[\rho u_i\left(h + \frac{1}{2}u_i u_j\right)\right] = \frac{\partial}{\partial x_j}\left[\left(\tau_{ij}\right)_{eff}u_i + k_{eff}\frac{\partial T}{\partial x_j}\right] \qquad k_{eff} = \frac{\mu_t}{Pr_t} + K \tag{3-3}$$

Following the recommendations of [40], k − ε turbulence model is chosen for this study. The standard k − ε model falls into the two equation turbulence category, which is based on transport equations for the turbulence kinetic energy (k) and its dissipation rate (ε). Transport equations for the standard k − ε model are as follow:

$$\frac{\partial}{\partial t}(\rho k) + \frac{\partial}{\partial x_i}(\rho k u_i) = \frac{\partial}{\partial x_j}\left[\left(\mu + \frac{\mu_t}{\sigma_k}\right)\frac{\partial k}{\partial x_j}\right] + G_k + G_b - \rho\varepsilon - Y_M + S_k \tag{3-4}$$

$$\frac{\partial}{\partial t}(\rho\varepsilon) + \frac{\partial}{\partial x_i}(\rho\varepsilon u_i) = \frac{\partial}{\partial x_j}\left[\left(\mu + \frac{\mu_t}{\sigma_\varepsilon}\right)\frac{\partial \varepsilon}{\partial x_j}\right] + C_{1\varepsilon}\frac{\varepsilon}{k}(G_k + C_{3\varepsilon}G_b) - C_{2\varepsilon}\rho\frac{\varepsilon^2}{k} + S_\varepsilon \tag{3-5}$$

Where;

G_k: the generation of turbulence kinetic energy due to the mean velocity gradients

G_b: the generation of turbulence kinetic energy because of buoyancy

Y_M: contribution of the fluctuating dilatation in compressible turbulence to the overall dissipation rate

σ_k and σ_ε: the turbulent Prandtl numbers for k and ε respectively

S_k and S_ε: user-defined source terms

$C_{1\varepsilon}$, $C_{2\varepsilon}$ and $C_{3\varepsilon}$ are constants.

3-3-2 Boundary conditions

The geometry of the model is identical to the vortex tube used in [37] (the EXAIR model 3202), which is shown in Figure 3-2. In the experimental study, CO_2 passed through 6 nozzles with a hot length of 78mm, tube diameter of 9.5mm and cold diameter of 3.5mm which are inner dimensions. In the current CFD modeling the exact model is simulated. However, because vortex tube has a symmetric geometry with 6 inlet nozzles, a 60° sector is modeled for the sake

of computational efficiency [43]. The experimental pressures at the nozzle inlet, hot exit and cold exit are applied directly to the CFD model. The no slip condition is assumed for the vortex inner walls and the inlet temperature is constant at 285 K. The simulation is done using the Pressure based Solver with SIMPLE algorithm. The vortex tube model is designed in ANSYS Design Modeler; the structural mesh is generated using ANSYS Meshing; the simulation is carried out in FLUENT.

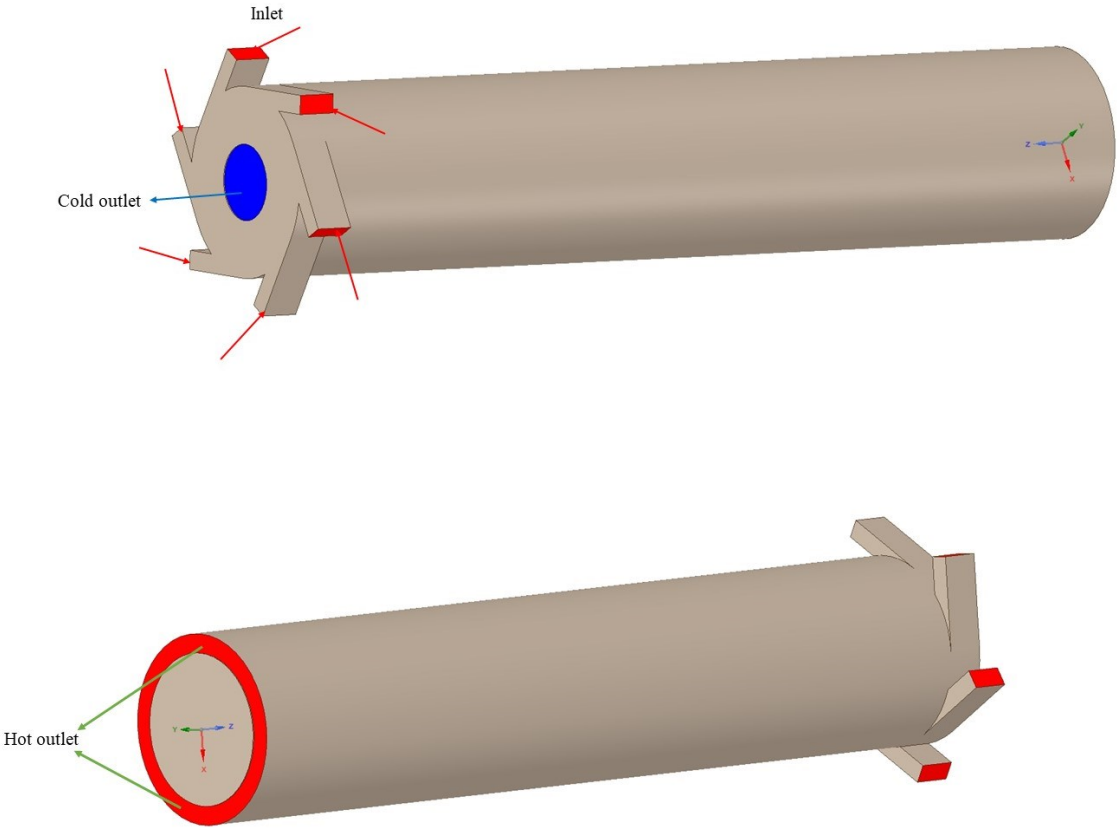

Figure 3-2. The geometry of EXAIR model 3202.

3-3-3 Mesh

The 3D CFD mesh grid around the nozzle inlet, cold exit, and hot exit is shown in Figure 3-3. In this model a regular organized mesh grid has been used. All radial lines of the meshing model are connected to the centerline and the circuit arcs are regularly constructed from the

wall to the centerline. This type of meshing model helps reduce computation time, and the computation procedure is more precise compared to irregular meshing [16].

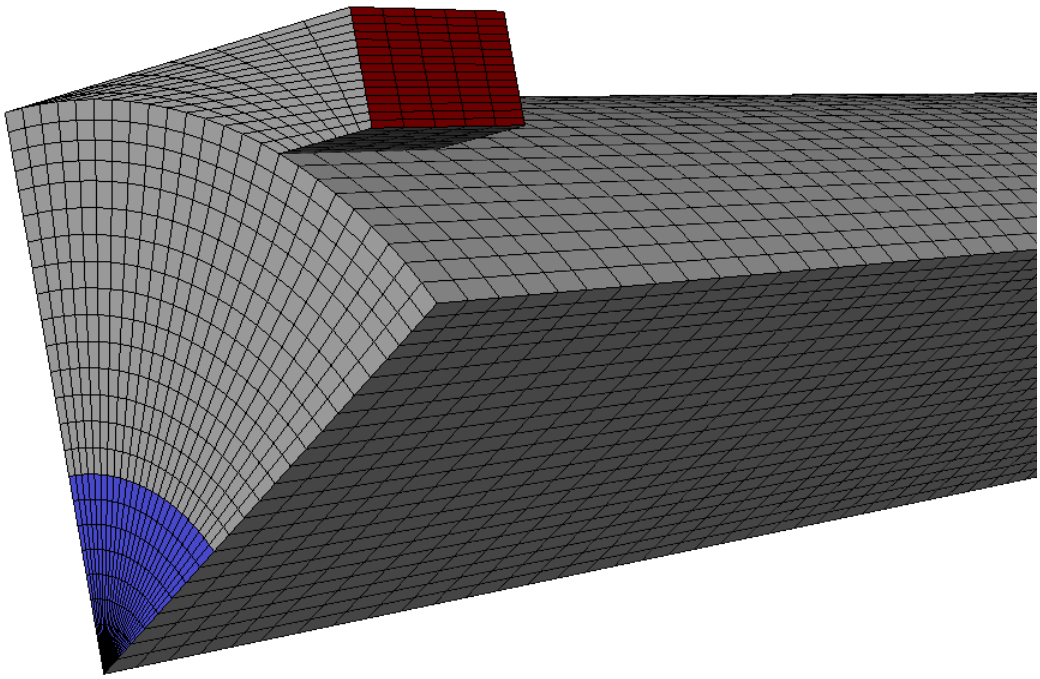

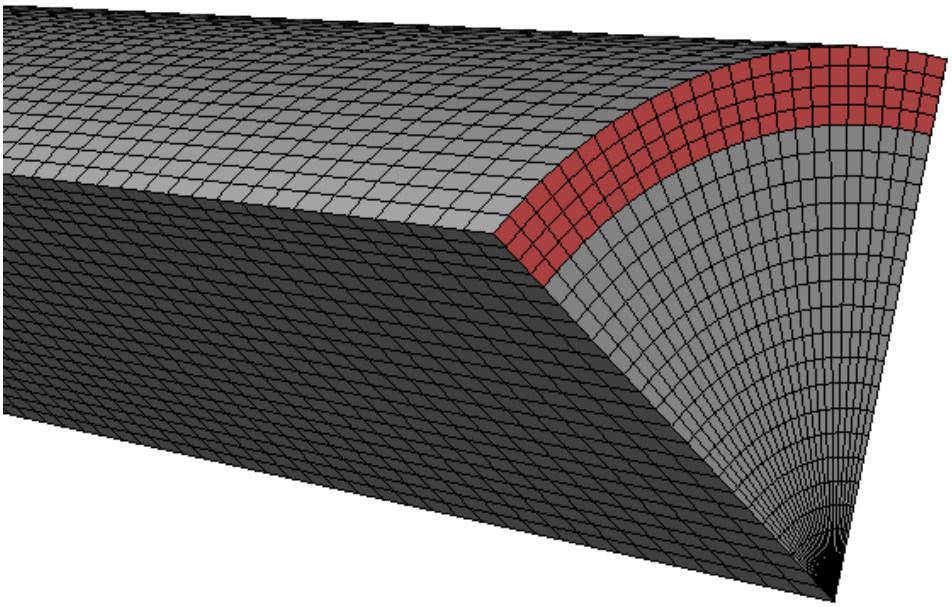

Figure 3-3. 3D CFD model of vortex tube.

3-3-4 Grid independency

Grid independency is important to determine the optimum mesh number, meaning that the solution is independent of the mesh resolution. Therefore, 3D CFD analysis was carried out using different mesh sizes, with 1187994, 1765194, and 2352794 cells. It found that the percentage of cold temperature difference at 1765194 and 2352794 cells are less than 0.5%. Therefore, the 1765194 cell grid is chosen for the simulation. Increasing the number of cells more than 1765194 does not have a significant impact on the results.

3-3-5 Validation

Figure 3-4 shows a comparison of the CFD results with the experimental data [37]. The hot exit results are shown in the upper part of the figure, with solid markers, while the cold exit results are in the low part. As it is obvious for both cold and hot exits, the achieved results from

k – ε model are precise and close to experimental results what means that the proposed turbulence model is capable of predicting the precise results.

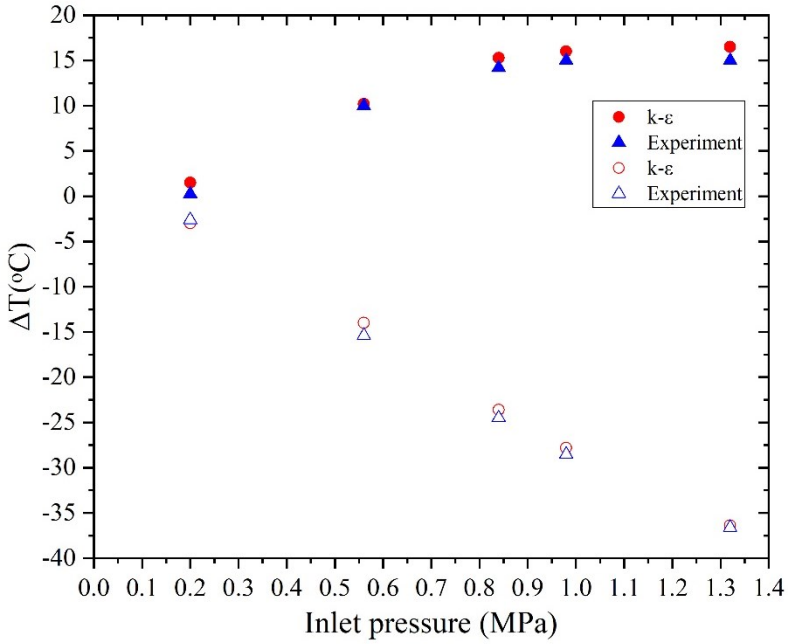

Figure 3-4. Comparison of CFD results with experimental results and hot exit results are shown in the upper part of the figure, with solid markers, while the cold exit results are in the low part.

3-4 Thermodynamic model of the vortex tube

The performance of the vortex tube relies on three main parameters: cold mass fraction, cold exit temperature difference, and hot exit temperature difference which are extracted from CFD modeling. The exergy efficiency will be applied to evaluate the vortex tube thermodynamic performance due to specific temperature differences, given some nominal information about the vortex tube. In the context of improving worldwide energy efficiency, it is important to analyze the performance of the vortex tube, which has not been considered in many research papers.

The cold mass fraction will be varied from 0 to 1 ($0 \leq \varepsilon \leq 1$) and defines as the ratio of the mass flow rate that is exhausted at the cold exit to the inlet mass flow rate.

$$\varepsilon = \frac{\dot{m}_c}{\dot{m}_{in}} \tag{3-6}$$

3-4-1 Cold and hot exit temperature difference

The cold exit temperature difference is defined as the difference between the average temperature at the cold exit and inlet temperature.

$$\Delta T_c = |T_c - T_{in}| \tag{3-7}$$

The hot exit temperature difference is defined as the difference between the average temperature at the hot exit and inlet temperature.

$$\Delta T_h = T_h - T_{in} \tag{3-8}$$

The first law of thermodynamics states that during an interaction between a system and its surroundings, the amount of energy that the system gains must be exactly equal to the amount of energy lost by the surroundings. The first law of thermodynamics can be written as:

$$\dot{E} = \sum_k \dot{Q}_k - \sum_k \dot{W}_k \tag{3-9}$$

$\dot{E}$ represents the sum of thermal energy, kinetic energy and etc.

Applying the first law on the vortex tube, it follows that

$$\dot{m}_{in} C_{p,in} T_{in} = \dot{m}_c C_{p,c} T_c + \dot{m}_h C_{p,h} T_h \tag{3-10}$$

Applying the second law of thermodynamics to the vortex tube with $\dot{Q} = 0$, gives

$$\dot{S}_{in} - \dot{S}_c - \dot{S}_h - \dot{S}_{irr} = 0 \tag{3-11}$$

$$\dot{S}_{irr} = \dot{m}_{in} s_{in} - \dot{m}_c s_c - \dot{m}_h s_h \tag{3-12}$$

$$\dot{S}_{irr} = \dot{m}_{in}[(1-\varepsilon)(s_h - s_{in}) + \varepsilon(s_c - s_{in})] \tag{3-13}$$

3-4-2 Efficiencies of the vortex tube system based on the first thermodynamics law

Thermal efficiencies are used to evaluate the cooling and heating power of the vortex tube. The vortex tube can not only be used as a cooler, but also as a heater, so the definition of the

efficiency should consider both effects. The cooling and heating powers of the vortex tube, when it acts as a refrigeration system and heat pump, are defined as:

$$\dot{Q}_c = \dot{m}_c C_{p,c}(T_{in} - T_c) \tag{3-14}$$

$$\dot{Q}_h = \dot{m}_h C_{p,h}(T_h - T_{in}) \tag{3-15}$$

The input work power is defined as the work required to compress the gas from the exhaust pressure up to the inlet pressure, using a reversible isothermal compression process [44]:

$$P = \dot{m}_{in} R T_{in}\, ln\left(\frac{P_{in}}{P_c}\right) \tag{3-16}$$

When the vortex tube acts as a refrigeration system, the coefficient of thermal performance is defined as the cooling power of the vortex tube divided by the input work power.

$$COP_{refrigeration} = \frac{\dot{Q}_c}{P} \tag{3-17}$$

When the vortex tube acts as a heat pump system, the coefficient of thermal performance is defined as the heating power of the vortex tube divided by the input work power.

$$COP_{heat\ pump} = \frac{\dot{Q}_h}{P} \tag{3-18}$$

3-4-3 Exergy efficiency

The thermomechanical specific exergy of the vortex tube inlet, cold and hot exits are given as [45]:

$$e_{in} = [h(P_{in}, T_{in}) - h(P_0, T_0)] - T_0.[s(P_{in}, T_{in}) - s(P_0, T_0)] + \frac{V_{in}^2}{2} \tag{3-19}$$

$$e_h = [h(P_h, T_h) - h(P_0, T_0)] - T_0.[s(P_h, T_h) - s(P_0, T_0)] + \frac{V_h^2}{2} \tag{3-20}$$

$$e_c = [h(P_c, T_c) - h(P_0, T_0)] - T_0.[s(P_c, T_c) - s(P_0, T_0)] + \frac{V_c^2}{2} \tag{3-21}$$

Therefore, the total input and output exergy for vortex tube can be calculated as:

$$\dot{E}_{in} = \dot{m}_{in}([h(P_{in}, T_{in}) - h(P_0, T_0)] - T_0.[s(P_{in}, T_{in}) - s(P_0, T_0)]) + \frac{\dot{m}_{in} V_{in}^2}{2} \quad (3\text{-}22)$$

$$\dot{E}_h = \dot{m}_h([h(P_h, T_h) - h(P_0, T_0)] - T_0.[s(P_h, T_h) - s(P_0, T_0)]) + \frac{\dot{m}_h V_h^2}{2} \quad (3\text{-}23)$$

$$\dot{E}_c = \dot{m}_c([h(P_c, T_c) - h(P_0, T_0)] - T_0.[s(P_c, T_c) - s(P_0, T_0)]) + \frac{\dot{m}_c V_c^2}{2} \quad (3\text{-}24)$$

The first definition of exergy efficiency for any process was proposed by Grassmann in 1950 as follows [46]:

$$\eta_{Gr} = \frac{\dot{E}_{out}}{\dot{E}_{in}} \quad (3\text{-}25)$$

Where, $\dot{E}_{out} = \dot{E}_c + \dot{E}_h$.

However, Brodyansky et al. [47] proposed excluding the transiting exergy flow from the numerator and denominator of equation (3-25). The transiting exergy flow is the part of exergy that enters the system and leaves it without transformation. As a result, the exergy efficiency is defined as:

$$\eta_{tr} = \frac{\dot{E}_{out} - \dot{E}_{tr}}{\dot{E}_{in} - \dot{E}_{tr}} = \frac{\Delta \dot{E}}{\nabla \dot{E}} \quad (3\text{-}26)$$

In both exergy efficiency definitions, exergy losses are the same but the useful effects presented in the numerator and the exergy expenses presented in the denominator are different. $\Delta\dot{E}$ and $\nabla\dot{E}$ are the produced and consumed exergies in the process, respectively.

Sorin and Khennich [48] applied the transiting exergy to evaluate the efficiency of the air vortex tube. As a result, $\Delta\dot{E}$ and $\nabla\dot{E}$ for the cold and hot streams were calculated as:

$$\Delta \dot{E}_c = \dot{m}_{in}.\varepsilon.[e(P_c, T_c) - e(P_{min}, T_0)] \quad (3\text{-}27)$$

$$\nabla \dot{E}_c = \dot{m}_{in}.\varepsilon.[e(P_{in}, T_{in}) - e(P_{min}, T_0)] \quad (3\text{-}28)$$

$$\Delta\dot{E}_h = \dot{m}_{in}.(1-\varepsilon).[e(P_h,\ T_h) - e(P_{min},\ T_{min})] \quad (3\text{-}29)$$

$$\nabla\dot{E}_h = \dot{m}_{in}.(1-\varepsilon).[e(P_{in},\ T_{in}) - e(P_{min},\ T_0)] \quad (3\text{-}30)$$

Where $\Delta\dot{E} = \Delta\dot{E}_h + \Delta\dot{E}_c$ and $\nabla\dot{E} = \nabla\dot{E}_h + \nabla\dot{E}_c$.

Calculation of the transiting exergy (the second term in each of the four previous equations) depends on three different situations.

If ($T_{in} > T_0$ and $T_{out} > T_0$): $\dot{E}_{tr} = \dot{m}.e_{tr}(P_{min},\ T_{min})$ (3-31)

If ($T_{in} < T_0$ and $T_{out} < T_0$): $\dot{E}_{tr} = \dot{m}.e_{tr}(P_{min},\ T_{max})$ (3-32)

If $(T_{in} > T_0$ and $T_{out} < T_0)$ OR $(T_{in} < T_0$ and $T_{out} > T_0)$ $\dot{E}_{tr} = \dot{m}.e_{tr}(P_{min},\ T_0)$ (3-33)

Where, P_{min} is the lowest pressure when comparing the inlet and outlet pressure values. Given that the considered CO_2 vortex tube works across the environmental temperature T_0 (280 K, 285 K and 290 K) and the environmental pressure $P_0 = 101.3\ kPa$ equation (3-33) is used to evaluate the terms $\Delta\dot{E}_h, \Delta\dot{E}_c, \nabla\dot{E}_h$ and $\nabla\dot{E}_c$ given in equations (27)-(30).

3-5 Results and discussion

In the present study, the effect of inlet pressure and cold mass fraction, which is varied by changing the pressure at the hot exit, are investigated on different aspects of vortex tube. Energy separation is discussed in terms of the hot exit and cold exit temperature differences, both with respect to the VT inlet temperature. Performance is characterized by cooling power, heating power, and both energy and exergy efficiencies. To better understanding the flow inside the vortex tube temperature, pressure, velocity in different sections of vortex tube and, the effect of inlet pressure and cold mass fraction are investigated on cooling and heating power, COP and exergy efficiency.

Figure 3-5 illustrates the effect of inlet pressure (P_{in}) and the cold mass fraction (ε) on the cold exit temperature difference (ΔT_c). The cold exit temperature difference increases with higher inlet pressure, which could be due to increasing swirl velocity. When the cold mass fraction increases, it means that more fluid leaves the cold outlet so cold fluid mixes with hot fluid and the temperature difference decreases. For inlet pressures of 550 kPa, 850 kPa and 1300 kPa, the cold exit temperature difference is 23.7 ˚C, 30.86 ˚C and 44.2 ˚C for a cold mass fraction of 0.2; For the same three inlet pressures, the cold exit temperature difference trend decreases to 7.2 ˚C, 8.7 ˚C and 9.7 ˚C for a cold mass fraction of 0.9.

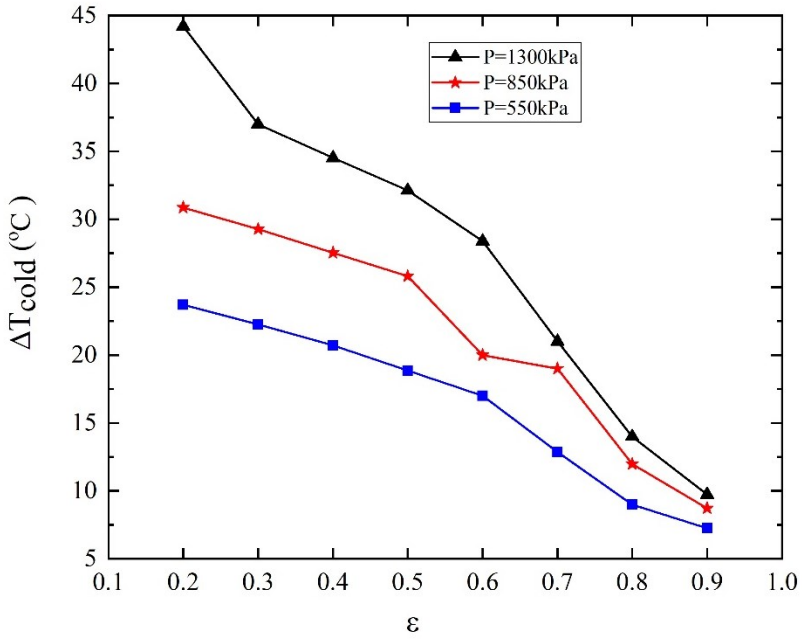

Figure 3-5. Effect of inlet pressure and cold mass fraction on cold exit temperature difference.

As shown in Figure 3-6, as the cold mass fraction (ε) increases, the hot exit temperature difference (ΔT_h) increases. As mentioned, increasing the inlet pressure causes an increase in the swirl velocity, leading to an increase in the hot exit temperature difference. The hot exit temperature difference is 5.5 ˚C, 9.4 ˚C and 10 ˚C at $\varepsilon = 0.2$, and 59.4 ˚C, 70.6 ˚C and 78.9 ˚C at $\varepsilon = 0.9$, corresponding to inlet pressures of 550 kPa, 850 kPa and 1300 kPa respectively.

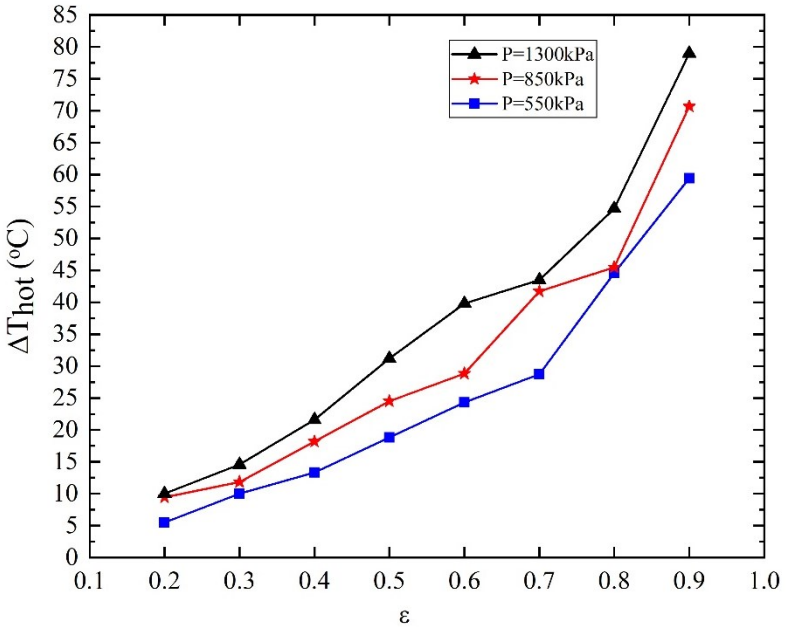

Figure 3-6. Effect of inlet pressure and cold mass fraction on hot exit temperature difference.

In addition to the temperature difference, the flow pattern inside the vortex tube is vital to understand the mechanism of energy separation.

Figure 3-7 depicts the swirl velocity as a function of dimensionless radial position ($\frac{r}{R}$, $0 \leq r \leq R$), for three dimensionless axial locations (x/L), and three inlet pressures. As CO_2 is admitted into the vortex tube, it expands, causing the static pressure to drop and the swirl velocity magnitude to increase. Velocity increases owing to increase the inlet pressure from 550 kPa to 1300 kPa, which causes higher expansion. Due to friction between peripheral stream and the wall, and friction between the CO_2 layers, the velocities of peripheral stream and inner core stream decrease as the streams move towards the hot exit of the vortex tube. The magnitude of the swirl velocity is very low near the core and increases with the increasing radius of the tube. Swirl velocity is zero at the wall because of the no-slip boundary condition. Therefore, the linear part of the swirl velocity diagram confirms the presence of a forced vortex (swirl velocity is directly proportional to the radius, $V \propto r$) near the centerline and a free vortex near the wall (swirl velocity is inversely proportional to the radius, $V \propto 1/r$).

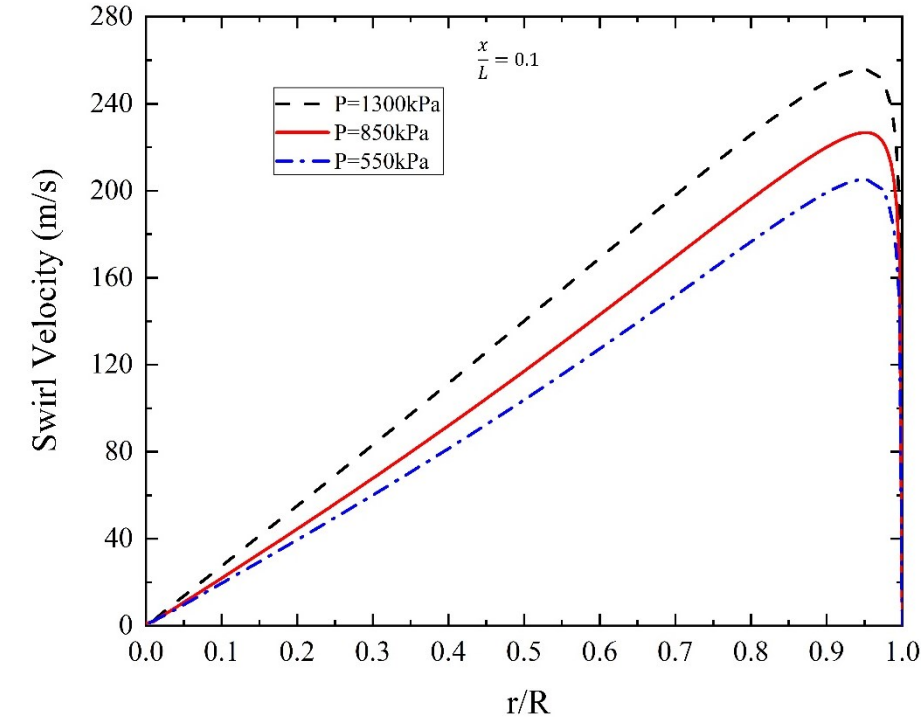
$\frac{x}{L} = 0.1$
P=1300kPa
P=850kPa
P=550kPa
Swirl Velocity (m/s)
r/R
0
40
80
120
160
200
240
280
0.0
0.1
0.2
0.3
0.4
0.5
0.6
0.7
0.8
0.9
1.0

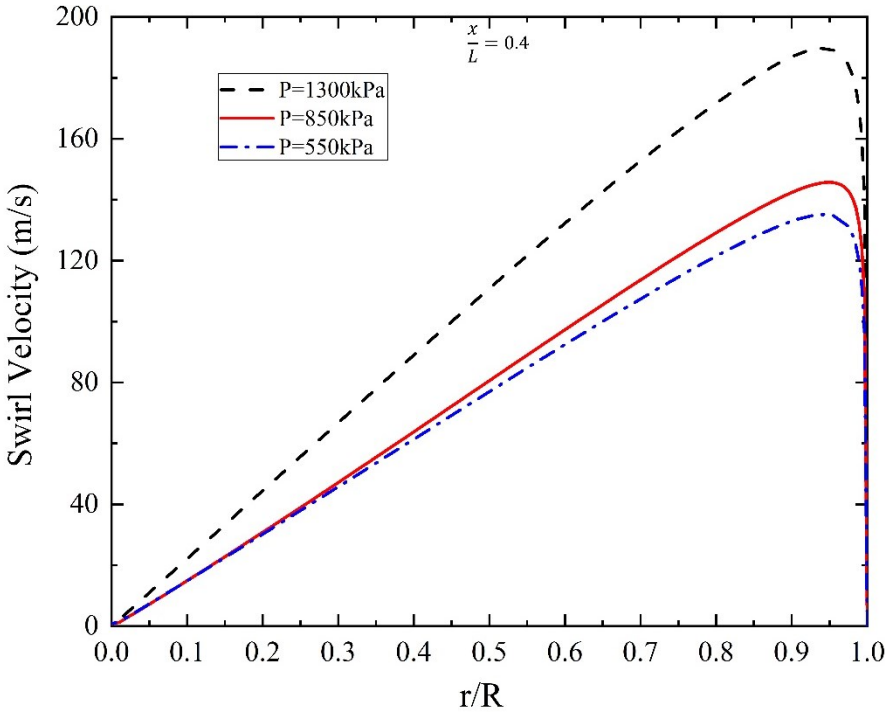
$\frac{x}{L} = 0.4$
P=1300kPa
P=850kPa
P=550kPa
Swirl Velocity (m/s)
r/R
0
40
80
120
160
200
0.0
0.1
0.2
0.3
0.4
0.5
0.6
0.7
0.8
0.9
1.0

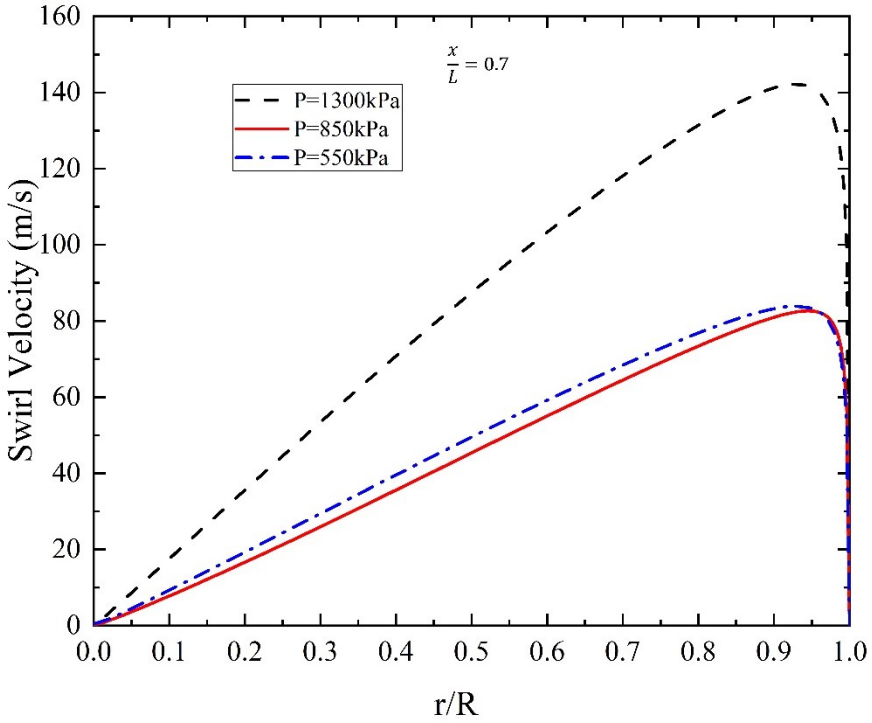

Figure 3-7. Radial profile of swirl velocity for inlet pressure 550, 850 and 1300kPa and dimensionless axial locations (x/ L) 0.1, 0.4 and 0.7.

Figure 3-8 illustrates the axial velocity as a function of dimensionless radial position (r/R), for three dimensionless axial locations (x/L), and three inlet pressures. According to the assumed sign convention for the axial velocity, positive values indicate movement toward the hot exit, while negative values indicate movement toward the cold exit. As the flow moves to the hot exit, it loses its kinetic energy and finally it cannot overcome the pressure difference between the hot and cold exits, hence it backs to the cold exit. As it is shown in Figure 3-8, as the cold mass fraction increases, the magnitude of the positive axial velocity decreases and the magnitude of the negative axial velocity increases, due to the increasing pressure gradient. The magnitude of swirl velocity is five times greater than the axial velocity in each x/L.

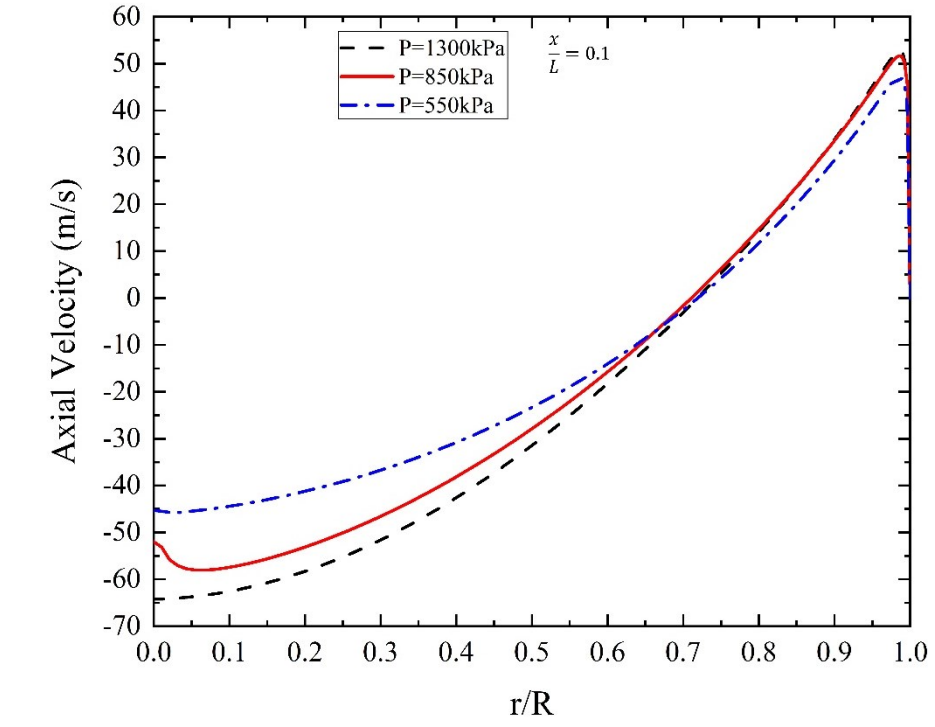
P=1300kPa
P=850kPa
P=550kPa
$\frac{x}{L} = 0.1$
Axial Velocity (m/s)
r/R

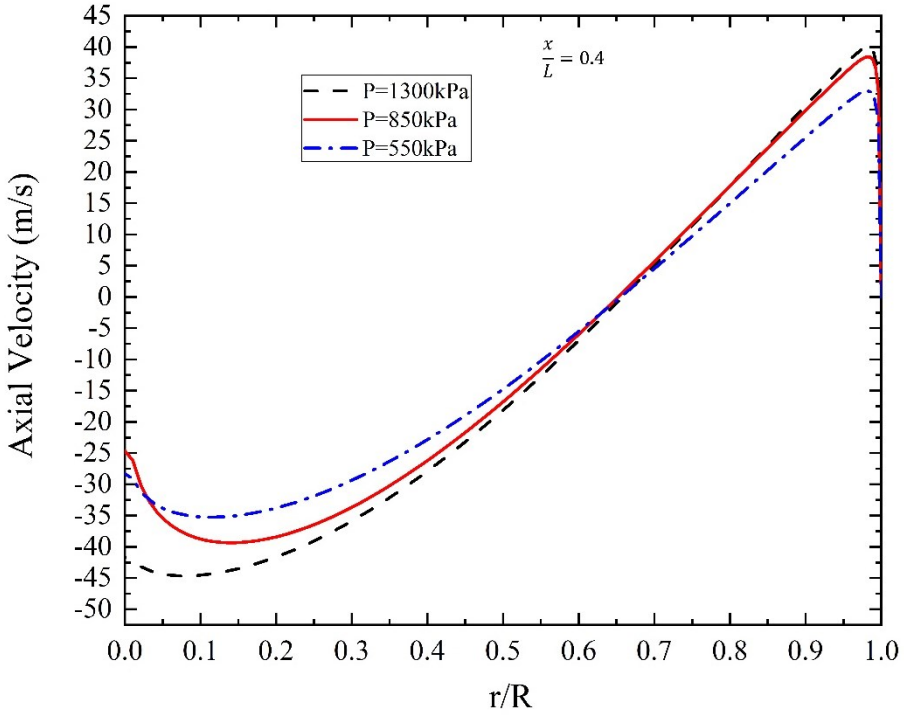
P=1300kPa
P=850kPa
P=550kPa
$\frac{x}{L} = 0.4$
Axial Velocity (m/s)
r/R

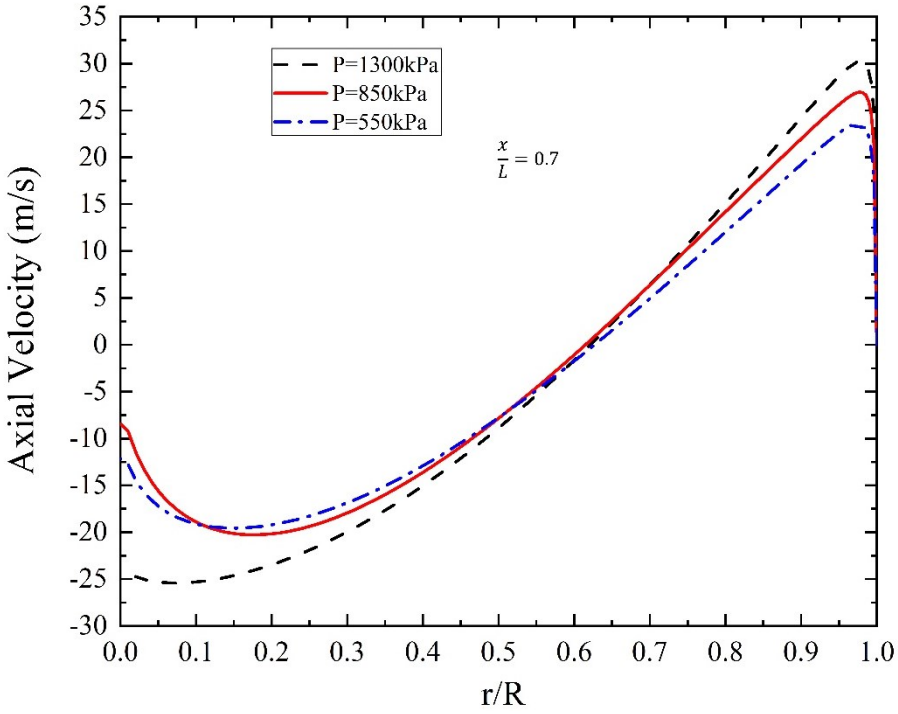

Figure 3-8. Radial profile of axial velocity for inlet pressure 550, 850 and 1300kPa and dimensionless axial locations (x/ L) .1, 0.4 and 0.7.

Figure 3-9 shows the profile of the static temperature as a function of dimensionless radial position (r/R), for three dimensionless axial locations (x/L), and three inlet pressures. The expansion process takes place in the inlet nozzle and leads to a drop in flow temperature and an increase in the tangential velocity. When inlet pressure increases, it causes higher expansion of the admitted gas into the vortex tube, which leads to lower static temperature. The inner flow has a higher static temperature than the peripheral flow and this static temperature difference between the two streams enhances heat transfer from the inner region to the peripheral region. The peripheral flow has the higher kinetic energy than core flow because of higher velocity so it has a lower static temperature with respect to the inner flow. The no-slip boundary condition at wall explains the sudden increase in static temperature. In addition, as the peripheral and flow the inner flows move toward the hot exit, its velocity decreases so the static temperature decreases owing to the conversion of kinetic energy to thermal energy.

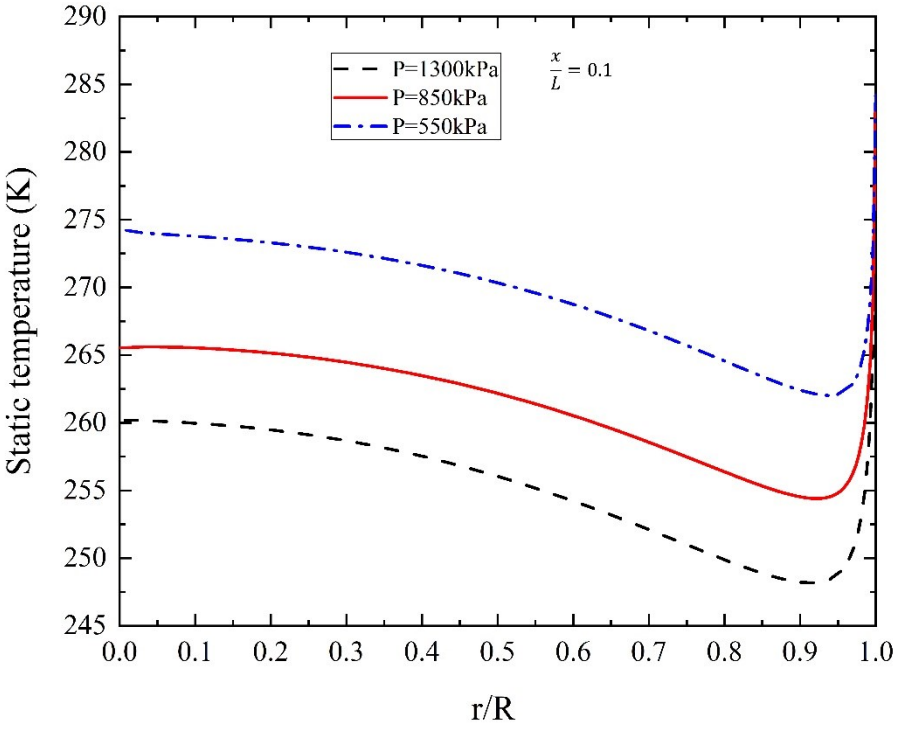
P=1300kPa
P=850kPa
P=550kPa
$\frac{x}{L} = 0.1$
Static temperature (K)
r/R
290
285
280
275
270
265
260
255
250
245
0.0
0.1
0.2
0.3
0.4
0.5
0.6
0.7
0.8
0.9
1.0

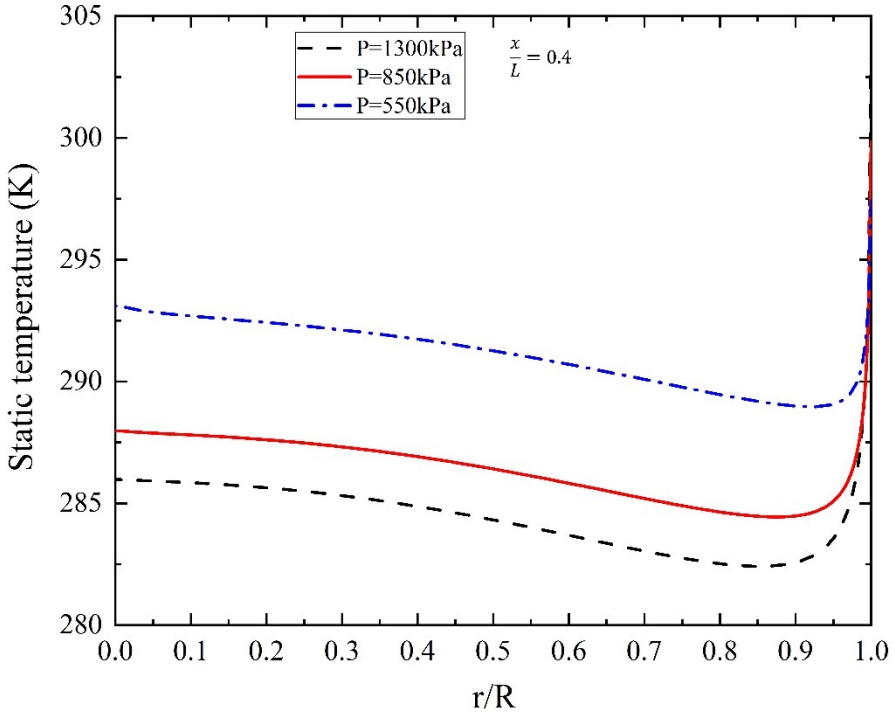
P=1300kPa
P=850kPa
P=550kPa
$\frac{x}{L} = 0.4$
Static temperature (K)
r/R
305
300
295
290
285
280
0.0
0.1
0.2
0.3
0.4
0.5
0.6
0.7
0.8
0.9
1.0

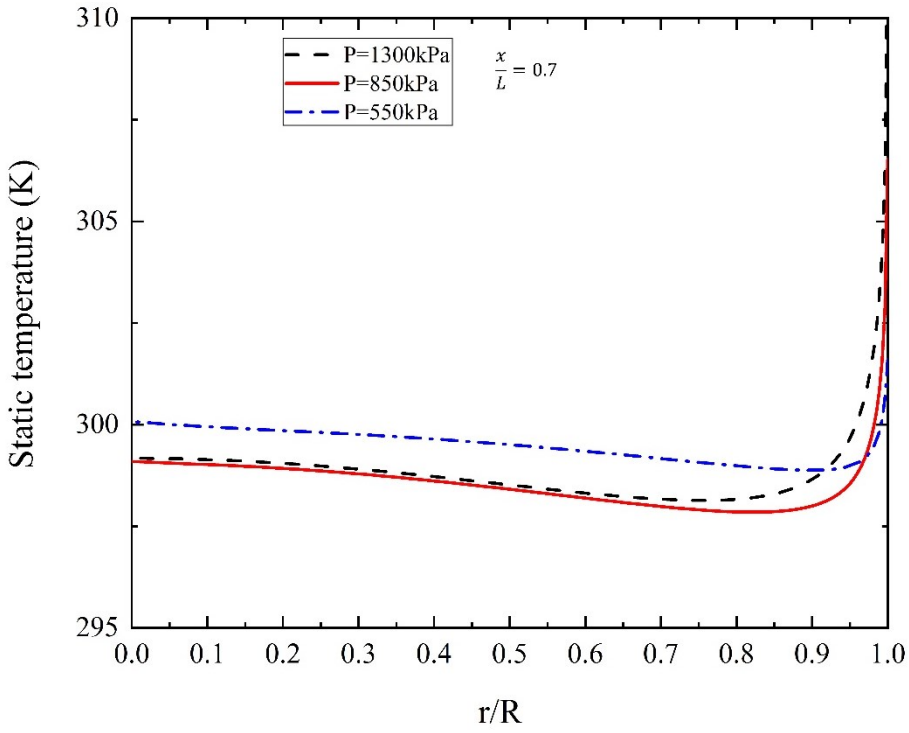

Figure 3-9. Radial profile of static temperature for inlet pressure 550, 850 and 1300kPa and dimensionless axial locations (x/ L) 0.1, 0.4 and 0.7.

Figure 3-10 illustrates the total temperature profile as a function of dimensionless radial position (r/R), for three dimensionless axial locations (x/L), and three inlet pressures at α=0.5. It is obvious that as flow moves toward the hot exit, the total temperature increases owing to the gain in the kinetic energy and this value decreases at the radius because of low velocity magnitude, which leads to low kinetic energy. The total temperature is calculated by following expression:

Total enthalpy is expressed in terms of a static enthalpy and the flow kinetic energy:

$$h_{tot} = h_{stat} + \frac{1}{2}(V.V) \tag{3-34}$$

Static enthalpy is calculated based on static temperature and static pressure where:

$$h_{stat} - h_{ref} = h(T_{stat}, P_{stat}) - h(T_{ref}, P_{ref}) \tag{3-35}$$

The entropy can be evaluated by the following equation:

$$s - s_{ref} = \int_{h_{ref}}^{h} \frac{1}{T} dh - \int_{P_{ref}}^{P} \frac{1}{\rho T} dP \quad (3\text{-}36)$$

Also,

$$h_{tot} - h_{ref} = h(T_{tot}, P_{tot}) - h(T_{ref}, P_{ref}) \quad (3\text{-}37)$$

Step 1: The Fluent solver calculates the total enthalpy and static pressure so the static enthalpy can be calculated by using the flow velocity (Eq. 3-34). Therefore, static temperature can be calculated by Eq. 3-35.

Step 2: Using the isentropic assumption $s_{tot} = s_{stat}$, total pressure will be evaluated by Eq. 3-36.

Step 3: Finally, by knowing the total enthalpy and total pressure, the total temperature can be calculated by Eq. 3-37.

The total temperature profile is similar to the velocity profile because from equation (3-34), total temperature depends on static temperature and velocity with an order one and two, respectively. Therefore, increasing the velocity leads to an increase in the total temperature. Maximum total temperature is near the radius and equals 289.2 K, 291.6 K, 293.1 K at x/L=0.1, 303.1 K, 308.3 K and 313.2 K at x/L=0.4 and 308.1 K, 313.2 K, 321.5 K at x/L=0.7 for inlet pressures of 550 kPa, 850 kPa and 1300 kPa.

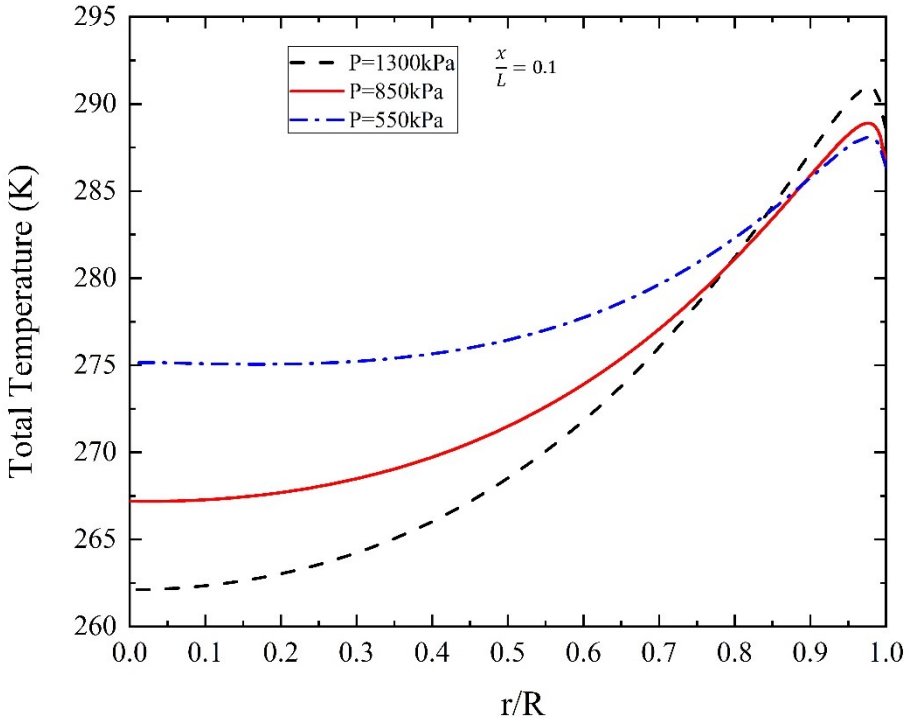
P=1300kPa
P=850kPa
P=550kPa
$\frac{x}{L} = 0.1$
Total Temperature (K)
r/R
295
290
285
280
275
270
265
260
0.0
0.1
0.2
0.3
0.4
0.5
0.6
0.7
0.8
0.9
1.0

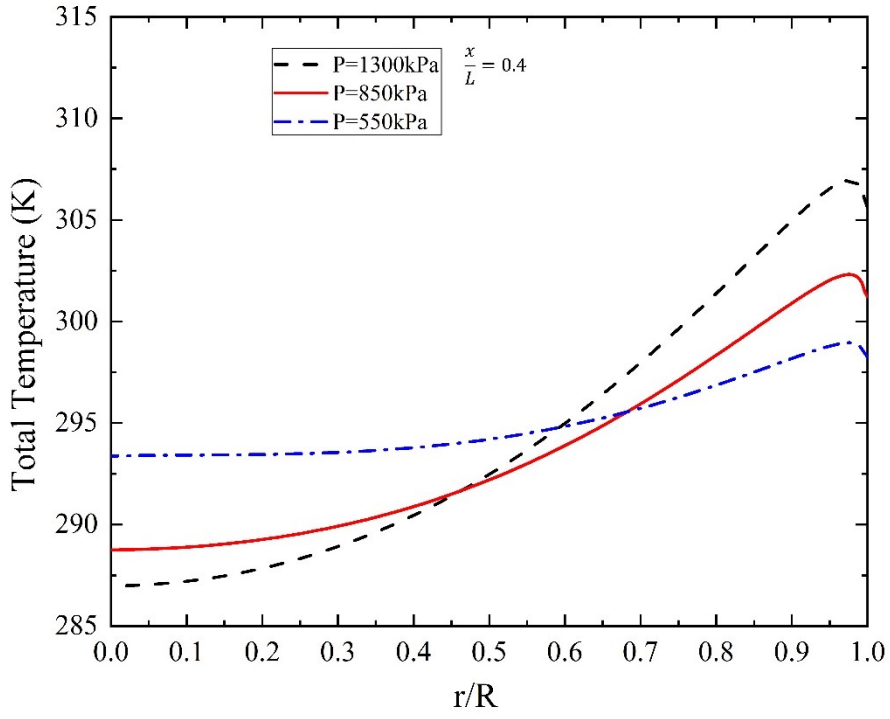
P=1300kPa
P=850kPa
P=550kPa
$\frac{x}{L} = 0.4$
Total Temperature (K)
r/R
315
310
305
300
295
290
285
0.0
0.1
0.2
0.3
0.4
0.5
0.6
0.7
0.8
0.9
1.0

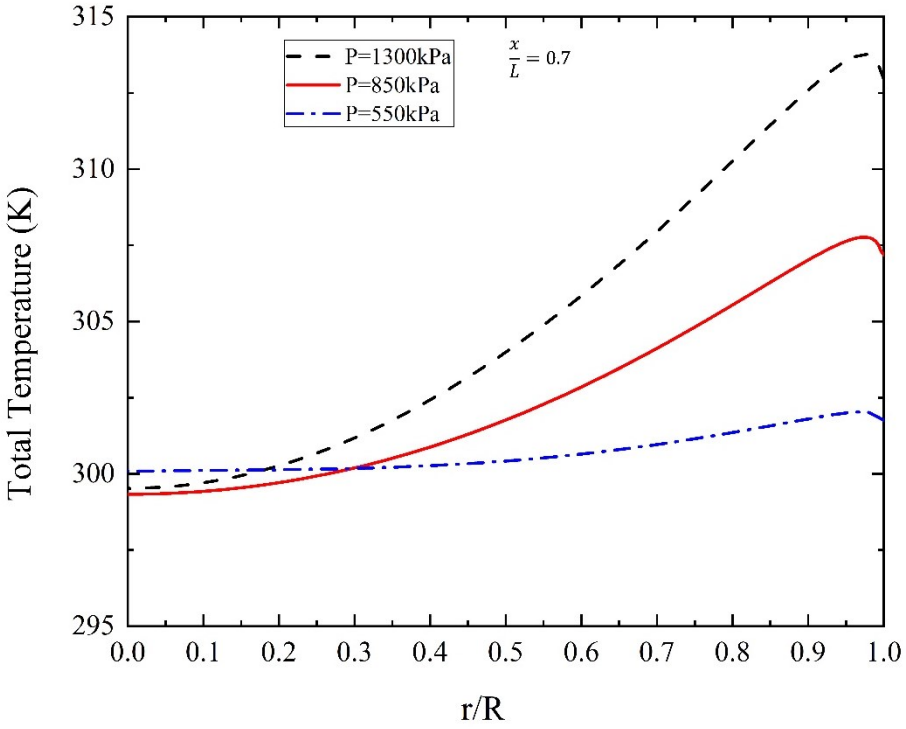

Figure 3-10. Radial profile of total temperature for inlet pressure 550, 850 and 1300kPa and dimensionless axial locations (x/ L) 0.1, 0.4 and 0.7.

Figure 3-11 illustrates the static pressure profile as a function of dimensionless radial position (r/R), for three dimensionless axial locations (x/L), and three inlet pressures. It is observed that at the inlet, the static pressure of the stream is decreased due to the expansion process after the inlet nozzle, the inner core floe has the lower static pressure because of expansion while the peripheral flow has the higher static pressure because of the compression. As the flow moves to the hot exit of the vortex tube, the static pressure is reduced because of internal friction between the gas layers and between the gas and the wall. This is obvious that static pressure is enhanced owing to the increasing the inlet pressure.

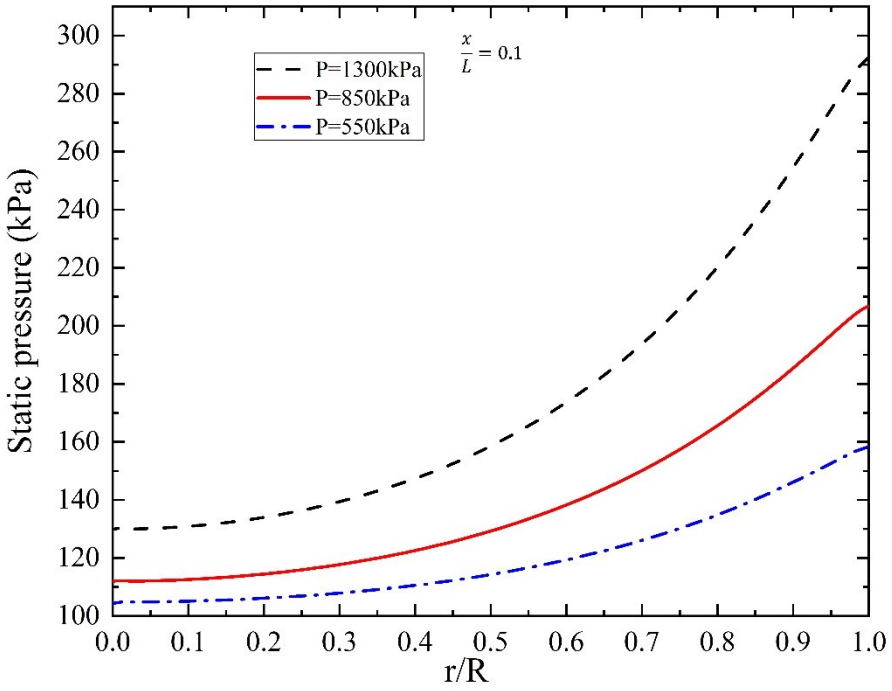
P=1300kPa
P=850kPa
P=550kPa
$\frac{x}{L}$ = 0.1
Static pressure (kPa)
r/R
300
280
260
240
220
200
180
160
140
120
100
0.0
0.1
0.2
0.3
0.4
0.5
0.6
0.7
0.8
0.9
1.0

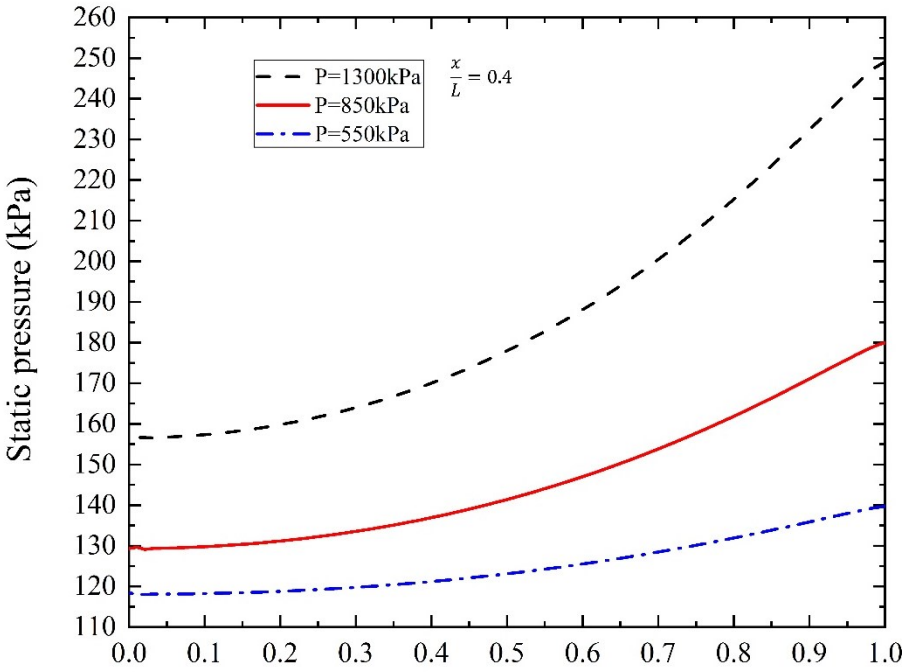
P=1300kPa
P=850kPa
P=550kPa
$\frac{x}{L}$ = 0.4
Static pressure (kPa)
260
250
240
230
220
210
200
190
180
170
160
150
140
130
120
110
0.0
0.1
0.2
0.3
0.4
0.5
0.6
0.7
0.8
0.9
1.0

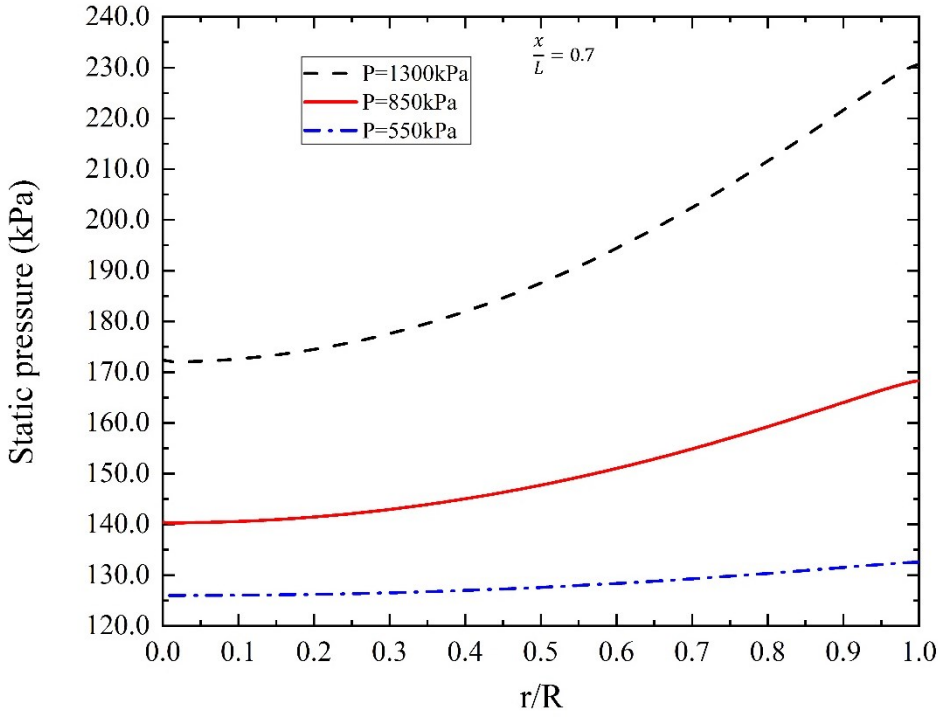

Figure 3-11. Radial profile of static pressure for inlet pressure 550, 850 and 1300kPa and dimensionless axial locations (x/ L) 0.1, 0.4 and 0.7.

Figure 3-12 illustrates the total pressure profile as a function of dimensionless radial position (r/R), for three dimensionless axial locations (x/L), and three inlet pressures. Total pressure depends on static pressure and velocity with an order one and two, respectively. Therefore, increasing the velocity leads to increase the total pressure even though static pressure decreases. As the flow goes to the hot exit of the vortex tube, due to friction, the total pressure decrease. Total pressure gains the highest value, because the velocity near the wall has the highest value and at the wall, total pressure decreases because velocity is zero at the wall and it has a negative effect of total pressure rise.

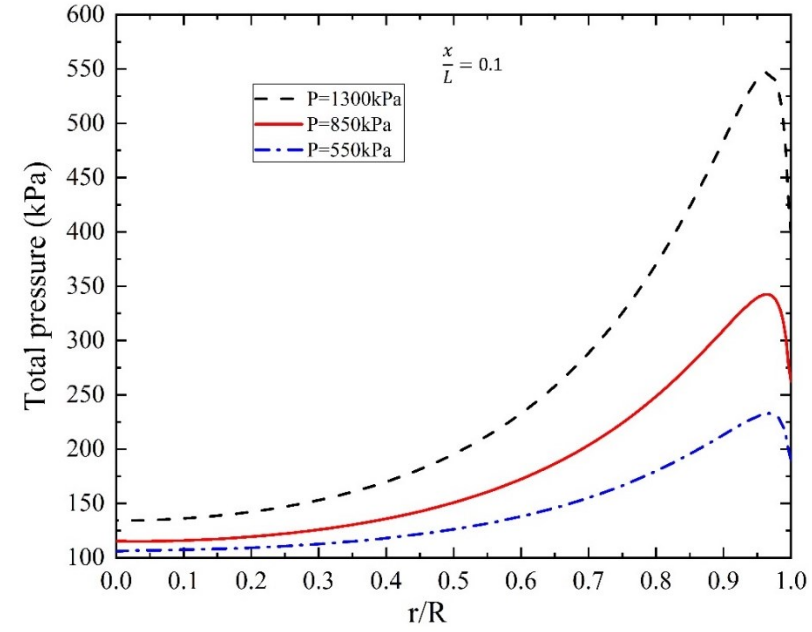
$\frac{x}{L} = 0.1$
P=1300kPa
P=850kPa
P=550kPa
Total pressure (kPa)
r/R

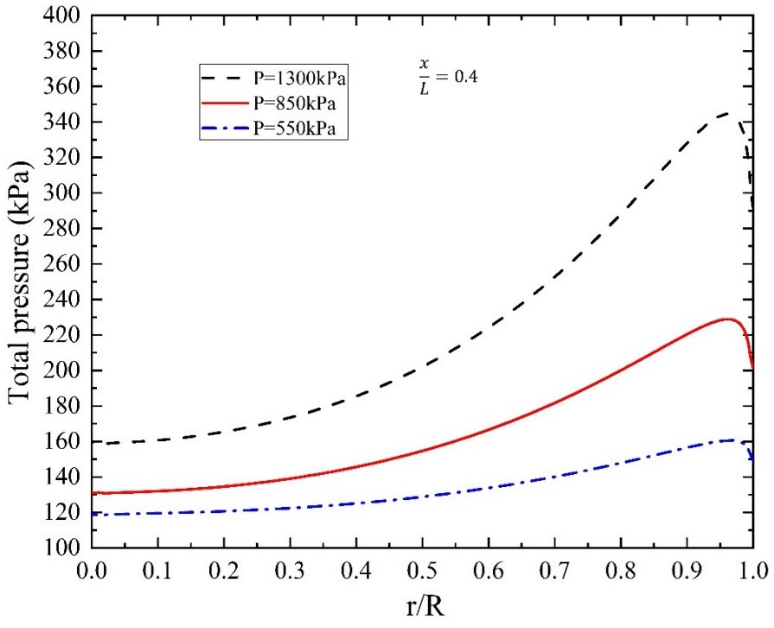
$\frac{x}{L} = 0.4$
P=1300kPa
P=850kPa
P=550kPa
Total pressure (kPa)
r/R

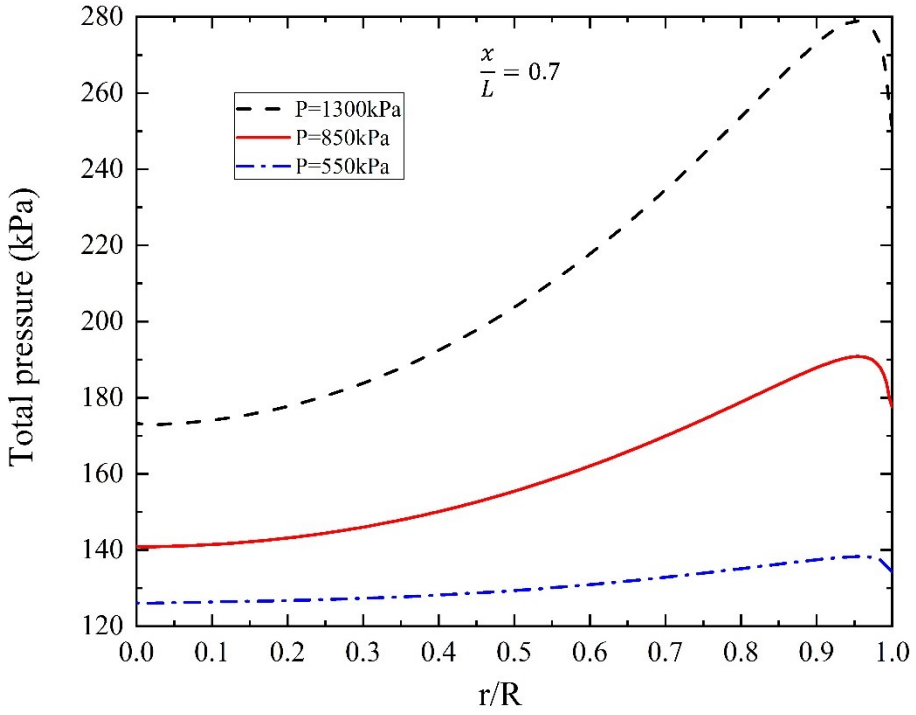

Figure 3-12. Radial profile of total pressure for inlet pressure 550, 850 and 1300kPa and dimensionless axial locations (x/ L) 0.1, 0.4 and 0.7.

Figure 3-13 shows the profile of the turbulence kinetic energy as a function of dimensionless radial position (r/R), for three dimensionless axial locations (x/L), and three inlet pressures at α=0.5. As it is shown, as the flow goes to the hot exit of the vortex tube, its turbulence kinetic energy decreases and when the inlet pressure increases, turbulence kinetic energy increases due to increasing the velocity.

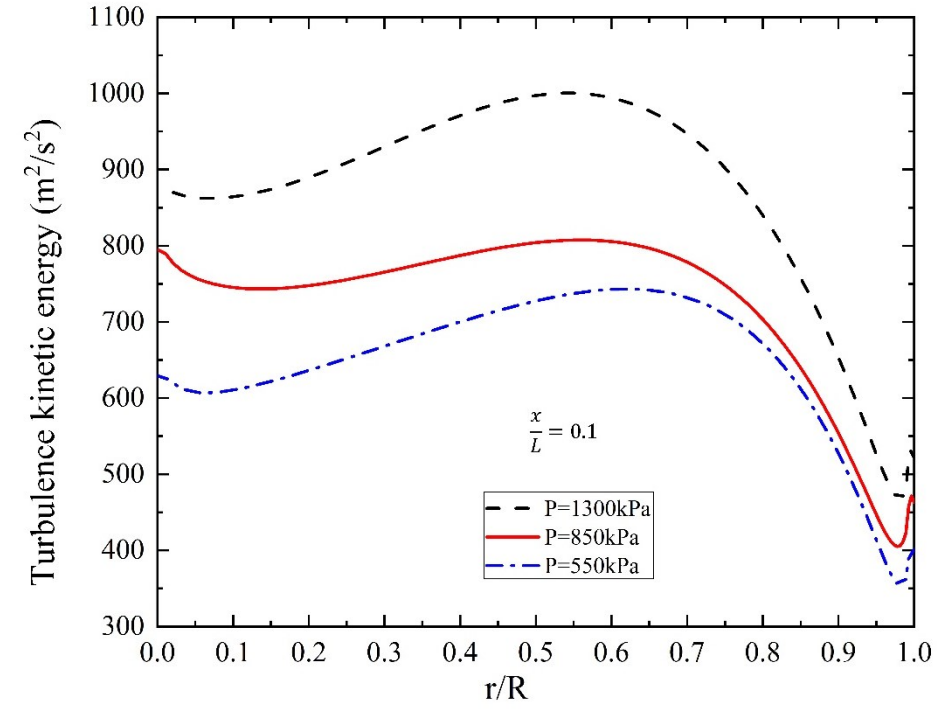
Turbulence kinetic energy (m²/s²)
r/R
x/L = 0.1
P=1300kPa
P=850kPa
P=550kPa

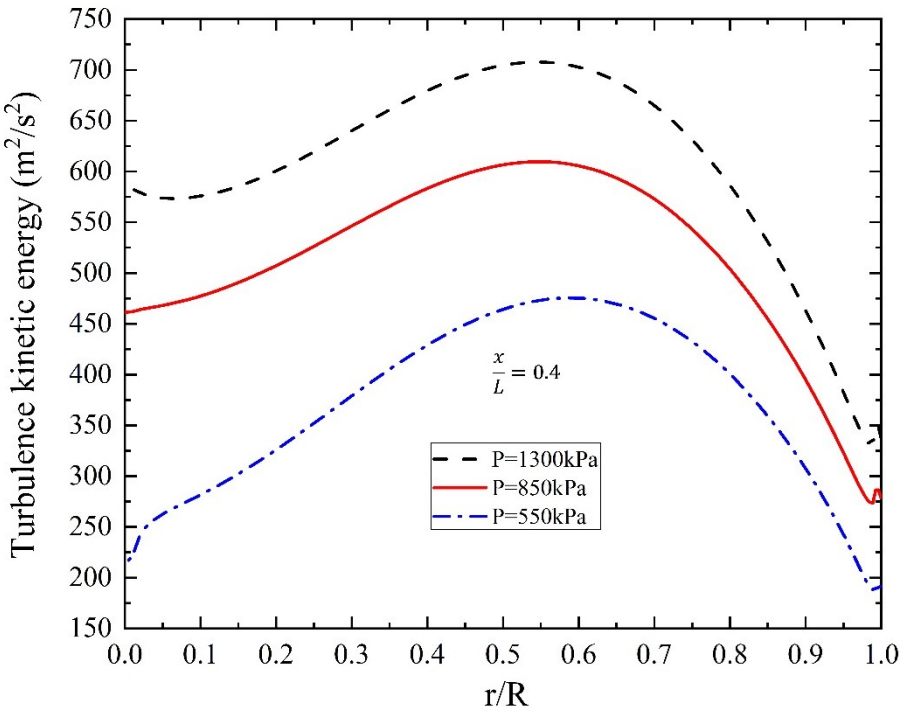
Turbulence kinetic energy (m²/s²)
r/R
x/L = 0.4
P=1300kPa
P=850kPa
P=550kPa

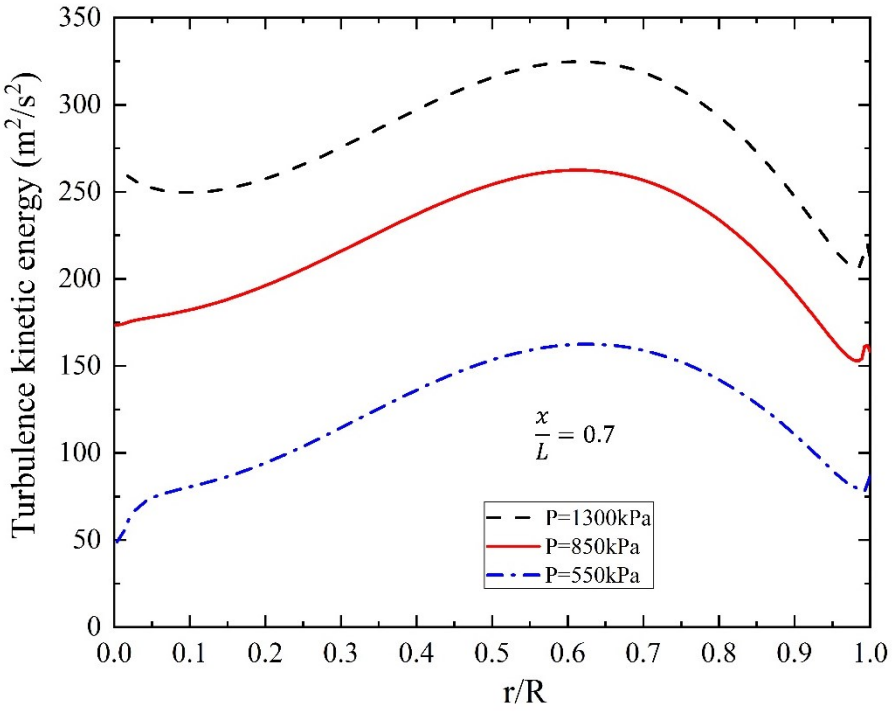

Figure 3-13. Radial profile of turbulence kinetic energy for inlet pressure 550, 850 and 1300kPa and dimensionless axial locations (x/ L) 0.1, 0.4 and 0.7.

The temperature difference just gives some nominal information about the vortex tube, and this is important to analyze the performance of the vortex tube as well, which has not been considered in many research papers. Figure 3-14 depicts the effect of the inlet pressure (P_{in}) and cold mass fraction (ε) on the cooling and heating powers. Cooling and heating powers are not only related to the temperature difference at the cold and hot exits, but also depend on mass fraction and heat capacity. The maximum cooling and heating powers at P=1300 kPa are 70.5 W and 82.5 W, occurring at $\varepsilon = 0.55$ and $\varepsilon = 0.6$ respectivly; the maximum cooling and heating powers at P=850 kPa are 32.25 W and 42.45 W, both at $\varepsilon = 0.57$; the maximum cooling and heating powers are 14.7 W and 24.2 W at P=550 kPa, occurring at $\varepsilon = 0.62$ and $\varepsilon = 0.57$ respectively.

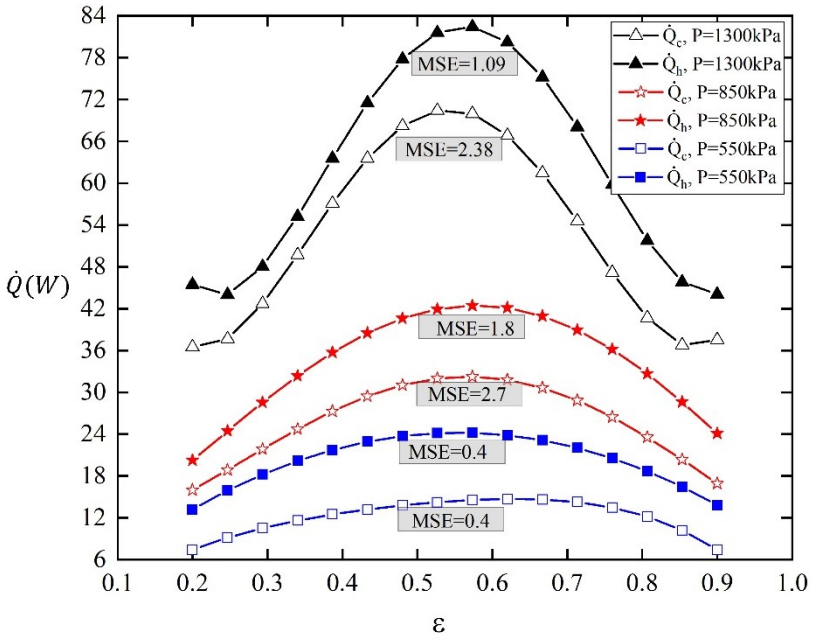

Figure 3-14. Effect of inlet pressure and cold mass fraction on cooling and heating powers.

Figure 3-15 illustrates the effect of inlet pressure (P_{in}) and the cold mass fraction (ε) on COP_c and COP_h. COP depends on heat and cold rate powers and inlet power (Eqs. (3-17 and (3-18) which inlet power for each inlet pressure is constant hence the only effective parameter on COP is power rate so COP_c and COP_h display similar trend with the cold mass fraction that heating and cooling power rates showed. Hence for the inlet pressure of 1300 kPa, maximum values of heat and cold rate powers occur at $\varepsilon = 0.6$ and $\varepsilon = 0.55$, respectively that leads to maximum COP_c and COP_h. However, for the inlet pressure of 850kPa, the maximum value of heat and cold rate powers occur at $\varepsilon = 0.57$ which leads to the maximum value of COP. Moreover, for inlet pressure of 550 kPa the maximum value of heat and cold power rate occur at different cold mass fraction because two parameters which are temperature gradient and mass fraction affect on heat and cold rate so maximum COP_c and COP_h occur at $\varepsilon = 0.65$ and $\varepsilon = 0.59$, respectively. Maximum values for COP_c are 0.095, 0.107 and 0.12 and COP_h are 0.15, 0.138 and 0.142 for inlet pressure 550 kPa, 850 kPa and 1300 kPa, respectively. As it is shown in Figure 3-15, the vortex tube performance is higher when it acts as a heat pump.

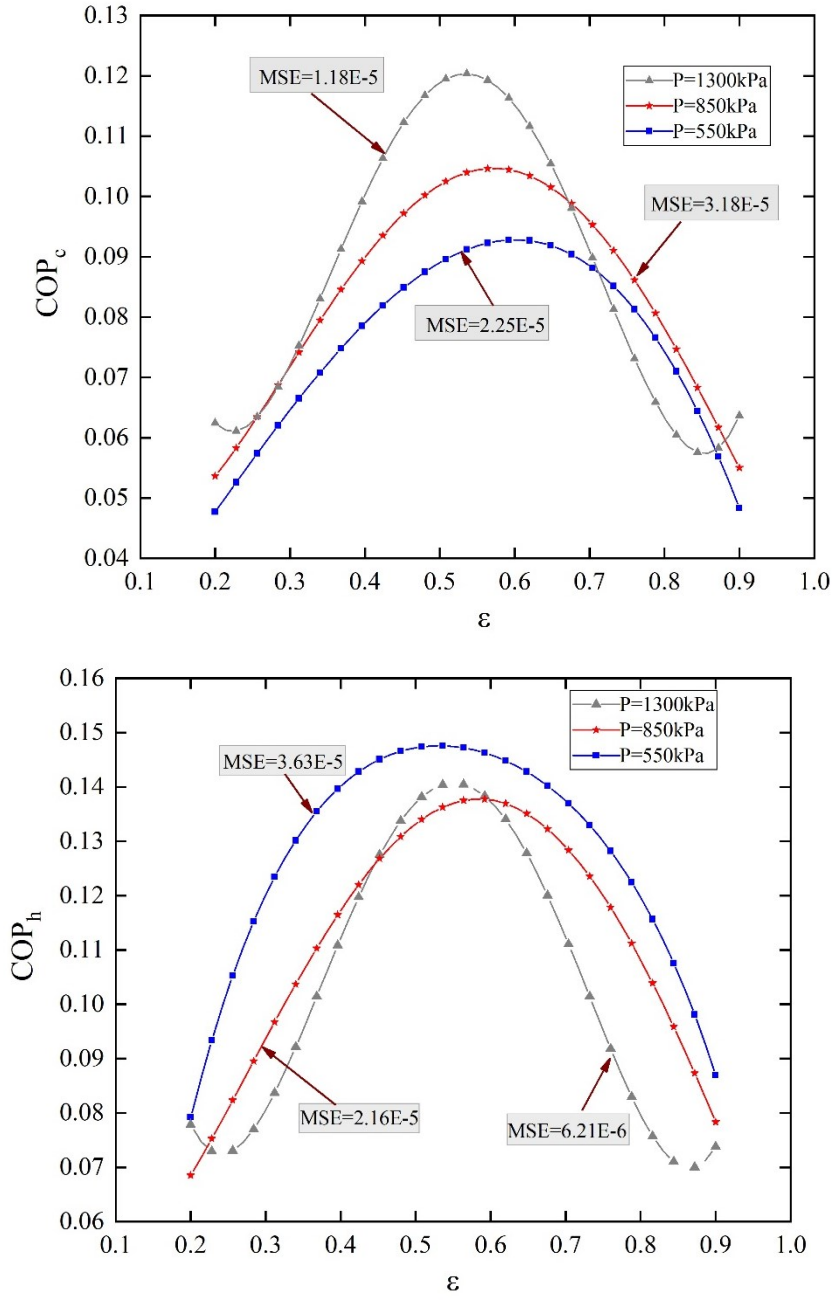

Figure 3-15. The effect of inlet pressure and cold mass fraction on a: COPc, b: COPh.

Figure 3-16 illustrates the effect of inlet pressure (P_{in}) and the cold mass fraction (ε) on exergy efficiency based on Grassmann and transiting definitions for three reference temperatures (280 K, 285 K and 290 K). The exergy depends on the cold mass fraction, temperature difference and reference temperature hence for the exergy efficiency variation

these three parameters should be considered. As it was mentioned, at P_{in}=1300 kPa and P_{in}=850 kPa, both heating and cooling power rates occur at $0.55 \leq \varepsilon \leq 0.6$ so the maximum exergy efficiency occurs at $0.55 \leq \varepsilon \leq 0.6$. Therefore, the maximum value of exergy efficiency at P_{in}=1300 kPa occur at $\varepsilon = 0.59$ and $\varepsilon = 0.57$ and at P_{in}=850 kPa occur at $\varepsilon = 0.57$ and $\varepsilon = 0.6$ based on Grassmann and transiting exergy efficiencies, respectively. Moreover, at P_{in}=550 kPa, the maximum of Grassmann and transiting exergy efficiencies occur at $\varepsilon = 0.65$ and $\varepsilon = 0.8$. As it is shown in Figure 3-16, with rising the inlet pressure, the maximum of transiting exergy efficiency occurs at the lower cold mass fraction. The value of Grassmann exergy efficiency is ten times bigger than the transiting exergy efficiency which means 90% of inlet exergy has not undergone transformation within an analyzed process. The exergy efficiency variation with reference temperature for both definitions is close to each other.

Two important observations follow from analysis of the graphs presented on Figures 3-14 and 3-15. The first one is that with the rise of inlet pressure the maximum values (function of ε) of the three performance metrics (COP_c; Grassmann and transiting exergy efficiencies) increase. This is not the case of COP_h, which decreases. This phenomenon is explained by the fact that the exergy of the cold flow surpasses the exergy of the hot flow in the numerators of equations (3-25) and (3-26). At the same time, contrary to COP_c, exergy efficiencies evaluate the energy and its quality of the hot flow. The second observation is that the variation in optimal ε with the inlet pressure, while maximizing the Grassmann exergy efficiency, in relatively small (6%). Meanwhile, the variation in optimal ε with the inlet pressure, while maximizing transiting exergy efficiency, is 29%. This can be explained by the different nature of the exergy terms presented in the numerators of equations (3-25) and (3-26). Indeed, the exergies of cold and hot flows are presented in the numerator of (3-25), however the numerator of equation (3-26) is the exergy rise due to the temperature decrease for the cold flow and temperature increase for the hot flow. As a result, the transiting exergy efficiency is a more sensitive performance metric compared to Grassmann exergy efficiency and it is thus recommended as an objective function for thermodynamic optimization of Vortex tubes.

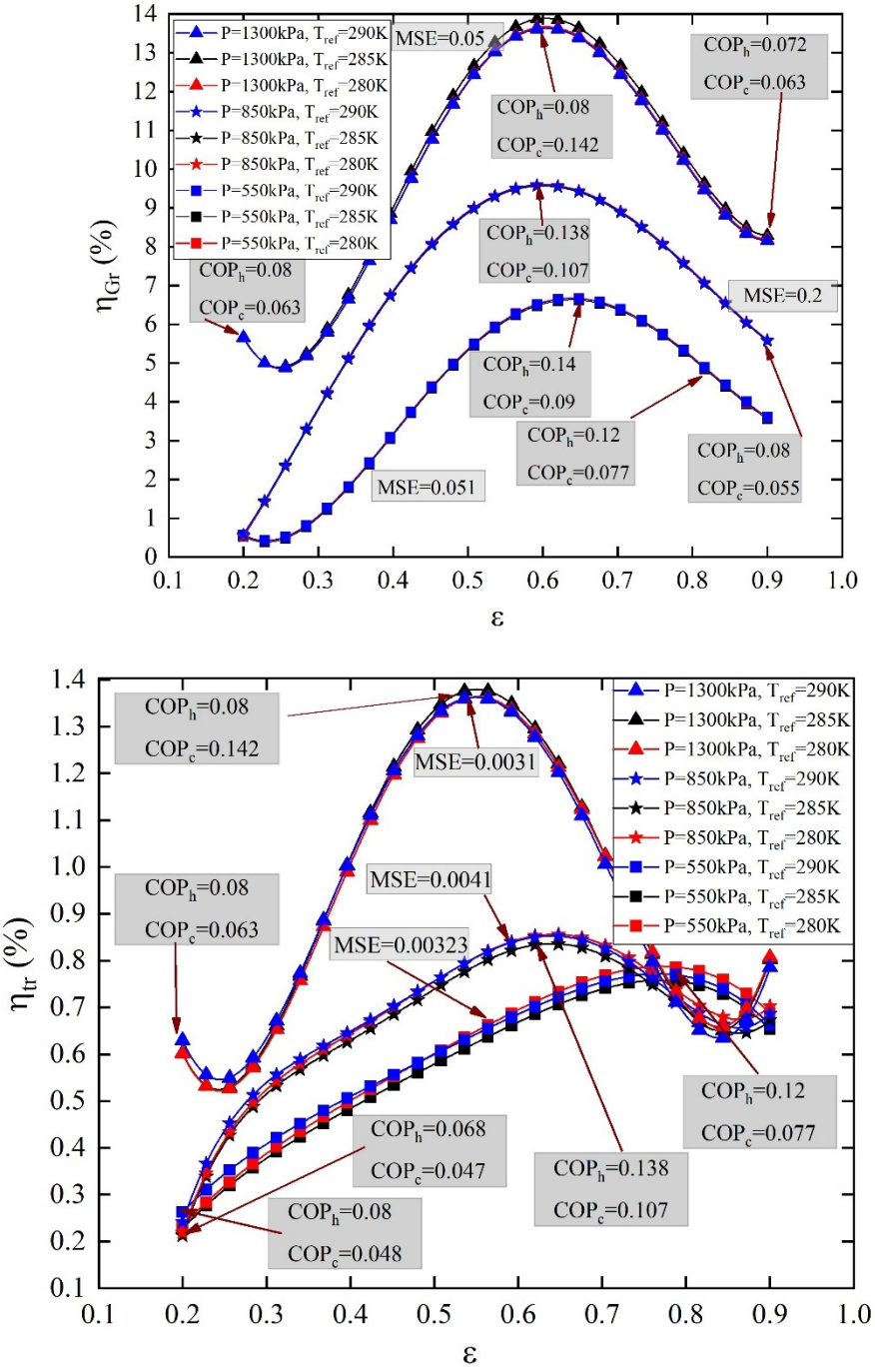

Figure 3-16. Effect of inlet pressure and cold mass fraction on exergy efficiency.

3-6 Conclusions

In the present study, CFD analysis was conducted to illustrate the energy separation in the vortex tube with CO_2 as a real gas at the different inlet pressure and cold mass fraction. Energy separation was discussed in terms of the hot exit and cold exit temperature differences, both with respect to the VT inlet temperature. Performance is characterized by cooling power, heating power, and both energy and exergy metrics. With increasing inlet pressure, the cold exit temperature decreases while the hot exit temperature increases. Increasing the inlet pressure leads to increasing the magnitude of the velocity and increasing the vortex tube performance. The value of swirl velocity is five times greater than the axial velocity. The COP of the vortex tube was investigated when it is understood to acts as a heat pump and refrigeration. Even though, increasing the pressure causes the rising the cooling and heating power, and goes through the maximum. The maximum value for exergy efficiency depends on both heating and cooling power rates directly ($\eta_{exe} \propto (\dot{Q}_c + \dot{Q}_h)$) hence maximum value of either heating or cooling power rate at specific cold mass fraction is not concluded that maximum efficiency occurs at the same cold mass fraction. The maximum value of Grassmann exergy efficiency is ten times bigger than transiting exergy efficiency. The transiting exergy efficiency is recommended as an objective function for thermodynamic optimization of Vortex tubes.

3-7 Acknowledgments

This project is a part of the Collaborative Research and Development (CRD) Grants Program at “Université de Sherbrooke”. The authors acknowledge the support of the Natural Sciences and Engineering Research Council of Canada, Hydro-Québec, Rio Tinto, Alcan and Canmet ENERGY Research Center of Natural Resources Canada (RDCPJ451917-13).

3-8 Nomenclature

c_p	heat capacity at constant pressure, kJ kg^{-1} K^{-1}
D	diameter, mm
e	specific exergy, kJ kg^{-1} K^{-1}
$\dot{E}$	total energy, W
h	specific enthalpy, kJ kg^{-1}
H	enthalpy, W
k	turbulence kinetic energy, m^2 s^{-2}
L	length, m
MSE	mean square error
$\dot{m}$	mass flow rate, kg s^{-1}
P	pressure, kPa
Pr	prandtl number
$\dot{Q}$	thermal power, W
R	gas constant, J mol^{-1} K^{-1}
$\dot{S}$	entropy rate, W K^{-1}
s	specific entropy, kJ kg^{-1} K^{-1}
T	Time, s
$\dot{W}$	power, W
x_i	coordinates

Subscripts

c	cold
exe	exergy
Gr	grassmann
h	hot
in	inlet
irr	irreversibility
out	outlet
tr	transitive

Greek letters

ν	specific volume, $m^3\ kg^{-1}$
η	efficiency
ε	cold mass fraction
ρ	density, $kg\ m^{-3}$
μ	dynamic viscosity, $kg\ m^{-1}\ s^{-1}$

Chapter 4

3D CFD modelling and exergy loss minimization within a high-pressure vortex tube

Avant-propos

Auteurs et affiliation :

Abbas Aghagoli: étudiant au doctorat, faculté de génie, département de génie mécanique, Université de Sherbrooke.

Mikhail Sorin: professeur, faculté de génie, département de génie mécanique, Université de Sherbrooke.

Date d'acception: -

État de l'acceptation: à l'étude

Revue: International Journal of Refrigeration

Titre français: Modélisation CFD 3D et minimisation des pertes d'exergie dans un tube vortex haute pression

Contribution au document: Cet article contribue à la thèse par une application de tube vortex haute pression

Résumé français:

Le tube vortex est un appareil simple sans pièces mobiles qui peut fournir à la fois chauffage et refroidissement. Jusqu'à présent, toutes les études sur le tube vortex ont été réalisées à basse pression de fonctionnement. Dans la présente étude, le comportement du tube vortex à haute pression de fonctionnement est étudié. Pour ce faire, un modèle CFD 3D a été développé. Le gaz de travail est le CO_2, qui est considéré comme un gaz réel. En raison du

comportement non linéaire du CO_2 dans la région supercritique, un tableau des propriétés des gaz réels est couplé au solveur ANSYS CFX pour surmonter l'instabilité de la simulation dans la région supercritique. Les nœuds hexaèdres structurés sont générés par l'ICEM et le modèle de turbulence k-ε est appliqué pour simuler les caractéristiques d'écoulement moyen dans des conditions d'écoulement turbulent. En outre, l'approche d'équilibre homogène (HEM) est appliquée au modèle CFD. Grâce à l'application de ce modèle, l'impact de la modification de la pression d'entrée et de la fraction de masse froide est étudié en termes de pertes d'exergie dans le tube vortex. Les résultats montrent que les pertes d'exergie minimales se produisent à une fraction de masse froide égale à 0,5, tandis que l'efficacité exergétique atteint son maximum à une fraction de masse froide égale à 0,9. Cette différence s'explique par le fait que la capacité de refroidissement du tube se produit à une fraction massique de 0,9. De plus, il a été illustré que le frottement a un impact majeur sur la vitesse de génération d'entropie à proximité de la paroi et au centre du tube vortex.

4-1 Abstract

The vortex tube is a simple device with no moving parts that can provide both heating and cooling. So far, all of the studies on the vortex tube have been carried out at low operating pressure. In the present study, the behavior of the vortex tube at high operating pressure is investigated. To do so, a 3D CFD model has been developed. The working gas is CO_2, which is considered as a real gas. Due to the nonlinear behavior of CO_2 in the supercritical region, a real gas properties table is coupled with the ANSYS CFX solver to overcome the simulation instability in the supercritical region. Structured hexahedron nodes are generated by ICEM, and the $k-\varepsilon$ turbulence model is applied to simulate the mean flow characteristics for turbulent flow conditions. Further, the homogeneous equilibrium (HEM) approach is applied to the CFD model. Through application of this model, the impact of changing the inlet pressure and the cold mass fraction is investigated in terms of the exergy losses within the vortex tube. The results show that the minimum exergy losses occurs at cold mass fraction equals 0.5, meanwhile the exergy efficiency achieves its maximum at cold mass fraction equals 0.9. This difference is explained by the fact that the cooling capacity of the tube occurs at mass

fraction 0.9. Moreover, it has been illustrated that friction has a major impact on entropy generation rate near the wall and at the center of the vortex tube.

Keywords: Entropy generation rate, Vortex tube, Exergy loss, CFD

4-2 Introduction

A vortex tube is a simple device with no moving parts [13], which simultaneously produces both hot and cold streams from a highly compressed inlet gas. The high-pressure gas enters through tangential nozzles and produces a highly swirling flow inside the vortex tube and this flow ultimately separates into two different outlet streams. The inlet stream swirls peripherally, moves toward the hot outlet of the vortex tube, which is located far from the nozzles has a temperature higher than the inlet flow. A portion of the inlet stream swirls at the center of the tube and moves backward and is exhausted at the center of the tube, having a lower temperature than the inlet gas. The vortex tube was invented by Ranque (1933) but due to insufficient performance, it was abandoned for two decades. Even though much research has been carried out experimentally and numerically since the last 50s [49] to explain the complicated flow field inside the vortex tube, no agreement has been achieved on understanding the energy separation phenomenon. Adiabatic expansion and compression were proposed by Ranque [50] as the main reason for the energy separation inside the vortex tube, however there was no agreement that expansion corresponds to the temperature drop [51]. Ahlborn and Groves [31] observed that the mass flow rate that moves back toward the cold outlet is higher than the mass which leaves at the cold outlet and they proposed a secondary circulation. Later, Ahlborn et al. [32] proposed that the secondary circulation acts as a heat pump that transfers energy from the inner layer (near the core) to the outer layer (near the wall). However, the existence of the secondary circulation has not been acknowledged by all researchers. Hamdan et al. [34] investigated the effect of inlet pressure on the energy separation of the vortex tube. Their result showed that the inlet pressure has a major effect on the temperature difference of the vortex tube due to increasing the tangential velocity, which was confirmed by others [17,52,53]. In spite of the fact that the energy analysis of the vortex tube has gained more attention, exergy analysis could yet be a useful tool to improve vortex tube efficiency and find the sources of the energy losses.

Aghagoli and Sorin [54] proposed a new exergy efficiency definition called transiting exergy efficiency. Their findings showed that more than 90% of the inlet exergy is not transformed in the vortex tube process. The effect of the cold outlet pressure on the vortex tube exergetic efficiency was carried out in by Lagrandeur et al. [17], indicating that the maximum exergetic efficiency rises from 4.4% to 5.6% when the cold outlet pressure goes from 1 to 3 bars. Ouadha et al. [55] analyzed the exergy loss of the vortex tube with respect to the cold mass fraction and pressure and their results indicated that at lower inlet pressure, the effect of cold mass fraction is less on the total exergy loss. Kaya et al. [56] analyzed the influence of the inlet pressure on the vortex tube exergy loss, with CO_2 as a working fluid. Their results showed that increasing the inlet pressure leads to increasing the specific exergy loss and the same results are reported by Kirmaci [57]. Alternatively, entropy generation has attracted attention in the many industrial sectors, such as for heat exchangers [58] and ejectors [59]. There have been few papers regarding the analyzing the entropy generation rate on the vortex tube [60]. Entropy generation analysis was developed by Bejan [61], which is an effective method that demonstrates how energy is dissipated and thus can also help minimize exergy loss.

Thus far, air has been chosen predominantly as the working gas in experimental and numerical studies [62–65], while a minority of papers have focused on other types of the working fluids [37,54,66]. Wang and Suen [62] compared the effect of three different working gases (air, R134a, and R600) on the temperature difference of the vortex tube. The results showed that at constant inlet pressure, air has the highest temperature difference due to higher inlet velocity. Syed and Renganathan [67] carried out a CFD simulation on vortex tube for air and hydrogen and their result showed that the temperature separation is higher when air is chosen as a working fluid due to higher viscosity and lower specific heat. Liang et al. [52] applied the CFD modeling for the vortex tube at low and high operating pressure (0.9 and 9 MPa) with methane as a working fluid. Their results showed that at high pressure operating condition, the cold mass fraction has a no effect on the cold outlet temperature difference and hot outlet temperature difference is negative.

Aghagoli and Sorin [54] completed a CFD simulation of the vortex tube using the NIST real gas model where CO_2 thermodynamic properties were obtained using Refprop software

[68]. Most CFD studies have been carried out with air modeled as an ideal gas, which means that the CFD software applies the perfect gas equation of state and specific heat at constant pressure (c_p) is considered constant. However, thermodynamic properties of CO_2 vary with pressure and temperature, especially near the critical point (T = 304.12 K and P = 7.37 MPa), so choosing the correct equation of state (EoS) improves CFD simulation accuracy. A cubic EoS is preferred due to low computational cost, such as that of Soave−Redlich−Kwong (SRK) [69] or Peng−Robinson (PR) [70], but it cannot accurately represent density in the liquid phase. Fang et al. [71] implemented a tabulated EoS in their simulation and the result showed that the tabulated EoS is 66 times faster than the original Span-Wagner EoS. In order to overcome the instability of CO_2 in the supercritical region, Ameli et al. [72] implemented a CO_2 real gas properties (RGP) table.

In the present study, a three-dimensional CFD simulation of the vortex tube with CO_2 as the compressible working fluid is investigated where the CO_2 real gas properties table is implemented in ANSYS CFX solver. The CFD results of the vortex tube are used to evaluate exergy losses. The transiting exergy and transiting exergy efficiency is investigated as a function of the pressure and cold mass fraction. Besides, the local entropy generation rate is investigated on the vortex tube.

4-3 Mathematical modelling

4-3-1 Governing equations of CFD modelling

In this study, a 3D model of the vortex tube is developed, considering the flow as steady state. The flow pattern inside the vortex tube is highly turbulence, so choosing the proper turbulence model is important. Therefore, the standard k − ε turbulence model [65] is used to simulate the flow behavior in the vortex tube.

The mass, momentum, and energy equations for single-phase compressible flow in the vortex tube are:

$$\frac{\partial}{\partial x_j}\left(\rho u_j\right) = 0 \tag{4-1}$$

$$\frac{\partial}{\partial x_j}(\rho u_i u_j) = -\frac{\partial p}{\partial x_i} + \frac{\partial}{\partial x_j}\left[\mu\left(\frac{\partial u_i}{\partial x_j} + \frac{\partial u_j}{\partial x_i} - \frac{2}{3}\delta_{ij}\frac{\partial u_k}{\partial x_k}\right)\right] + \frac{\partial}{\partial x_j}\left(-\rho\overline{\acute{u}_i}\overline{\acute{u}_j}\right) \quad (4\text{-}2)$$

$$\frac{\partial}{\partial x_j}\left[\rho u_i\left(h + \frac{1}{2}u_i u_j\right)\right] = \frac{\partial}{\partial x_j}\left[\left(\tau_{ij}\right)_{eff} u_i + k_{eff}\frac{\partial T}{\partial x_j}\right] \quad k_{eff} = \frac{C_p \mu_t}{Pr_t} + K \quad (4\text{-}3)$$

The homogeneous equilibrium model (HEM) system considers the thermodynamic and mechanical equilibrium between liquid and gas phases. Hence, the velocity, pressure, and temperature are the same for both phases [73].

$$P_l = P_v = P_{sat}$$
$$T_l = T_v = T_{sat} \quad (4\text{-}4)$$
$$u_l = u_v = u$$

As a consequence, the fluid properties are a function of pressure and enthalpy:

$$\{\rho, \mu, c_p\} = f(P, h) \quad (4\text{-}5)$$

In the current study, the HEM is employed to a numerical model of CO_2 expansion in the vortex tube, due to its simplicity [74]. Lucas et al. [75] compared the experimental data with the HEM approach and their results showed that the difference was negligible.

4-3-2 Boundary conditions

The 3D geometry of the vortex tube is based on the experimental study of Han et al. [37] , which is shown in Figure 4-1. The vortex tube dimensions are given in Table 4-1. In the experimental study, CO2 passed through 6 nozzles with a hot length of 78 mm, tube diameter of 9.5 mm and cold diameter of 3.5 mm which are inner dimensions. Due to the symmetry of the geometry of the vortex tube, a 60˚ sector of the vortex tube is considered for the CFD simulation for the sake of reducing the computational time. The vortex tube is designed in ANSYS design modeler; the hexahedral grid is generated by ANSYS ICEM software and the commercial ANSYS CFX solver carries out the CFD simulation. The pressure outlet is assumed for the boundary condition of the cold and hot outlets and for the inlet of the nozzle, the pressure inlet is considered. The symmetry parts of the vortex tube were considered as a periodic boundary condition. The coupled algorithm is employed which solves the momentum and

pressure-based continuity equations together. The high resolution scheme is used to calculate the advection terms in the discrete finite volume equations. An adiabatic boundary condition is assumed for the walls. The convergence criteria for the mass, momentum, and energy are 10^{-6}, $10^{-6,}$ and 10^{-7}, respectively. The cold outlet pressure is fixed at 4 MPa and the inlet pressures are considered as 9, 10 and 11 MPa. In addition, the inlet temperature is constant at 35 ℃.

Table 4-1. Vortex tube dimensions.

Tube length	78 mm
Tube diameter	9.5 mm
Cold orifice diameter	3.5 mm

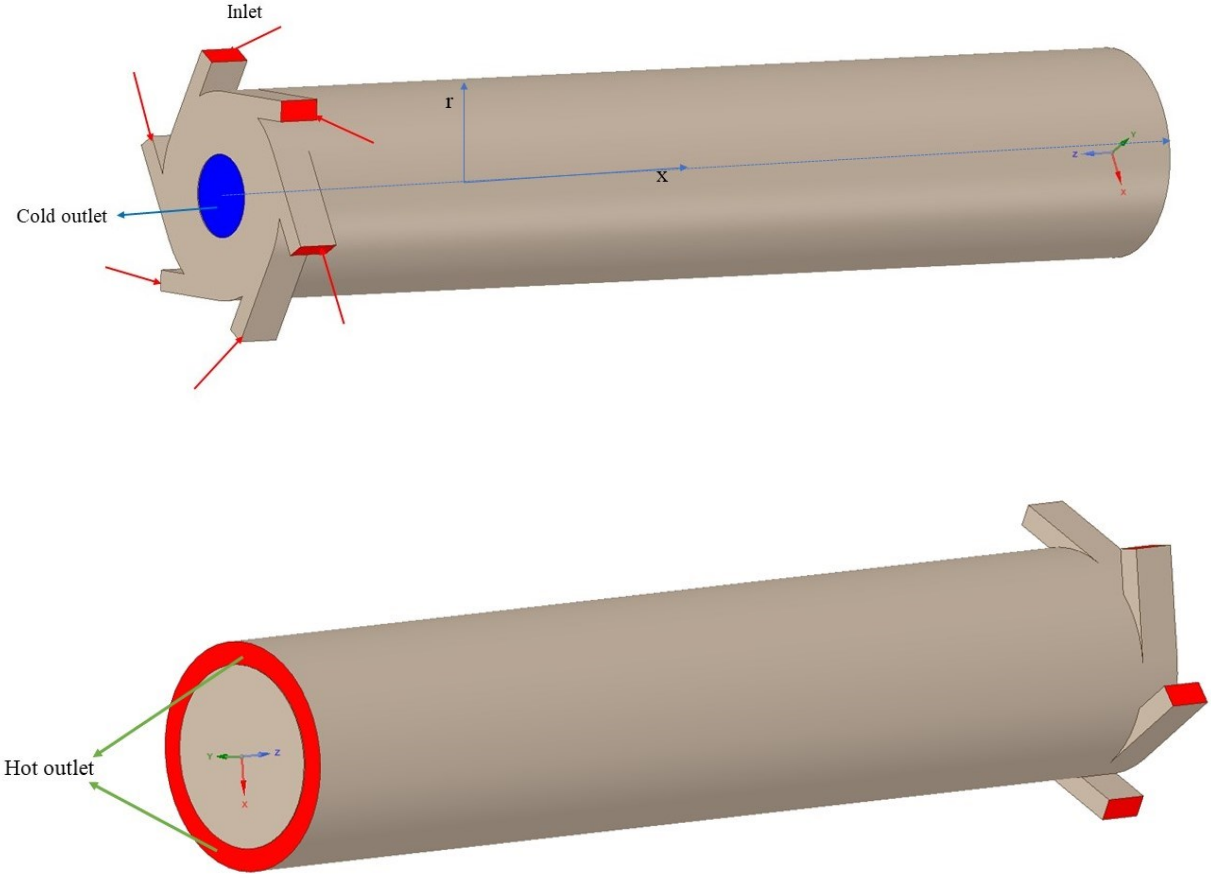

Figure 4-1. Vortex tube geometry.

4-3-3 Fluid Property Table

The accuracy of the results of the CFD simulation strongly depend on the EoS [71]. The nonlinear behavior of CO_2 is an issue that causes a major problem for the CFD simulation of CO_2. Figure 4-2 shows the isobaric specific heat (C_p) of CO_2 as a function of pressure and temperature. As illustrated in Figure 4-2, the C_P varies from 1 $kJ \cdot kg^{-1} \cdot K^{-1}$ to 140 $kJ \cdot kg^{-1} \cdot K^{-1}$.

In the present study, a very high resolution real gas properties (RGP) table is implemented into the commercial ANSYS CFX software. In the RGP table, there are nine parameters of CO_2 for both liquid and gas phases. These nine parameters are specific enthalpy, speed of sound, specific volume, specific heat at constant volume, specific heat at constant pressure, the partial derivative of pressure with respect to the specific volume at a constant temperature, specific entropy, dynamic viscosity, and thermal conductivity [76]. For the detailed regarding to the tabulated region of the CO_2 RGP table refer to Ref. [76].

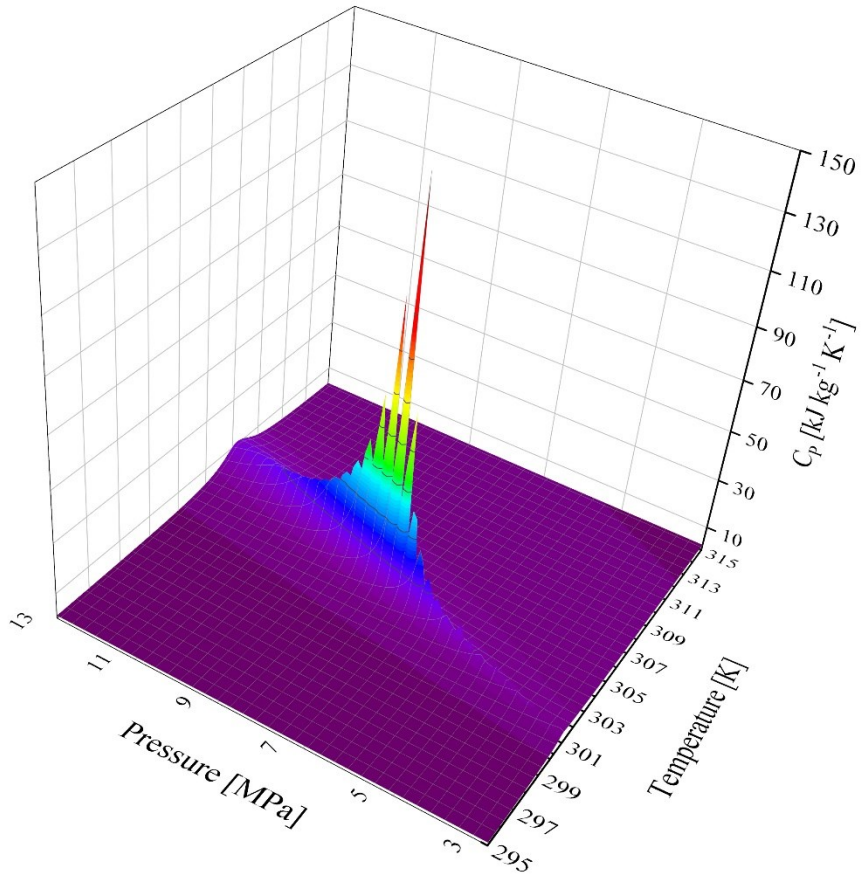

Figure 4-2. The isobaric specific heat of CO_2 as a function of pressure and temperature.

4-3-4 Mesh independency and validation

The validation of the vortex tube CFD simulation with CO_2 as a working gas was carried out on the previous study [54] and is given in Table 4-2. The structural grid of the vortex tube, shown in Figure 4-3, is generated by ICEM and is chosen over a non-structural grid, due to the former's higher precision and more accurate results [77].

Table 4-2. CFD validation against the experimental results.

Inlet pressure [MPa]	ΔT_{Exp} [K]	ΔT_{CFD} [K]	Error [%]
0.56	25.38	24.2	4.6
0.84	38.7	38.9	0.5
0.98	43.52	43.83	0.7
1.32	51.6	52.87	2.4

The mesh independency must be checked in order to find the optimum number of cells to decrease the computational time yet provide sufficient accuracy. Therefore, five numbers of cells were checked. Figure 4-4 depicts the pressure along the vortex tube length to detect the influence of the cell number on the pressure. The mesh with 1×10^6 hexahedral cells was chosen for the simulation.

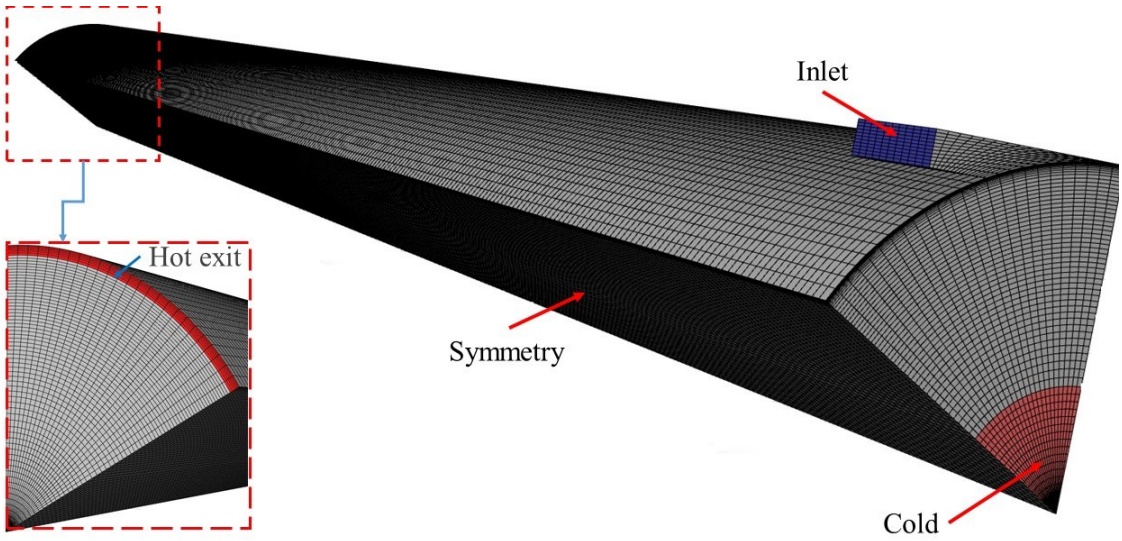

Figure 4-3. Structural mesh of the vortex tube.

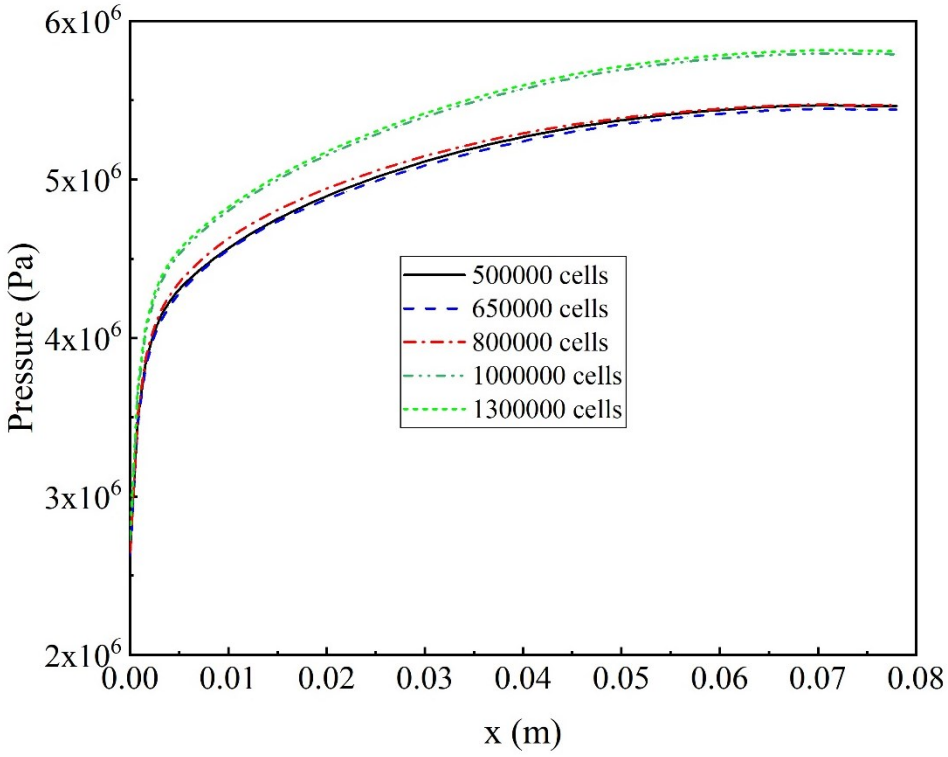

Figure 4-4. Variation of the pressure along the vortex tube for different numbers of cells.

4-4 Exergy analysis

Exergy analysis of the vortex tube is important in order to understand the reasons of the irreversibility and to help find the causes and locations of thermodynamic losses.

In the experimental procedure, opening or closing the hot outlet valve, the cold mass fraction decreases or increases. In the numerical simulation, however, by changing the hot outlet pressure, the cold mass fraction varies. The cold mass fraction of the vortex tube, which varies between 0 and 1, is the ratio between the mass flow at the cold outlet and mass flow at the inlet which is given as:

$$\alpha = \frac{\dot{m}_c}{\dot{m}_{in}} \tag{4-6}$$

4-4-1 Exergy loss and transiting exergy efficiency

The specific exergy of the vortex tube at the inlet, cold and hot outlets can be calculated as [45]:

$$e_{in} = ([h(P_{in}, T_{in}) - h(P_0, T_0)] - T_0 \cdot [s(P_{in}, T_{in}) - s(P_0, T_0)]) + \frac{V_{in}^2}{2} \quad (4\text{-}7)$$

$$e_h = (1-\alpha)([h(P_h, T_h) - h(P_0, T_0)] - T_0 \cdot [s(P_h, T_h) - s(P_0, T_0)]) + \frac{(1-\alpha)V_h^2}{2} \quad (4\text{-}8)$$

$$e_c = \alpha([h(P_c, T_c) - h(P_0, T_0)] - T_0 \cdot [s(P_c, T_c) - s(P_0, T_0)]) + \frac{\alpha V_c^2}{2} \quad (4\text{-}9)$$

The specific exergy loss is given as:

$$I = e_{in} - (e_h + e_c) \quad (4\text{-}10)$$

The transiting exergy efficiency is given as [48]:

$$\eta_{tr} = \frac{\dot{E}_{out} - \dot{E}_{tr}}{\dot{E}_{in} - \dot{E}_{tr}} = \frac{\Delta\dot{E}}{\nabla\dot{E}} \quad (4\text{-}11)$$

where $\Delta\dot{E}$ and $\nabla\dot{E}$ are the exergy produced and exergy consumed in the process. $\dot{E}_{tr}$ is the exergy that has not undergone transformation within an analysed process. $\Delta\dot{E}$, $\nabla\dot{E}$ and $\dot{E}_{tr}$ for the cold and hot streams are calculated as [48]:

$$\Delta\dot{E}_c = \dot{m}_{in} \cdot \alpha \cdot [e(P_c, T_c) - e(P_c, T_0)] \quad (4\text{-}12)$$

$$\nabla\dot{E}_c = \dot{m}_{in} \cdot \alpha \cdot [e(P_{in}, T_{in}) - e(P_c, T_0)] \quad (4\text{-}13)$$

$$\dot{E}_{trc} = \dot{m}_{in} \cdot \alpha \cdot e(P_c, T_0) \quad (4\text{-}14)$$

$\Delta\dot{E}_c$, $\nabla\dot{E}_c$ and $\dot{E}_{trc}$ are the exergy produced, consumed and transiting exergy within the cold stream, respectively.

$$\Delta\dot{E}_h = \dot{m}_{in} \cdot (1-\alpha) \cdot [e(P_h, T_h) - e(P_h, T_0)] \quad (4\text{-}15)$$

$$\nabla\dot{E}_h = \dot{m}_{in} \cdot (1-\alpha) \cdot [e(P_{in}, T_{in}) - e(P_h, T_0)] \quad (4\text{-}16)$$

$$\dot{E}_{trh} = \dot{m}_{in} \cdot (1-\alpha) \cdot e(P_h, T_0) \quad (4\text{-}17)$$

$\Delta\dot{E}_h$, $\nabla\dot{E}_h$ and $\dot{E}_{trh}$ are the exergy produced, consumed and transiting exergy within the hot stream, respectively.

Where $\Delta\dot{E} = \Delta\dot{E}_h + \Delta\dot{E}_c$ and $\nabla\dot{E} = \nabla\dot{E}_h + \nabla\dot{E}_c$.

It can be noticed that the exergy losses can be calculated by subtracting the numerator from the denominator in equation (4-11). The equation (4-11) can be rewritten based on the cold mass fraction, pressure and temperature.

$$\eta_{tr} = \frac{\alpha \cdot [e(P_c,\, T_c) - e(P_c,\, T_0)] + (1-\alpha) \cdot [e(P_h,\, T_h) - e(P_h,\, T_0)]}{\alpha \cdot [e(P_{in},\, T_{in}) - e(P_c,\, T_0)] + (1-\alpha) \cdot [e(P_{in},\, T_{in}) - e(P_h,\, T_0)]} \tag{4-18}$$

4-4-2 Local entropy generation

Investigation of the local entropy generation during flow processes and within a vortex tube is important to find the sources of the energy degradation. The heat transfer and friction are two sources of entropy generation. According to the RANS (Reynolds averaged Navier–Stokes) approach the flow properties such as entropy can be split into the time-mean and fluctuating part due to turbulence. Therefore, four entropy generation terms can be identified. Entropy generation in a process can be evaluated [60,78,79]:

$$S_{PRO,\bar{D}} = \frac{\mu}{T}\left\{2\left[\left(\frac{\partial u}{\partial x}\right)^2 + \left(\frac{\partial v}{\partial y}\right)^2 + \left(\frac{\partial w}{\partial z}\right)^2\right] + \left(\frac{\partial u}{\partial y} + \frac{\partial v}{\partial x}\right)^2 + \left(\frac{\partial u}{\partial z} + \frac{\partial w}{\partial x}\right)^2 + \left(\frac{\partial w}{\partial y} + \frac{\partial v}{\partial z}\right)^2\right\} \tag{4-19}$$

$$S_{PRO,\acute{D}} = \frac{\rho\varepsilon}{T} \tag{4-20}$$

$$S_{PRO,\bar{C}} = \frac{\lambda}{T^2}\left[\left(\frac{\partial T}{\partial x}\right)^2 + \left(\frac{\partial T}{\partial y}\right)^2 + \left(\frac{\partial T}{\partial z}\right)^2\right] \tag{4-21}$$

$$S_{PRO,\acute{C}} = \frac{\lambda_t}{T^2}\left[\left(\frac{\partial T}{\partial x}\right)^2 + \left(\frac{\partial T}{\partial y}\right)^2 + \left(\frac{\partial T}{\partial z}\right)^2\right] \tag{4-22}$$

Where $S_{PRO,\bar{D}}$ demonstrates the entropy generation due to direct dissipation and $S_{PRO,\acute{D}}$ demonstrates the entropy generation due to turbulent dissipation. $S_{PRO,\bar{C}}$ and $S_{PRO,\acute{C}}$

demonstrate the entropy generation by heat transfer due to mean temperature gradients and fluctuating temperature gradients, respectively.

The Bejan number (Be) compares the contribution of the entropy generation due to the heat transfer to total entropy generation rate and varies between 0 and 1which could be as:

$$Be = \frac{S_{PRO,\bar{C}} + S_{PRO,\acute{C}}}{S_{PRO,\bar{D}} + S_{PRO,\acute{D}} + S_{PRO,\bar{C}} + S_{PRO,\acute{C}}} \quad (4\text{-}23)$$

When $Be < 0.5$, it implies that the flow friction irreversibility dominates otherwise heat transfer irreversibility dominates.

4-5 Results and discussion

The exergy analysis of a high-pressure CO_2 vortex tube is developed using the MATLAB environment coupled with the Refprop database. The effect of inlet pressure and cold mass fraction, which is varied by changing the pressure at the hot outlet, is investigated on the vortex tube. The axial and swirl velocities of CO_2 are investigated at various section of the vortex tube. The specific exergy as a function of the inlet pressure and cold mass fraction is investigated. The exergy analysis aims to find the exergy losses for different inlet conditions as well as the location entropy generation within the vortex tube [60]. The entropy generation rate analysis aims to evaluate the contribution of the heat transfer and friction within the tube on thermodynamic losses. For the sake of brevity the work “specific” will not be repeated throughout the article and the summation of the specific outlet exergies will simply be referred to the outlet exergy.

The radial profile of the axial and swirl velocities of the vortex tube are given in Figure 4-5 with respect to the inlet pressure and vortex tube location. It was observed that the maximum value of the axial velocity is near the wall of the vortex tube and then reaches to zero due to the no-slip wall condition. In addition, the direction of the flow near the wall is toward the hot outlet. The radial profile of the axial velocity indicates that the flow direction is reversed near r/R = 0.75.

The swirl velocity of the working gas increases with respect to the radius of the tube and near the wall reaches its highest value and there, due to wall condition, the swirl velocity is

zero. The axial and swirl velocities decrease when the working gas moves to the hot outlet due to the friction between different layers of the flow. Increasing the inlet pressure leads to raising the swirl velocity of the working fluid increases due to expansion.

(a)

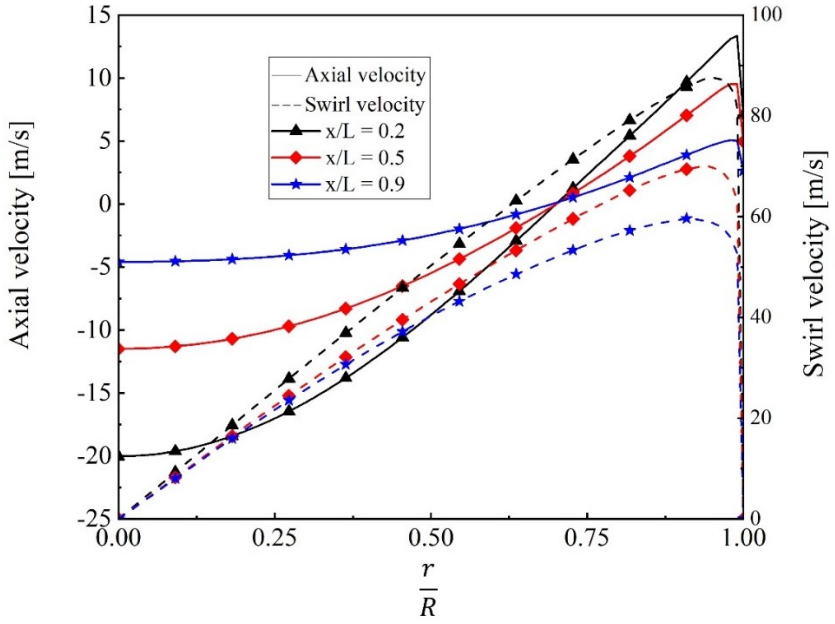

(b)

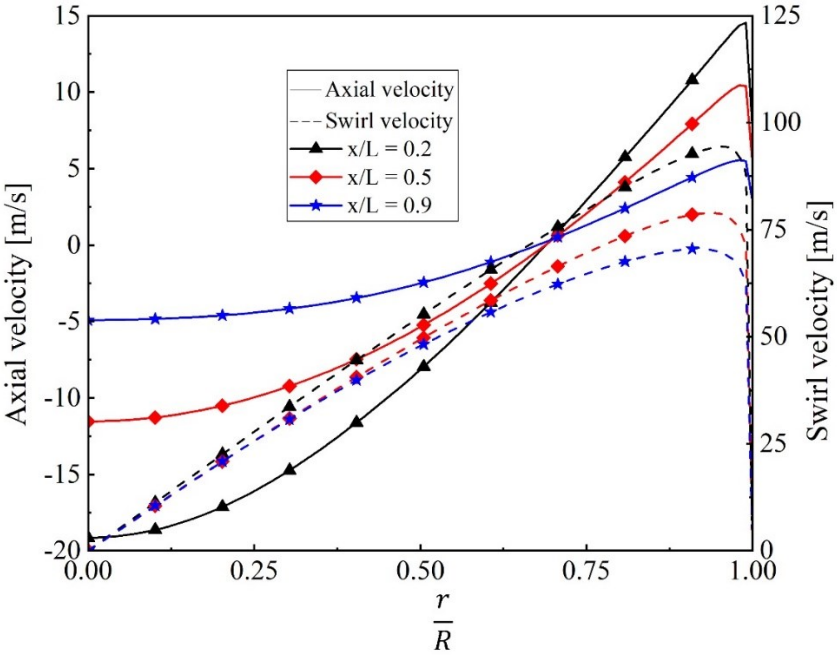

Figure 4-5. The radial profile of the axial and swirl velocities at different vortex tube locations and different inlet pressures (a) 9 MPa and (b) 11 MPa.

Figure 4-6 illustrates the radial profile of the temperature and pressure as a function of three different inlet pressures at x/L = 0.9 and α = 0.9. As CO_2 is admitted into the vortex tube through the nozzle, a centrifugal force occurs inside the vortex tube due to rotational movement. Some of the CO_2 is pressed toward the wall creating a high-pressure region (compression), while at the center of the tube expansion occurs. Therefore, the pressure raises with increasing (r/R) due to expansion of the inner stream and compression of the peripheral stream. With increasing the inlet pressure, the static pressure in the vortex tube increases. With increasing the inlet pressure, due to higher expansion of admitted CO_2 in the inlet nozzle, the static temperature decreases. The temperature increases rapidly due to heat transfer from the inner layer to the peripheral layer. It is worth noting that the inlet temperature was assigned 35℃ but the temperature at the nearest line to the hot outlet is less than the inlet temperature which could be due to the low velocity. By comparing the swirl velocity in the present study with Aghagoli and Sorin [54], it can be concluded that the maximum value of swirl velocity in this paper is less than 125 m/s, however, this value in [54] is 260 m/s which is approximately twice and the effect of velocity on the temperature is reported in [62]. Here, it is essential to note that positive values of axial velocity indicate flow moves toward the hot end while negative values indicate the flow directed towards cold end of the tube.

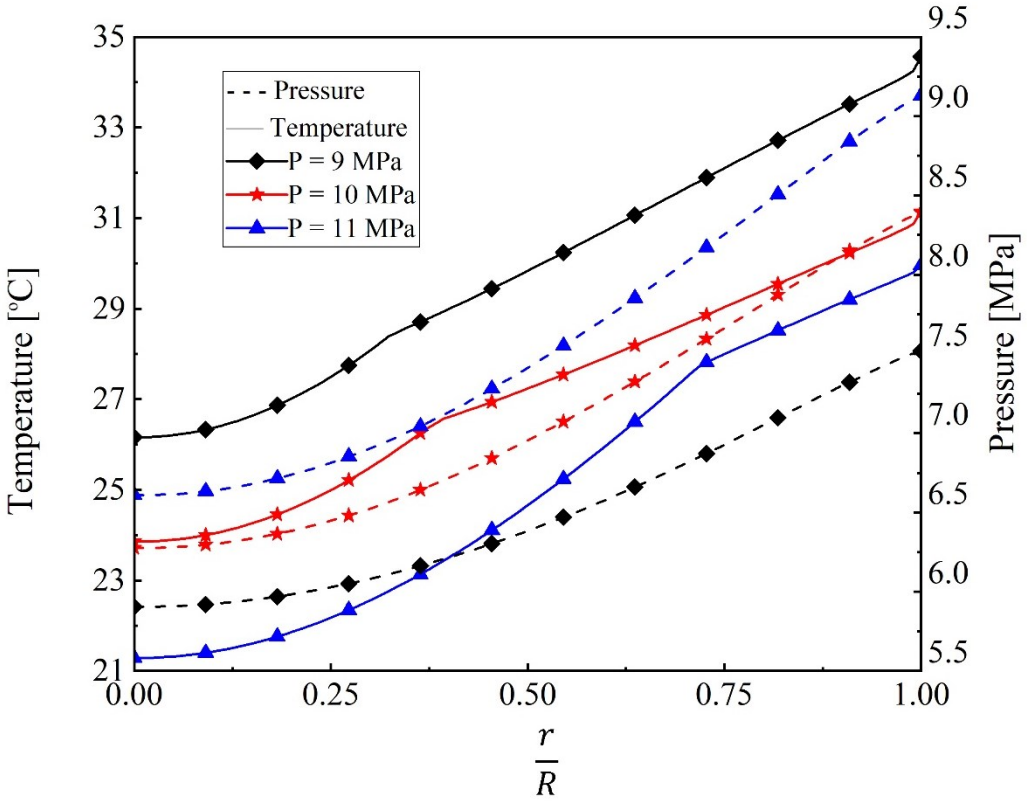

Figure 4-6. The radial profile of the temperature and pressure at three different inlet pressures at x/L = 0.9 and α = 0.9.

The outlet exergy and exergy loss of the vortex tube is given in Figure 4-7 with respect to the inlet pressure and cold mass fraction. For a given inlet pressure, as the cold mass fraction increases, the outlet exergy increases until an optimum value of α, beyond which it decreases. The optimum value of α decreases with rising inlet pressure: for P_{in} = 11 MPa, optimum cold mass fraction equals to 0.45; for P_{in} = 10 MPa, optimum cold mass fraction equals to 0.5; for P_{in} = 9 MPa, optimum cold mass fraction equals to 0.55. The result clarifies the tendency of the outlet exergy to ascend with raising inlet pressure. This effect of the inlet pressure on the outlet exergy is in agreement with the results reported by Kirmaci et al. [80]. The result shows that the inlet pressure has a major effect on the exergy loss that with increasing the inlet pressure, the entropy generation increases. Generally, with increasing cold mass fraction, the exergy loss of the vortex tube decreases, however the exergy loss decreases until specific cold mass fraction and then it increases [81,82]. The exergy loss is defined as the difference between the inlet

exergy and outlet exergies. The inlet exergy is constant and the only parameter that has any effect on the exergy loss is the outlet exergies. The minimum exergy losses occur at cold mass fractions equal to 0.55, 0.5 and 0.45 at P_{in} = 9 MPa, P_{in} = 10 MPa and P_{in} = 11 MPa, respectively.

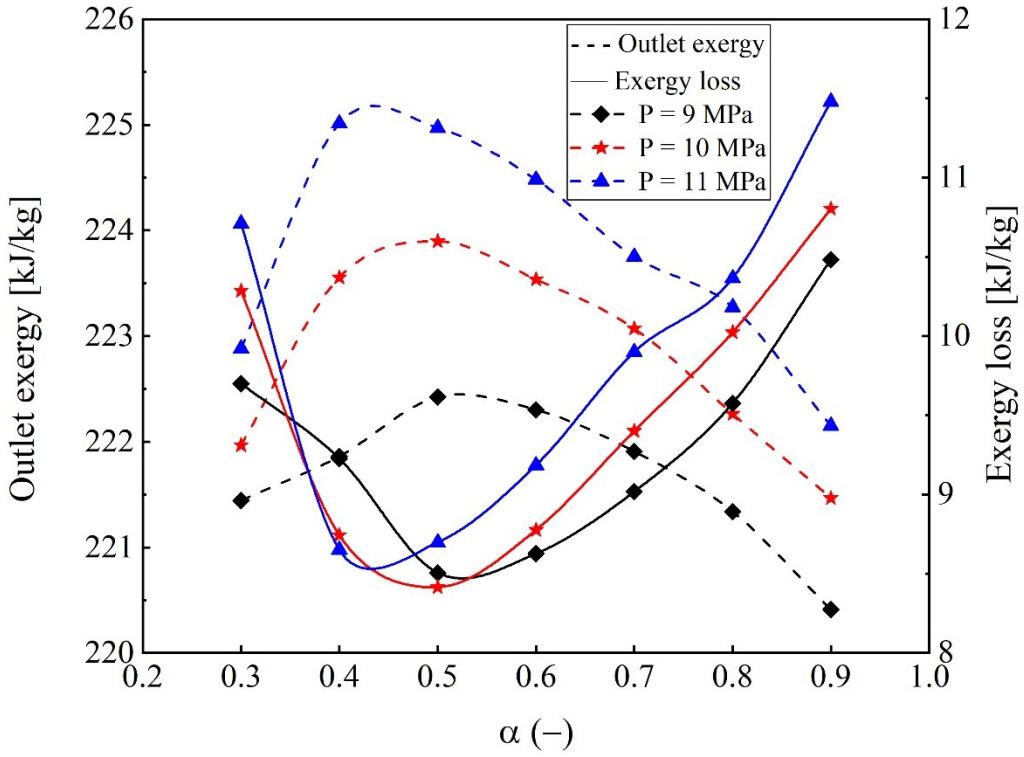

Figure 4-7. Outlet exergy and exergy loss of the vortex tube.

The exergy efficiency and transiting exergy of the vortex tube is illustrated in Figure 4-8 with respect to the inlet pressure and cold mass fraction. The transiting exergy is the summation of the transiting exergy at hot and cold outlets and it achieves its maximum at cold mass fraction equals to 0.5, where the exergy loss achieve its minimum (see Figure 4-7) .The rise in transiting exergy surpasses the reduction in exergy losses; the result is the minimum of exergy efficiency. Meanwhile for the interval of mass fraction between 0.5 and 0.9 the transiting exergy drops with α and the efficiency increases by achieving its maximum at α=0.9. As can be seen in Table 4-3, this maximum in exergy efficiency corresponds to the maximum in the cooling capacity of the tube. Figure 4-8 illustrates also that the rise the inlet pressure leads to the higher transiting exergy. As a result, the exergy efficiency drops with the inlet pressure.

Table 4-3. Variation in exergy metrics with the cold mass fraction for a vortex tube.

α	$\Delta\dot{E}_c$	$\nabla\dot{E}_c$	$\Delta\dot{E}_h$	$\nabla\dot{E}_h$	$\dot{E}_{tr,c}$	$\dot{E}_{tr,h}$	η_{tr}	$\dot{I}$	$\dot{Q}_c$
[-]	[kW]	[kW]	[kW]	[kW]	[kW]	[kW]	[%]	[kW]	[kW]
0.3	0.255	0.436	0.4	0.724	3.172	7.696	56.57	0.504	0.095
0.4	0.337	0.569	0.288	0.539	4.137	6.519	56.12	0.482	0.056
0.5	0.355	0.613	0.130	0.254	4.455	4.813	55.67	0.381	0.032
0.6	0.412	0.712	0.066	0.141	5.175	3.784	56.10	0.375	0.035
0.7	0.456	0.785	0.027	0.068	5.707	2.714	56.67	0.369	0.046
0.8	0.505	0.856	0.010	0.034	6.223	1.735	57.93	0.374	0.075
0.9	0.543	0.929	0.002	0.013	6.753	0.841	58.12	0.396	0.11

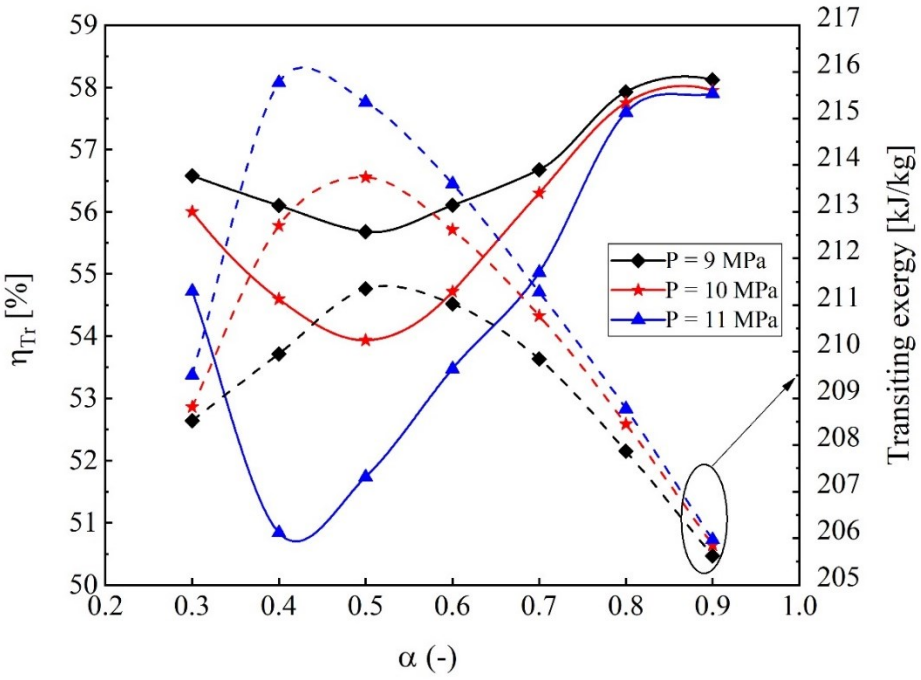

Figure 4-8. The transiting exergy efficiency and transiting exergy of the vortex tube.

The flow structure of high pressure CO_2 is illustrated in Figure 4-9. There is a pressure gradient between the hot and cold outlets inside the vortex tube and while CO_2 moves from the inlet toward the hot outlet, the momentum of CO_2 decreases until the momentum is zero. Therefore, some CO_2 particles aren't able to overcome the pressure gradient and they move

back to the cold outlet. The stagnation points can be seen in Figure 4-9 where the flow direction is changed and the local velocity is zero. The presence of the secondary circulation flow is observed near the inlet nozzle, which causes a reduction in temperature difference between the hot and cold streams. The presence of the secondary circulation pattern near the inlet nozzle was reported in [40,52].

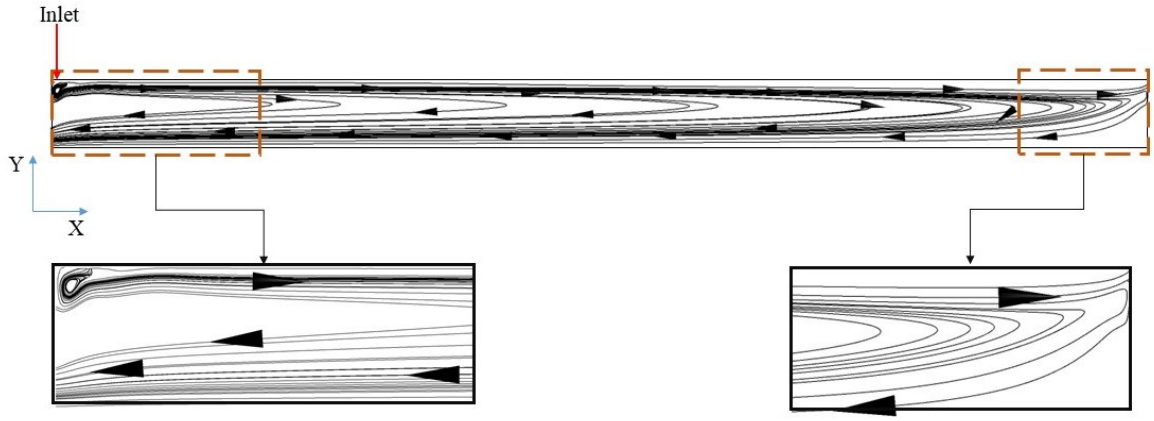

Figure 4-9. The streamline of the high pressure CO_2.

The entropy generation rate in the vortex tube could be generated due to the heat transfer and flow friction. The Bejan number is the ratio between the entropy generation due to heat transfer and total entropy generation [61]. Figure 4-10 illustrates the Bejan number at three different planes (inlet, $\frac{x}{L} = 0.5$ and $\frac{x}{L} = 0.9$) on the vortex tube. As the results reveal, the contribution of the entropy generation rate due to the heat transfer near the radius and at the center of the vortex tube is negligible and the friction is responsible for the entropy generation rate at these locations. In other words, the Bejan number is less than 0.5, where $\frac{r}{R}$ is greater than 0.9 or less than 0.17.The contribution of the entropy generation rate due to the heat transfer (Bejan number is greater than 0.5) can be seen where $0.17 < \frac{r}{R} < 0.9$, and has predominant effect on the entropy generation rate. As the flow goes to the hot outlet of the vortex tube, the effect of the entropy generation rate due to heat transfer decreases.

inlet

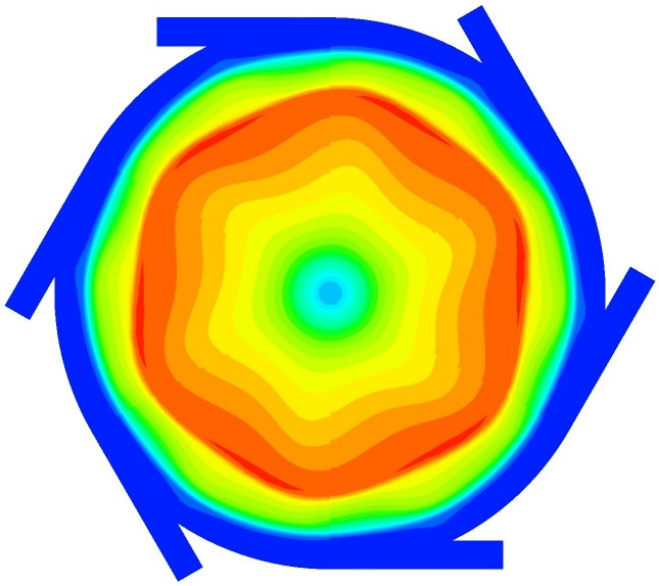

$\frac{x}{L} = 0.5$

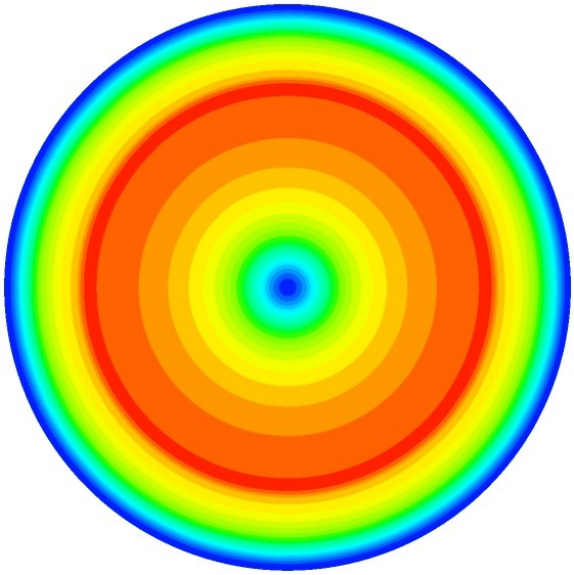

$\frac{x}{L} = 0.9$

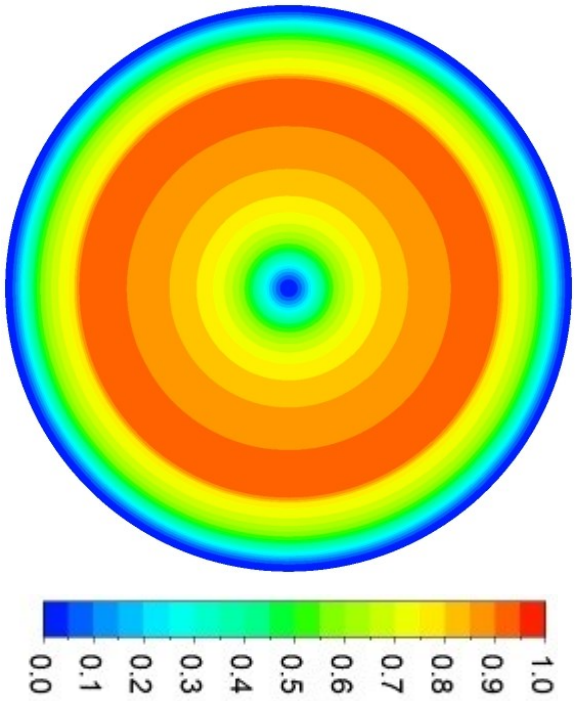

Figure 4-10. The Bejan number at different vortex tube length.

4-6 Conclusion

In the present study, a three-dimensional CFD simulation of the vortex tube with CO_2 as the compressible working fluid is investigated where a real gas properties table is implemented in ANSYS CFX solver. The results showed that the velocity has a major impact on the energy separation inside the vortex tube and that higher inlet pressure produces the higher axial and swirl velocities. The inlet pressure has a positive impact on the temperature difference inside the vortex tube, where the temperature is highest at P_{in} = 11 MPa. The minimum exergy loss occurs at cold mass fractions equal to 0.55, 0.5 and 0.45 at P_{in} = 9 MPa, P_{in} = 10 MPa and P_{in} = 11 MPa. With increasing inlet pressure, the minimum exergy loss corresponds to a lower cold mass fraction. The analysis of the local entropy generation rate showed that at the vortex tube center and near the tube wall, friction is responsible for the production of entropy. Otherwise, where $0.17 < \frac{r}{R} < 0.9$, heat transfer has the predominant effect on the entropy generation rate. The secondary circulation flow is observed near the inlet nozzle of the vortex tube. The exergy efficiency of the tube drops with the inlet pressure in the range from 11 to 9 MPa and achieves

its maximum at α =0.9. This maximum also corresponds to the maximum of the tube cooling capacity.

4-7 Acknowledgments

This project is a part of the Collaborative Research and Development (CRD) Grants Program at "Université de Sherbrooke". The authors acknowledge the support of the Natural Sciences and Engineering Research Council of Canada , Hydro-Québec, Rio Tinto, Alcan and Canmet ENERGY Research Center of Natural Resources Canada (RDCPJ451917-13).

4-8 Nomenclature

Be	Bejan number
c_p	heat capacity at constant pressure, kJ kg^{-1} K^{-1}
$\dot{E}$	total energy, W
h	specific enthalpy, kJ kg^{-1}
I	specific exergy loss, kJ kg^{-1}
$\dot{m}$	mass flow rate, kg s^{-1}
P	pressure, kPa
Pr	prandtl number
s	specific entropy, kJ kg^{-1} K^{-1}
T	temperature, °C or K
t	turbulence
u	Velocity in X direction, m s^{-1}
v	Velocity in Y direction, m s^{-1}
w	Velocity in Z direction, m s^{-1}
x_i, x_j, x_k	coordinates

Subscripts

c	cold
eff	effective
h	hot
in	inlet
l	liquid
min	minimum
sat	saturate
v	vapor

Greek symbols

α	Cold mass fraction
ε	turbulence dissipation rate, $m^2\ s^{-3}$
λ	thermal conductivity, $W\ m^{-1}\ K^{-1}$
ρ	density, $kg\ m^{-3}$
μ	dynamic viscosity, $kg\ m^{-1}\ s^{-1}$

Chapter 5

Thermodynamic analysis of a novel transcritical CO_2 vortex tube heat pump cycle

Avant-propos

Auteurs et affiliation :

Abbas Aghagoli: étudiant au doctorat, faculté de génie, département de génie mécanique, Université de Sherbrooke.

Mikhail Sorin: professeur, faculté de génie, département de génie mécanique, Université de Sherbrooke.

Sébastien Poncet: professeur, faculté de génie, département de génie mécanique, Université de Sherbrooke.

Date d'acception: 29 Mai 2019

État de l'acceptation: version finale publiée

Revue: Proceedings of the 27th CANCAM

Titre français: Analyse thermodynamique d'un nouveau cycle de pompe à chaleur à tube vortex de CO_2 transcritique.

Contribution au document: Cet article contribue à la thèse par une application du tube vortex dans le système de pompe à chaleur.

Résumé français:

Le cycle des pompes à chaleur CO_2 a attiré l'attention en raison de son respect de l'environnement et de ses caractéristiques thermodynamiques. Cependant, le cycle de pompe à

chaleur transcritique à CO_2 présente une perte d'étranglement importante en raison d'une haute chute de pression pendant la détente. La présente étude se concentre sur l'étude de la performance d'un nouveau cycle de pompe à chaleur à tube vortex de CO_2. Le tube vortex remplace le détendeur pour récupérer partiellement les pertes d'étranglement et améliorer les performances du cycle de la pompe à chaleur. L'effet de la pression du refroidisseur de gaz sur le coefficient de performance (COP) du cycle a été étudié et le COP de la pompe à chaleur à tube vortex est comparé au cycle de pompe à chaleur transcritique CO_2 conventionnel. Les résultats montrent qu'en remplaçant partiellement le tube vortex, le coefficient de performance est amélioré de 8% et avec l'augmentation de la pression du refroidisseur de gaz, le COP diminue pour le système de pompe à chaleur à tube vortex. De plus, l'utilisation d'un tube vortex produit une plus grande charge thermique de refroidisseur à gaz et de l'évaporateur que le cycle de pompe à chaleur conventionnel.

5-1 Abstract

CO_2 heat pumps cycle have drawn many attentions due to its environmental friendliness and thermodynamic features. However, the transcritical CO_2 heat pump cycle has a large throttling loss due to high-pressure change during expansion in a throttling process. The present study focuses on the investigation of the performance of a novel CO_2 vortex tube heat pump cycle. The vortex tube replaces the expansion valve to partially recover the throttling losses and improve the heat pump cycle performance. The effect of the gas cooler pressure on the coefficient of the performance (COP) of the cycle is investigated and COP of the vortex tube heat pump is compared with conventional transcritical CO_2 heat pump cycle. The results show that by partially replacing the vortex tube, the coefficient of the performance is improved by 8%, and with increasing the gas cooler pressure, COP decreases for the vortex tube heat pump system. In addition, employing a vortex tube produces greater gas cooler and evaporator heat load than the conventional heat pump cycle.

Keywords: Heat pump, vortex tube, COP, CO_2

5-2 Introduction

The high energy consumption, serious pollution of buildings and low efficiency have drawn increasing attention to solve this problem. The heat pump system is an excellent way to replace traditional building energy supply technology and reduce building energy consumption which can significantly reduce the consumption of fossil fuel [83]. Carbon dioxide (CO_2) is an appropriate replacement for conventional refrigerants due to its minimal impacts on climate change [84]. In addition, since scientists understood the negative effects of chlorofluorocarbons (CFCs) on global warming and ozone depletion, the use of CFCs decreased and there were some attempts to find a promising substitute refrigerant in order to preserve environment. Carbon dioxide is considered as an attractive refrigerant due to zero ozone depression potential and low global warming potential [83].

Generally, conventional heat pump consists of a compressor, gas cooler, expansion valve and evaporator. In the conventional heat pump system, the whole system works under critical region and heat absorption by evaporator and heat rejection by condenser occur under conditions of low and high pressures, respectively. However, in the transcritical heat pump system, evaporator absorbs heat at low pressure but heat rejection occurs in the gas cooler at pressure above the critical point [85]. Unlike the combustion kind heating system, where the delivered heat is much less than the input energy, the delivered heat by the heat pump is greater than the input work. The pressure difference between the heat rejection and the heat absorption is high in a transcritical CO_2 system and leads to large thermodynamic losses during the expansion process [86]. Hence, employing vortex tube instead of throttling valve, will reduce the throttling losses and improve the cycle performance. The vortex tube is a simple device that separates a compressed gas into cold and hot streams simultaneously. In other words, the high-pressure gas is an engine of the vortex tube. Due to no moving part and simple structure, it has received many attentions [87].

Yingfu et al. [88] used the vortex tube with isentropic assumption in the transcritical heat pump cycle. They used hot exit flow in the gas cooler and COP improvement was between 5.8% and 13.9%. Zhao and Ning [89] analyzed the effect of vortex tube one the performance

of heat pump cycle. The results showed that COP of the heat pump is improved by 3.9 to 16.8% compared to the conventional heat pump cycle.

This paper aims to employ the vortex tube in a CO_2 heat pump cycle and evaluate the coefficient of the performance of the vortex tube heat pump system. In addition, the effect of gas cooler pressure is investigated on the COP of the system, gas cooler and evaporator heat loads.

5-3 System description

Figure 5-1 shows the schematic diagram of proposed CO_2 vortex tube heat pump cycle. CO_2 leaves the evaporator in the saturated vapor (state 1) and goes into the compressor (2). In the compressor, the pressure and temperature of CO_2 increase and this high pressure and temperature gas enters into the gas cooler (3). During the constant pressure process, the temperature of CO_2 decreases due to heat rejection to the external fluid (3). In the conventional heat pump cycle, high-pressure CO_2 goes into the expansion valve and causes thermodynamic losses. However, in the proposed cycle, the high-pressure CO_2 goes into the vortex tube. In the vortex tube, gas is divided into two streams (high-temperature and low-temperature streams). A flow that has a higher temperature than inlet named hot flow leaves at state 5 and gets into the second gas cooler and an another flow that has a lower temperature than inlet named cold flow gets into the first expansion valve (4). In the gas cooler, the superheated CO_2 rejects heat during the constant pressure process, its temperature reduces (4). Cold flow is introduced into the first expansion valve and hot flow after the second gas cooler is introduced into the second expansion valve. After expansion valves, both flows mix and get to the evaporator.

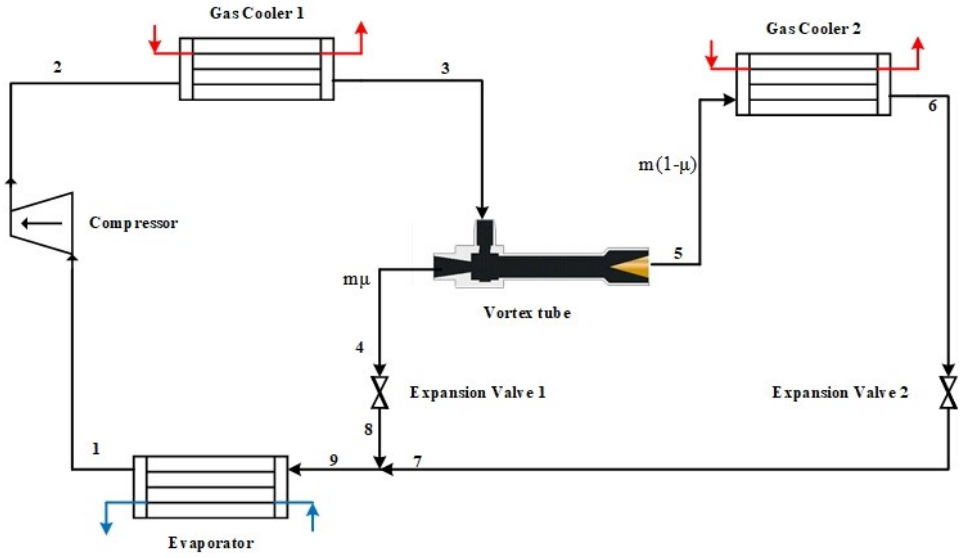

Figure 5-1. Schematic diagram of proposed CO_2 vortex tube heat pump cycle.

5-4 Mathematical simulation

The following assumptions have been considered for the analysis before establishing the mathematical models:

- The pressure losses in the gas cooler, evaporator and pipes are neglected [90].
- The flow across the expansion valve is isenthalpic [7].
- The working fluid after the evaporator is saturated vapor.

The mass conservation law in the vortex tube is calculated as:

$$\dot{m}_3 = \dot{m}_4 + \dot{m}_5 \tag{5-1}$$

The cold mass fraction in the vortex tube is given as:

$$\mu = \frac{\dot{m}_4}{\dot{m}_3} \tag{5-2}$$

The energy conservation in the vortex tube is calculated as:

$$\dot{m}_3 h_3 = \dot{m}_4 h_4 + \dot{m}_5 h_5 \tag{5-3}$$

The isentropic efficiency of the compressor is obtained by [91]:

$$\eta_c = \frac{h_{2s} - h_1}{h_2 - h_1} \tag{5-4}$$

The energy balance at the inlet of the evaporator writes:

$$\dot{m}_9 h_9 = \dot{m}_9 \mu\, h_8 + \dot{m}_9 (1-\mu) h_7 \quad (5\text{-}5)$$

The compressor power is expressed as:

$$\dot{W}_C = \dot{m}_1 (h_2 - h_1) \quad (5\text{-}6)$$

The heating load of the gas coolers and evaporator are expressed as:

$$\dot{Q}_G = \dot{m}_1 [(h_3 - h_2) + (1-\mu)(h_6 - h_5)] \quad (5\text{-}7)$$

$$\dot{Q}_E = \dot{m}_1 (h_1 - h_9) \quad (5\text{-}8)$$

Coefficient of performance (COP) of CO_2 vortex tube heat pump is calculated as:

$$COP = \frac{\dot{Q}_G}{\dot{W}_C} \quad (5\text{-}9)$$

5-5 Results and Discussion

The main operating conditions for the simulation of the vortex tube heat pump are summarized in Table 5-1. Thermodynamic properties of CO_2 are obtained with the Engineering Equation Solver (EES) software, which combines non-linear equations with thermophysical property functions. The effect of vortex tube and gas cooler pressure on the coefficient of performance of the heat pump cycle, gas cooler heat load and evaporator heat load are investigated.

Table 5-1. Operating conditions for the vortex tube heat pump cycle.

Evaporator	-15 ℃
Gas cooler pressure	90 bar
Gas cooler	37℃
Compressor efficiency	0.85
μ	0.9

Figure 5-2 shows the effect of the hot exit pressure on the COP of the heat pump at two different constant gas cooler pressures (90 bar and 95 bar) and three different cold exit pressures (78, 79 and 80 bar). At constant cold exit pressure of the vortex tube, the hot exit pressure increases that leads to increase the second heat pump heat load and increases the COP. As the

cold exit pressure of the vortex tube increases, enthalpy at the cold exit decreases, causing the hot exit enthalpy to rise so the COP of the system increases too.

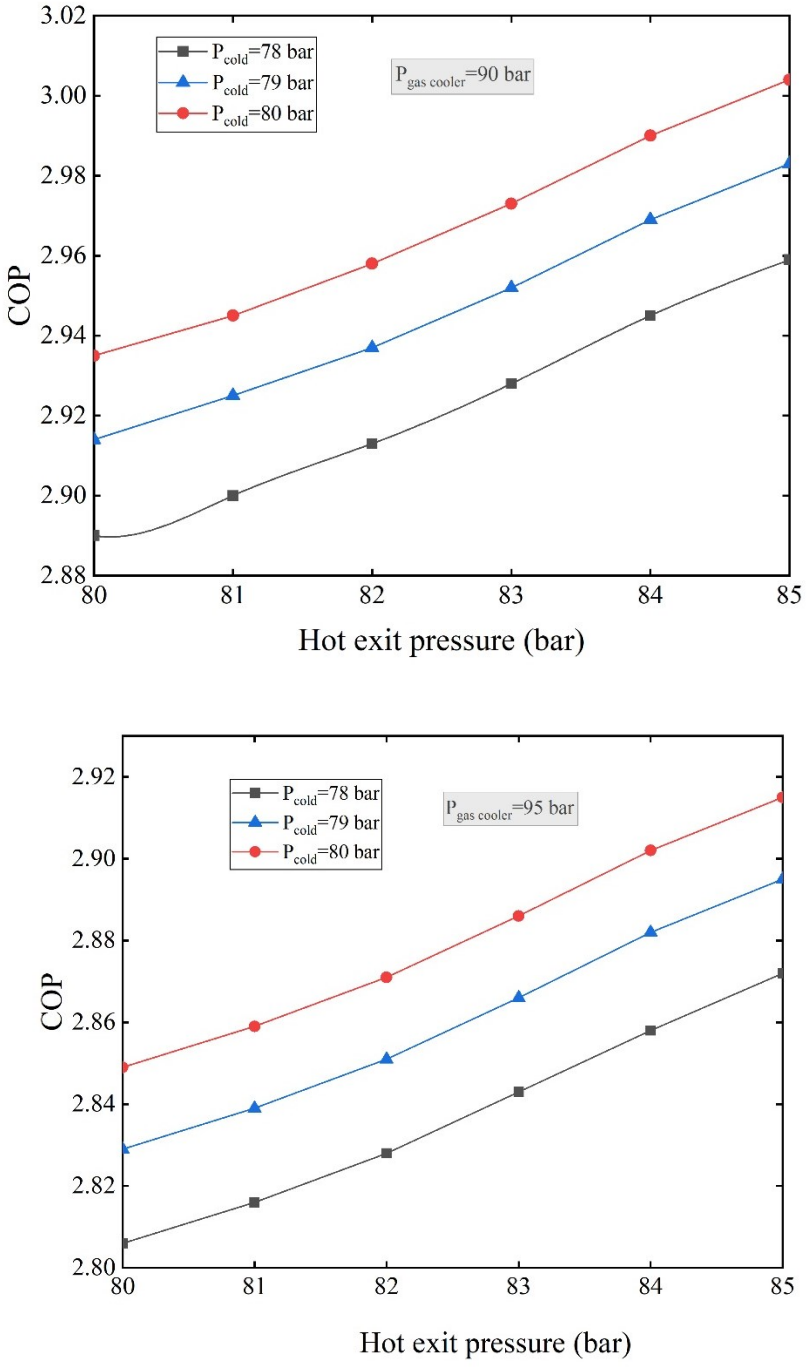

Figure 5-2. The effect of the hot exit pressure on the COP of the vortex tube heat pump.

Figure 5-3 displays the effect of hot exit pressure of the vortex tube on the heating load of the evaporator and gas cooler of the vortex tube heat pump. By increasing the hot exit pressure, the quality of the working fluid at state 8 is constant. However, the quality of the working fluid after the second expansion valve decreases so the quality of the working fluid at the inlet of the evaporator decreases (state 9), causing the rise of the evaporator heat load. In addition, by increasing the hot exit pressure, the enthalpy at the hot exit of the vortex tube increases so the second gas cooler heat load increases with constant first gas cooler heat load. By rising the cold exit pressure, at the hot exit of the vortex tube, the enthalpy increases so the gas cooler heat load increases.

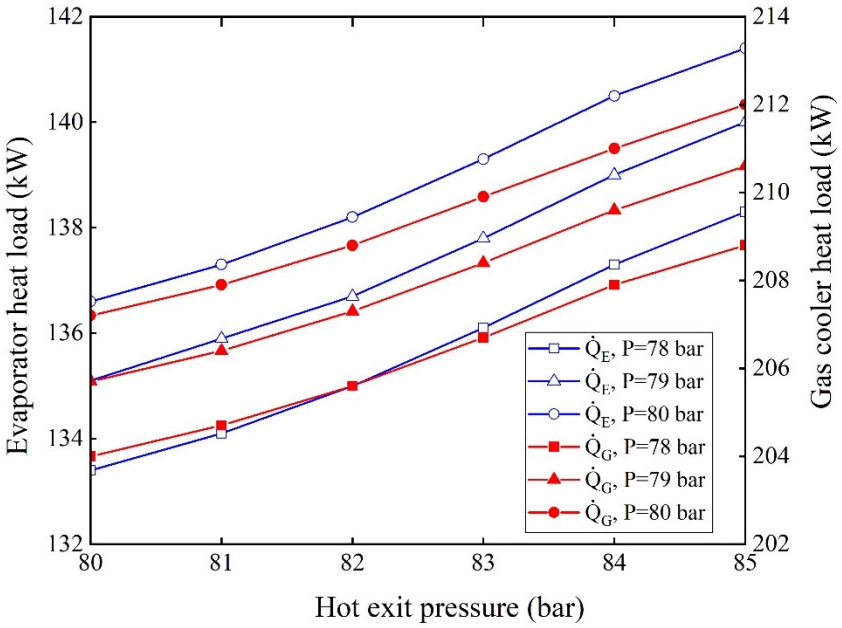

Figure 5-3. The effect of the hot exit pressure on the heat load of evaporator and gas cooler of the vortex tube heat pump.

Figure 5-4 shows the effect of the gas cooler pressure on the COP of the heat pump. Even though as the gas cooler pressure rises, the heat load of the gas cooler increases but compressor power increases as well, causing the decrease of the COP of the system (Equation (5-9)). As it is shown in Figure 5-3, the gas cooler heat load difference between traditional heat pump and vortex tube heat pump indicates the effect of second gas cooler heat load in the vortex tube heat pump system that decreases by increasing the gas cooler pressure. COP of the vortex tube heat pump system and traditional heat pump system are 2.97 and 2.76, respectively.

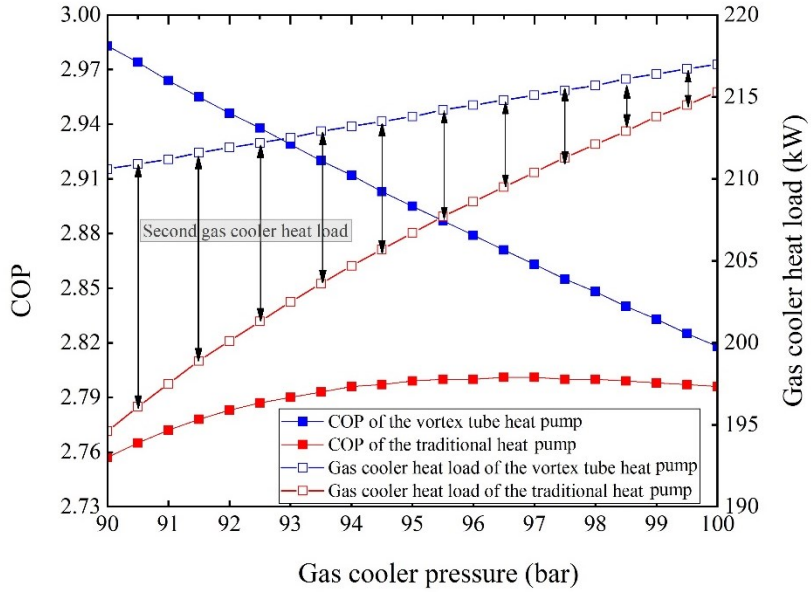

Figure 5-4. The effect of the gas cooler pressure on the COP of the heat pump.

5-6 Conclusion

This paper studied the effect of vortex tube on the COP, gas cooler and evaporator heat loads of the heat pump system using the first law of thermodynamics. Increasing both cold and hot exit pressures has a positive impact on the COP of the vortex tube heat pump system. Even though increasing the gas cooler pressure leads to increase in the first gas cooler heat load, but causing a decrease of the second gas cooler heat load due to the decrease of the enthalpy at the vortex tube hot exit. COP of the vortex tube system is 8% greater than traditional heat pump system at P_G=90 bar and 1% greater at P_G=100 bar. By partially replacing the vortex tube, gas cooler heat load increases from 194 kW to 210 kW that means 16 kW is generated due to the use of the vortex tube. Using partially the vortex tube in the heat pump cycle causes the quality of the working fluid to fall so the heating load of the evaporator increases.

5-7 Nomenclature

h	Enthalpy (kJ.kg^{-1})
$\dot{m}$	Mass flow rate (kg. s^{-1})
$\dot{Q}$	Heat load (kW)

P	Pressure (bar)
T	Temperature (K)
$\dot{W}$	Work power (kW)

Subscripts

C	Compressor
E	Evaporator
G	Gas cooler

Greek letters

μ	Cold mass fraction
η	Efficiency

Chapter 6

CFD modeling and exergy analysis of a heat pump cycle with Tesla Turbine using CO_2 as a working fluid

Avant-propos

Auteurs et affiliation :

Abbas Aghagoli: étudiant au doctorat, faculté de génie, département de génie mécanique, Université de Sherbrooke.

Mikhail Sorin: professeur, faculté de génie, département de génie mécanique, Université de Sherbrooke.

Date d'acception: 9 Juin 2020

État de l'acceptation: version finale publiée

Revue: Applied Thermal Engineering

Titre français: Modélisation CFD et analyse exergétique d'un cycle de pompe à chaleur avec turbine Tesla utilisant le CO_2 comme fluide de travail.

Contribution au document: Cet article contribue à la thèse par une application de la turbine Tesla dans le système de pompe à chaleur.

Résumé français:

Le cycle de la pompe à chaleur transcritique au dioxyde de carbone a suscité beaucoup d'intérêt pour la recherche en faveur de son respect de l'environnement et des caractéristiques thermodynamiques du dioxyde de carbone. Cependant, il y a un problème préoccupant, qui est

l'énorme perte d'exergie associée au processus isenthalpique dans le détendeur. Dans l'étude actuelle, un nouveau cycle de pompe à chaleur transcritique au dioxyde de carbone est proposé, dans lequel une turbine Tesla remplace le détendeur. La turbine Tesla est une turbine sans pales qui fonctionne avec n'importe quel fluide diphasique, ce qui est le cas pour l'expansion du CO_2 supercritique. Un modèle numérique de dynamique des fluides en 3D est d'abord développé pour simuler l'écoulement de dioxyde de carbone dans une turbine Tesla, puis les résultats extraits sont utilisés comme données pour la modélisation thermodynamique ultérieure du cycle de la pompe à chaleur. La production d'énergie de la turbine Tesla et les pertes d'exergie, ainsi que le coefficient de performance du cycle de pompe à chaleur proposé sont étudiés en termes de vitesse angulaire du rotor de turbine et des pressions du refroidisseur de gaz et de l'évaporateur. Il est démontré que le coefficient de performance du cycle où une turbine Tesla est intégrée est jusqu'à 16,3% plus élevé que le cycle traditionnel avec le détendeur. De plus, à une vitesse angulaire du rotor égale à 1000 rad / s, la puissance de la turbine est maximale et l'augmentation de la pression d'entrée conduit à un couple plus élevé et par conséquent à la puissance de turbine plus élevée. À une pression d'entrée inférieure, le coefficient de performance du cycle de la pompe à chaleur est plus élevé. L'existence d'un compromis thermodynamique est illustré entre la production d'énergie de la turbine Tesla et la qualité de la vapeur en sortie de la turbine Tesla, en fonction de la vitesse angulaire du rotor. Il est prouvé numériquement que la vitesse angulaire optimale du rotor correspond au rendement exergétique maximal de la turbine Tesla, ce qui conduit à son tour au coefficient maximal de performance de l'ensemble du cycle.

6-1 Abstract

The transcritical carbon dioxide heat pump cycle has been drawing much research interest due to its environmental friendliness and the thermodynamic features of carbon dioxide. However, there is one concerning issue, which is the huge exergy loss associated with the isenthalpic process in the expansion valve. In the current study, a new transcritical carbon dioxide heat pump cycle is proposed, where a Tesla turbine replaces the expansion valve. The Tesla turbine is a bladeless turbine that works with any two-phase fluid, which is the case for the expansion of supercritical CO_2. A 3D computational fluid dynamics model is first developed

to simulate the flow of carbon dioxide within a Tesla turbine, and then the extracted results are used as data for subsequent thermodynamic modeling of the heat pump cycle. The Tesla turbine power production and exergy losses, as well as the proposed heat pump cycle coefficient of performance are investigated in terms of the turbine rotor angular velocity and the gas cooler and evaporator pressures. It is demonstrated that the coefficient of performance of the cycle where a Tesla Turbine is integrated is up to 16.3% higher than the traditional cycle with the expansion valve. In addition, at rotor angular velocity equals to 1000 rad/s, the turbine power is maximum and increasing the inlet pressure leads to the higher torque and consequently higher turbine power. At lower inlet pressure, the coefficient of performance of the heat pump cycle is higher. A thermodynamic trade-off is illustrated between the power production from the Tesla turbine and the vapor quality at the outlet of the Tesla turbine, as a function of rotor angular velocity. It is numerically proven that the optimum rotor angular velocity corresponds to the maximum exergy efficiency of the Tesla turbine, which in turn leads to the maximum coefficient of the performance of the whole cycle.

Keywords: Tesla turbine, supercritical CO_2, CFD, heat pump, COP, exergy efficiency

6-2 Introduction

The high energy consumption and serious pollution from the burning of fuels for buildings heating have drawn increasing attention, with the goal of alleviating these problems. A heat pump system is an excellent way to replace traditional building heating technology and reduce building energy consumption. In addition, CO_2 as a working fluid in the heat pump system has attracted much attention not only due to its zero ozone depletion potential and low global warming potential, but also for its specific thermodynamic properties, such as low critical temperature [92]. In a subcritical heat pump, heat rejection occurs below the critical point, which leads to poor performance [93,94]. In a transcritical heat pump, heat rejection is not limited by the critical temperature, which leads to higher performance. However, the most important cause of thermodynamic imperfection of a transcritical heat pump cycle is the large throttling exergy destruction due to the refrigerant passing from the supercritical state (80-120 bar) to subcritical state (30-40 bar). In other words, the greater pressure difference between the

gas cooler and the evaporator causes important exergy loses due to expansion. One key approach to improving the performance of a heat pump cycle is to recover part of these throttling losses by producing useful work. Therefore, a large number of studies have been done to enhance the performance of the heat pump cycle and different system designs have been proposed [3,95]. The ejector was proposed as an expansion device that can partially recover energy from the expansion process [7,27,91]. Many research works have been carried out on the performance of the ejector transcritical CO_2 heat pump cycle [10,84,96], which show a rise in the overall efficiency. Elbel and Hrnjak [97] carried out an experimental study on a transcritical R744 system using an ejector; their results showed that the cooling capacity and COP improved by 8% and 7%, respectively. The ejector recovered 14.5% of throttling losses. However, they found that ejector efficiency is lower when the pressure of the primary flow is high. Taslimi Taleghani et al. [85] analyzed two-phase transcritical CO_2 ejectors. They investigated the effect of compression ratio on the entrainment ratio and the results showed that by increasing the primary flow pressure, the entrainment ratio decreases. In addition, CFD modeling of a two-phase ejector showed that droplets have a negative effect on the ejector performance [98]. Moreover, the low COP is the main disadvantage of the cycle which is integrated by the ejector [99]. Yang et al. [100] compared the exergy efficiency and COP of a heat pump cycle integrated with either an expander or with an expansion valve. Their results showed the exergy efficiency and COP of a heat pump cycle with an expander increases by 30% and 33%, respectively. For the purpose of work recovery, there is some equipment that can be used as an expander: e.g. the Tesla turbine. The Tesla turbine isn't a competitive turbomachinery device in many applications where traditional turbines are used. However, in some situations, such as in the presence of two-phase or highly viscous fluids, conventional turbomachinery is not suitable. In these situations, a Tesla turbine can operate effectively [24,101,102].

The Tesla turbine, which is also known as a bladeless turbine, was invented by Nikolas Tesla in 1913 [21]. A Tesla turbine is characterized as a radial expander and is comprised of several parallel disks, instead of blades, that works through the generation of torque by fluid wall shear stress on the disks. The Tesla turbine has a simple structure with low-cost

manufacturing, which can be a potentially reliable expander [103]. The working fluid goes to the stator of the turbine through the series of nozzles (stator entrance). The flow enters the interface between the outer stator and inner rotor and reaches its high tangential velocity. The strong tangential flow enters into the disk channels (the narrow space between two disks) and rotates the disks due to friction, and finally exhausts along the rotor axis. In this way the working fluid delivers its kinetic energy to the disks.

Recently, there has been much interest in the application of the Tesla turbine in Organic Rankine Cycles, due to power generation in small scales [22,103,104]. There are many parameters that affect the Tesla turbine performance, such as the gap between the rotating disks, the disk rotation speed, and the number of nozzles, and thus some experimental and numerical studies focused on the geometrical parameters. Lampart and Jędrzejewski [105] showed in their numerical study that the Tesla turbine efficiency decreases as the number of nozzles increases. Pandey et al. [106] carried out the computational fluid dynamics (CFD) analysis of a 1kW Tesla turbine with water as a working fluid. Choon et al. [107] optimized the Tesla turbine efficiency with a CFD procedure and the Tesla turbine generated a torque of 0.033 N m, with the maximum efficiency of 10.7%. The maximum efficiency of the Tesla turbine was reported as 69% at rotor angular velocity equals to 3000 rpm [108].

The accuracy of the CFD simulation strongly relies on the thermodynamic properties of the working fluid, which are extracted from the equation of state (EoS) [71].

The NIST real gas model of CO_2 employed by Aghagoli and Sorin [54] in a vortex tube study was based on the Helmholtz-energy equation of state. Fang et al. [71] computed the computational time for different equations of state and demonstrated that the tabulated EoS is 66 times faster than the original Span-Wagner EoS.

Due to the nonlinear behavior of CO_2 in the supercritical region, Ameli et al. [72] implemented a CO_2 real gas properties (RGP) table in the ANSYS-CFX solver to overcome the simulation instability in the supercritical region for the radial turbine. In addition, they studied the effect of look-up table resolution and the ideal gas assumption for a supercritical CO_2 radial turbine. Their studies showed that when the compressibility factor is close to one, the simulation

error is not noticeable; when the initial condition is close to the critical point, there is approximately 22% error in the enthalpy drop.

In the present study, the Tesla turbine is introduced as a potential device to recover the throttling losses in a heat pump cycle. The Tesla turbine power production and exergy losses, as well as the proposed heat pump cycle coefficient of performance (COP), are investigated as a function of turbine rotor angular velocity, gas cooler pressure, and evaporator pressure. For this purpose, a three-dimensional CFD simulation of the Tesla turbine is first investigated, with CO_2 as the compressible working fluid, where the CO_2 RGP table is coupled with ANSYS CFX solver. The CFD results of the Tesla turbine are then used for thermodynamic modeling of the heat pump cycle. A thermodynamic trade-off will be illustrated between the power production from the Tesla turbine and the vapor quality at the outlet of the Tesla turbine, as a function of rotor angular velocity. Finally, the relationship between the Tesla turbine exergy efficiency and the overall heat pump cycle COP will be discussed in terms of the operating conditions.

6-3 Heat pump cycle description

The schematic and temperature-entropy diagram of the heat pump cycle integrated with the Tesla turbine (TeslaHPC) is presented in Figure 6-1a and Figure 6-1b, respectively. The process path 1-2-3-4-1 presents the heat pump integrated with the Tesla turbine, and the process path 1-2-3-4'-1 presents the conventional heat pump with the expansion valve. Saturated vapor CO_2 leaves the evaporator and enters the compressor. During the isentropic process in the compressor, the temperature and pressure of the carbon dioxide increase. At the supercritical pressure, the carbon dioxide isobarically cools as it passes through the gas cooler. In the conventional transcritical heat pump cycle, the CO_2 adiabatically expands (3-4') through the expansion valve.

In contrast, in the proposed cycle, the CO_2 expands in the Tesla turbine (3-4) and the turbine produces usable work. Finally, the working fluid returns to the evaporator (4-1). The following assumptions are considered for analyzing this cycle:

There is no pressure drop through pipes [109,110].

The heat pump cycle operates in steady-state.

The working fluid state at the evaporator outlet is saturated vapor [7,111].

The evaporator heat load is 5 kW.

There is no heat loss to the environment.

ΔT =5 K between the CO_2 and external fluids in the gas cooler and evaporator, at the cold end of the heat exchangers.

The isentropic efficiency of the compressor is calculated according to an approximation [112]:

$$\eta_C = 0.9343 - 0.04478 \cdot P_2/P_1 \quad (6\text{-}1)$$

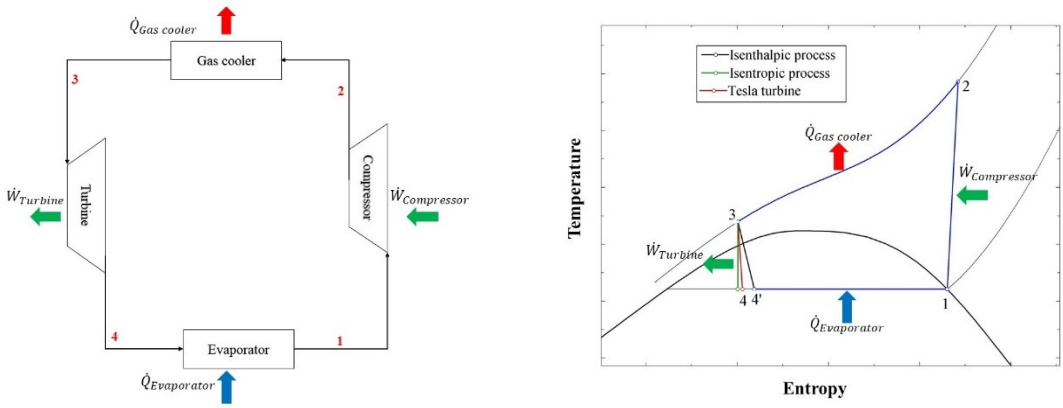

Figure 6-1. Schematic (a) and temperature-entropy diagram (b) of the heat pump cycle integrated with the Tesla turbine.

6-3-1 Internal-external exergy losses and exergy efficiency of Tesla turbine.

In order to evaluate the influence of the Tesla Turbine irreversibility on the overall cycle COP, it is proposed to first study a semi-ideal transcritical CO_2 cycle. This semi-ideal cycle is defined as a cycle where all components work under ideal conditions, except the Tesla turbine: i.e. there is no exergy loss in the compressor, evaporator and gas cooler. In other words, the efficiency of the compressor is assumed to be 100%, and the temperature difference between

the CO_2 and the external fluids is zero in the gas cooler and evaporator. The internal exergy losses within the Tesla turbine are here defined by the Gouy-Stodola relation [113]:

$$\dot{I}_{internal} = \dot{m} \cdot T_0 \cdot (s_{out} - s_{in}) \quad (6\text{-}2)$$

The external losses represent the kinetic energy of flow leaving the turbine:

$$\dot{I}_{external} = 0.5 \cdot \dot{m} \cdot V_{out}^2 \quad (6\text{-}3)$$

This kinetic energy is dissipated within the evaporator, but for the purpose of this analysis, it is represented as the external exergy losses of the turbine. The work produced by the turbine is:

$$\dot{W}_T = \dot{m} \cdot (h_{\text{in}} - h_{\text{out}}) \quad (6\text{-}4a)$$

$$\dot{W}_T = \sigma \cdot \Omega \quad (6\text{-}4b)$$

Where, σ and Ω are torque and rotor angular velocity, respectively.

The general exergy efficiency expression was first proposed by Grassmann [46]. Some authors used this expression for the optimization of the sub environmental process [5,114,115]. However, Brodyansky et al. [47,48] discussed the shortcomings of this expression while it is applied to expansion processes across the environmental temperature. They proposed a new definition of exergy efficiency, called transiting exergy efficiency. The transiting exergy flow is the part of exergy that enters the system and leaves it without transformation, and as a result, it is excluded from the numerator and denominator of the Grassmann coefficient and is defined as:

$$\eta_{\text{tr}} = \frac{\dot{E}_{out} - \dot{E}_{Tr} + \dot{W}_T}{\dot{E}_{in} - \dot{E}_{Tr}} = \frac{\Delta\dot{E}_{out} + \dot{W}_T}{\nabla\dot{E}_{in}} \quad (6\text{-}5)$$

Given that the expansion process in the Tesla turbine goes through the environmental temperature T_0, $\Delta\dot{E}$ and $\nabla\dot{E}$ are the produced and consumed exergies in the process, respectively [48].

$$\Delta\dot{E}_{out} = \dot{m} \cdot [e(P_{out}, T_{out}) - e(P_{min}, T_0)] \quad (6\text{-}6)$$

$$\nabla\dot{E}_{in} = \dot{m} \cdot [e(P_{in}, T_{in}) - e(P_{min}, T_0)] \quad (6\text{-}7)$$

Where, P_{min} is the lowest pressure between the inlet and outlet values. The term $\Delta\dot{E}_{out}$ in equation (6-6) represents the increase in the thermal exergy component due to an isobaric temperature drop from T_0 to T_{out}. The symbol $\nabla\dot{E}_{in}$ in equation (6-6) represents the decrease in thermo-mechanical exergy, due to the combined effects of the thermal exergy destruction resulting from the temperature drop from T_{in} to T_0, and the decrease of mechanical exergy because of the pressure drop from P_{in} to P_{out}.

The attention of the reader is drawn to the fact that the difference between the denominator and the numerator of equation (6-5) equals the sum of internal and external losses.

6-4 CFD model

Computational fluid dynamics (CFD) has been applied to analyze the fluid flow phenomena as a powerful tool to simulate and optimize engineering problems. CFD modeling requires some steps in order to simulate the flow behavior and obtain reliable results which are; select the appropriate working fluid EoS, turbulence model, Boundary condition and mesh grid.

6-4-1 Fluid Property Table

The accuracy of the CFD simulation strongly relies on the thermodynamic properties of the working fluid, which are extracted from the equation of state [71]. The major difficulty CFD studies involving CO_2 is related to the nonlinear behavior of CO_2 near the critical point. Figure 6-2 shows the specific heat at a constant pressure of CO_2 as a function of pressure and temperature.

In the current study, a CO_2 real gas properties (RGP) table with very-high-resolution is generated and is coupled with commercial CFD software ANSYS CFX solver. There are nine important properties of CO_2 (specific enthalpy, speed of sound, specific volume, specific heat at constant volume, specific heat at constant pressure, the partial derivative of pressure with respect to the specific volume at a constant temperature, specific entropy, dynamic viscosity, and thermal conductivity) that are extracted from REFPROP libraries and are stored in the RGP table. For each phase (liquid and vapor) there is one RGP table that is coupled with CFX solver and the supercritical region exists in both liquid and vapor RGP tables.

In the current study, the RGP table pressure values range from 1 MPa to 30 MPa, and the temperatures range from 220 K to 400 K, in order to cover a wider range than the simulation criteria. The tabulated region in the CO_2 phase diagram is shown in Figure 6-3. The relative error of the CO2 properties between the RGP table and Refprop software are shown in Figure 6-3.

In this study, the homogeneous equilibrium model (HEM) is applied to a three-dimensional numerical model of CO_2 expansion inside the Tesla turbine. The HEM is chosen due to its simplicity [74], and Lucas et al. [75] compared the experimental data of the quality of CO_2 in a two-phase ejector with the HEM approach and their results showed that the difference was negligible.

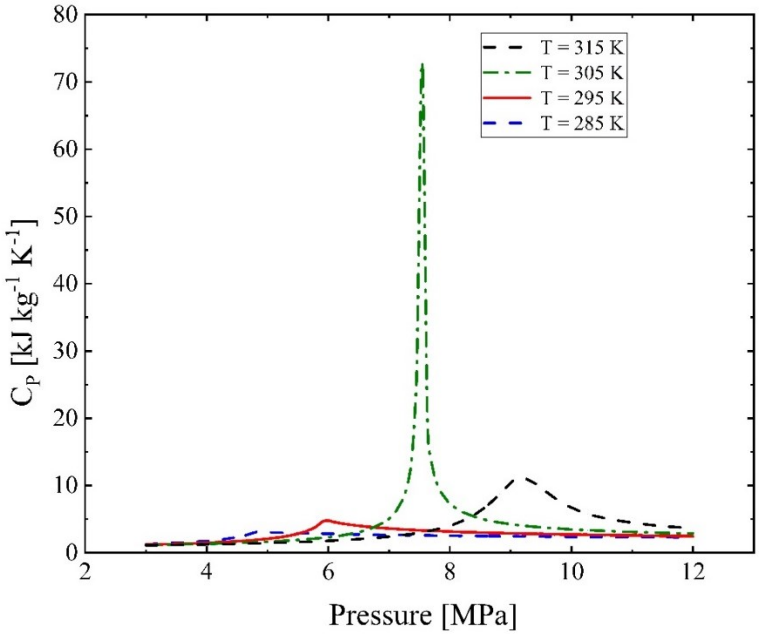

Figure 6-2. Specific heat at constant pressure for CO_2 as a function of pressure and temperature.

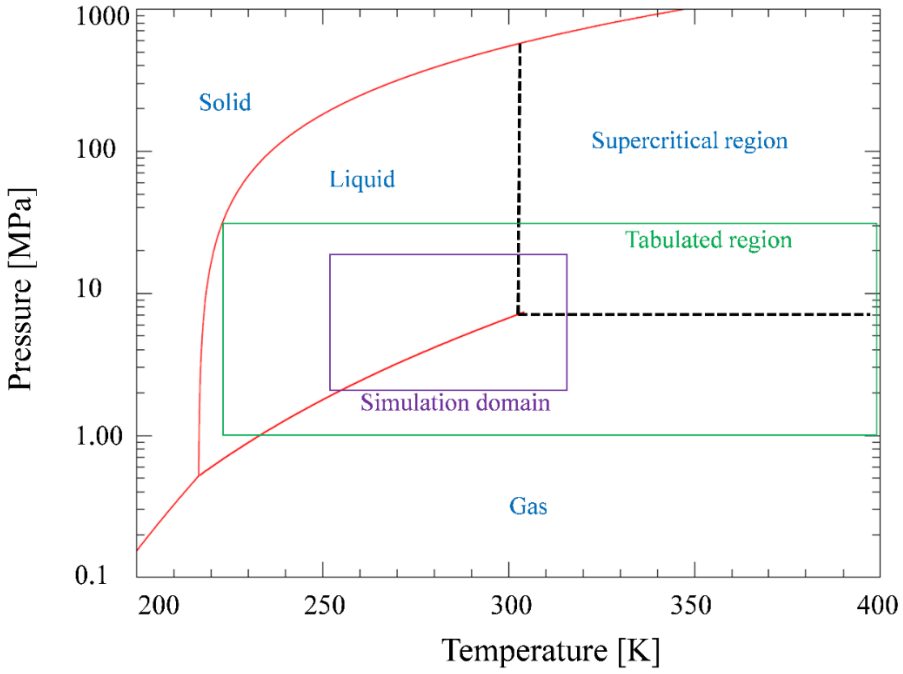

Figure 6-3. P-T diagram for CO_2.

Table 6-1. The relative error of the CO_2 properties.

	RGP table	Refprop software	Error [%]
Pressure [MPa]	10	10	-
Temperature [˚C]	35	35	-
Enthalpy [kJ.kg^{-1}]	279.73	279.75	0.007
Entropy [kJ.kg^{-1}.K^{-1}]	1.24	1.241	0.08
Density [kg.m^{-3}]	765.62	765.7	0.013

The mass, momentum and energy equations for compressible single-phase turbulent flow are:

$$\frac{\partial}{\partial x_j}\left(\rho u_j\right) = 0 \tag{6-8}$$

$$\frac{\partial}{\partial x_j}\left(\rho u_i u_j\right) = -\frac{\partial p}{\partial x_i} + \frac{\partial}{\partial x_j}\left[\mu\left(\frac{\partial u_i}{\partial x_j} + \frac{\partial u_j}{\partial x_i} - \frac{2}{3}\delta_{ij}\frac{\partial u_k}{\partial x_k}\right)\right] + \frac{\partial}{\partial x_j}\left(-\rho\bar{u}_i\bar{u}_j\right) \tag{6-9}$$

$$\frac{\partial}{\partial x_j}\left[\rho u_i\left(h+\frac{1}{2}u_i u_j\right)\right]=\frac{\partial}{\partial x_j}\left[\left(\tau_{ij}\right)_{eff}u_i+k_{eff}\frac{\partial T}{\partial x_j}\right] \quad (6\text{-}10)$$

Where, $k_{eff}=\frac{\mu_t}{Pr_t}+K$.

Moreover, a similar numerical method can be applied for the HEM system by considering the thermodynamic and mechanical equilibrium between both phases [73].

$$\begin{aligned} P_l &= P_v = P_{sat} \\ T_l &= T_v = T_{sat} \\ u_l &= u_v = u \end{aligned} \quad (6\text{-}11)$$

As a consequence, the fluid properties are a function of pressure and enthalpy:

$$\{\rho,\mu,c_p\}=f(P,h) \quad (6\text{-}12)$$

6-4-2 The shear stress transport model

The shear stress transport (SST) turbulence model is chosen following the recommendation of [116–118] to simulate mean flow characteristics for flow conditions inside the Tesla turbine. Even though the $k-\varepsilon$ turbulence model is used to predict the turbulent flow due to robustness and economy, it fails to predict the turbulence flow near the wall, such as a turbine blade. Therefore, the SST model has been developed that has $k-\omega$ turbulence model characteristics near the wall and k − ε turbulence model characteristics in the bulk flow.

$$\frac{\partial}{\partial x_j}(\rho k u_j)=\frac{\partial}{\partial x_j}\left[\left(\mu+\frac{\mu_t}{\sigma_{k2}}\right)\frac{\partial k}{\partial x_j}\right]+P_k-\acute{\beta}\rho k\omega \quad (6\text{-}13)$$

$$\frac{\partial}{\partial x_j}(\rho\omega u_j)=\frac{\partial}{\partial x_j}\left[\left(\mu+\frac{\mu_t}{\sigma_{\omega 3}}\right)\frac{\partial \omega}{\partial x_j}\right]+2\rho(1-F1)\frac{1}{\sigma_{\omega 2}\omega}\frac{\partial k}{\partial x_j}\frac{\partial \omega}{\partial x_j}+\alpha\frac{\omega}{k}P_k - \beta_3\rho\omega^2 \quad (6\text{-}14)$$

For the detailed coefficients in equations (6-13) and (6-14), refer to Ref. [119].

6-4-3 Boundary conditions

In the present study, the geometry of the Tesla turbine is taken from [120] and is shown in Figure 6-4. All simulations are based on the Second Order Upwind scheme. The Tesla turbine model is designed in ANSYS Design Modeler; the structural mesh is generated using

commercial ANSYS package ICEM; the simulation is carried out in commercial CFD software ANSYS CFX solver. The turbine inlet boundary conditions are considered to be the inlet pressure and temperature, whereas the outlet conditions are characterized by the outlet pressure. In other words, the inlet and outlet conditions of the Tesla turbine is the condition of the working fluid after the gas cooler and the evaporator, respectively. The adiabatic and no-slip boundary condition is considered for all walls; for the rotor-stator interface, the frozen rotor method is applied [120].

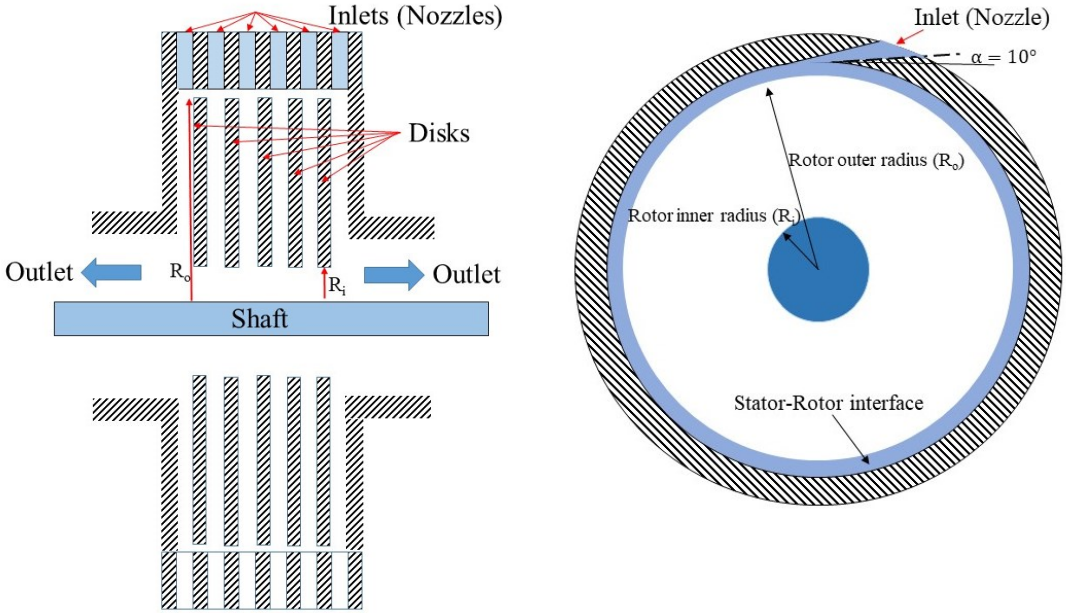

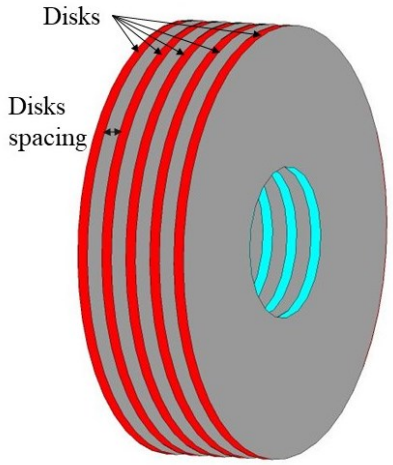

Figure 6-4. The geometry of the Tesla turbine (Stator and Rotor).

Table 6-2. The boundary condition of the Tesla turbine.

Inlet pressure	9-12 [MPa]
Inlet temperature	35 [°C]
Outlet pressure	3-4 [MPa]
Rotor speed	100, 500, 1000, 1500 and 2000 [rad/s]

Table 6-3. The Tesla turbine design dimensions [116].

Rotor outer diameter	100 [mm]
Rotor inner diameter	38.4 [mm]
Rotor disk thickness	1 [mm]
disk spacing	0.5 [mm]
Inlet nozzle angle	10˚
Number of disks	5

6-4-4 Mesh and grid independency

The mesh grid for the Tesla turbine is shown in Figure 6-5. A regular mesh is chosen rather than an irregular mesh, due to higher precision and lower computational time.

Mesh independency is important in CFD simulation. An optimum mesh number that means the results are independent of the grid number choice. Therefore, a 3D CFD analysis with three different mesh sizes (1.331 million, 1.425 million, and 2.05 million cells) was carried out. It found that the percentage of the relative variation of turbine power at1.331 million and 1.425 million cells is 1.7% and at 1.425 million and 2.05 million cells is 0.5%. Hence, a 1.425 million cell grid is chosen for the simulation. As it is shown in Figure 6-5, the mesh density between the rotor and stator is higher than the nozzle and rotor to capture the CO_2 flow behavior because of the CO_2 expansion after nozzle, its velocity increases (CO_2 Mach number reaches 1).

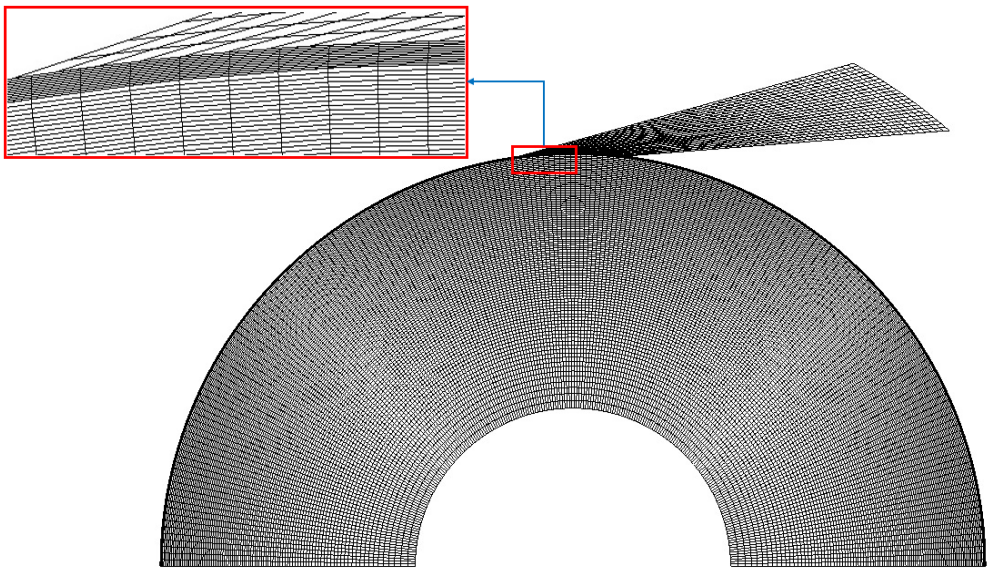

Figure 6-5. The Tesla turbine structural mesh.

6-4-5 Model validation

Table 6-4 compares the efficiency of the Tesla turbine of the current simulation with [120]. The inlet pressure is fixed at 346 kPa with Air as a working gas. It is observed that the result of the numerical model agrees well with [120] that the maximum difference is 8.6% at $\Omega = 30000$

r/min which the quality of the mesh could be the main reason to explain the differences. In the present study, grid quality is higher than 0.65.

Table 6-4. The Tesla turbine CFD validation.

Rotor angular velocity (r/min)	Efficiency in [120] (%)	Efficiency in the Current study (%)	Difference (%)
10000	12.1	12.8	5.7
20000	20.5	21.3	3.9
30000	24.4	26.5	8.6
40000	22.2	23.1	4

6-5 Thermodynamic analysis

The numerical analysis for the energy and exergy evaluation of a heat pump system with integration of the Tesla turbine was developed using the Engineering Equation Solver (EES) software. This section presents the CFD results of the Tesla turbine simulation and thermodynamic analysis of the heat pump cycle integrated with the Tesla turbine. The transiting exergy efficiency of the turbine will be used that takes into account internal and external losses (Equation (6-5)). In addition, the comparison between the semi-ideal heat pump cycle and the real heat pump cycle will be investigated to illustrate the vital effect of the Tesla turbine performance on the cycle. For the real cycle, the exergy loss in each component is not zero, which means the compressor efficiency is less than 100% and is calculated according to equation (6-1) ; it is also assumed that there is a 5 K temperature difference between the CO_2 and external fluids in the gas cooler and evaporator, at the cold end of the heat exchangers. The flow chart of the CFD simulation and thermodynamic analysis of the heat pump cycle is illustrated in Figure 6-6.

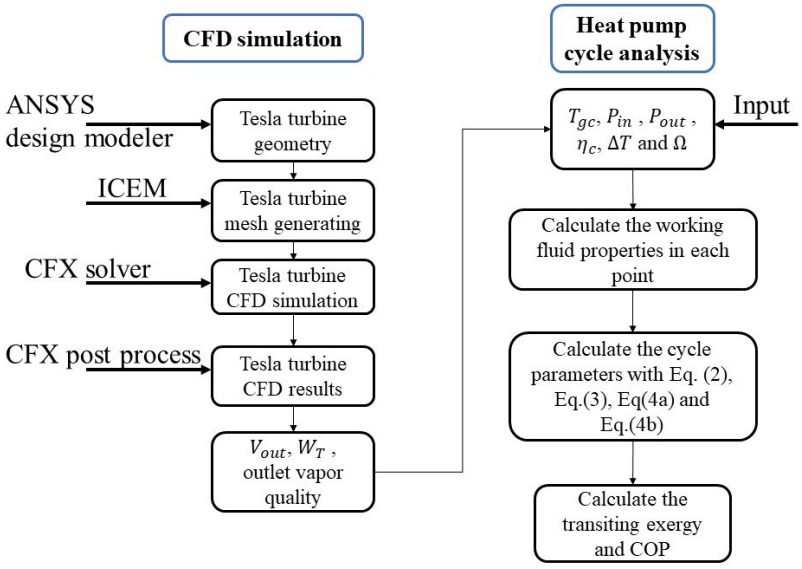

Figure 6-6. The flow chart of the heat pump analysis.

6-5-1 Flow coefficient and isentropic efficiency of the Tesla turbine

Figure 6-7 illustrates the Flow coefficient and isentropic efficiency of the Tesla turbine at 12 MPa. The flow coefficient and the isentropic efficiency of the Tesla turbine are calculated by equation (6-15) and equation (6-16):

$$C_m = \frac{V_r}{\Omega r} \tag{6-15}$$

$$\eta_{isentropic} = \frac{W_t}{\Delta h_{is}} \tag{6-16}$$

The flow coefficient depends on the average radial velocity of the working fluid and linear velocity of the rotor. With increasing the rotor angular velocity, the radial velocity and linear velocity increase however, the augmentation of linear velocity overcome the augmentation of the redial velocity that leads to decreasing the flow coefficient. The isentropic efficiency depends on the produced power of the turbine and isentropic power of the turbine. The isentropic power depends on the inlet condition and outlet pressure so it is constant for all rotor angular velocity at constant inlet and outlet pressures. With increasing the rotor angular velocity, the isentropic efficiency increases until optimum rotor angular velocity (1000 rad/s) and after that it decrease.

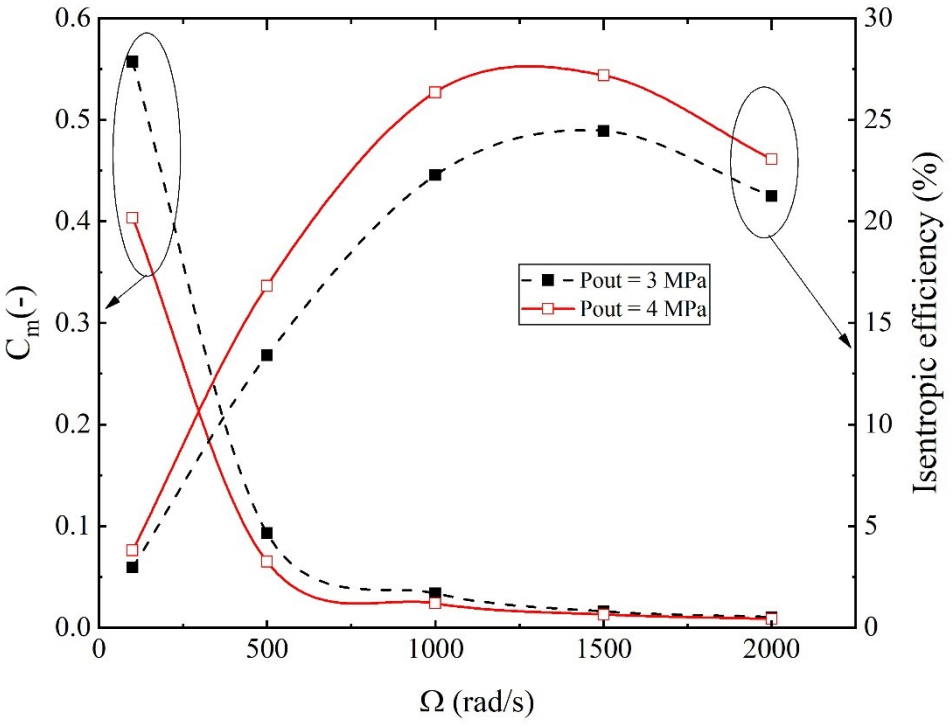

Figure 6-7. The Flow coefficient and isentropic efficiency.

The velocity triangle of the turbine and the enthalpy-entropy diagram of the expansion process in the tesla turbine for P_{in} = 12 MPa and P_{out} = 3 MPa is illustrated in Figure 6-8.

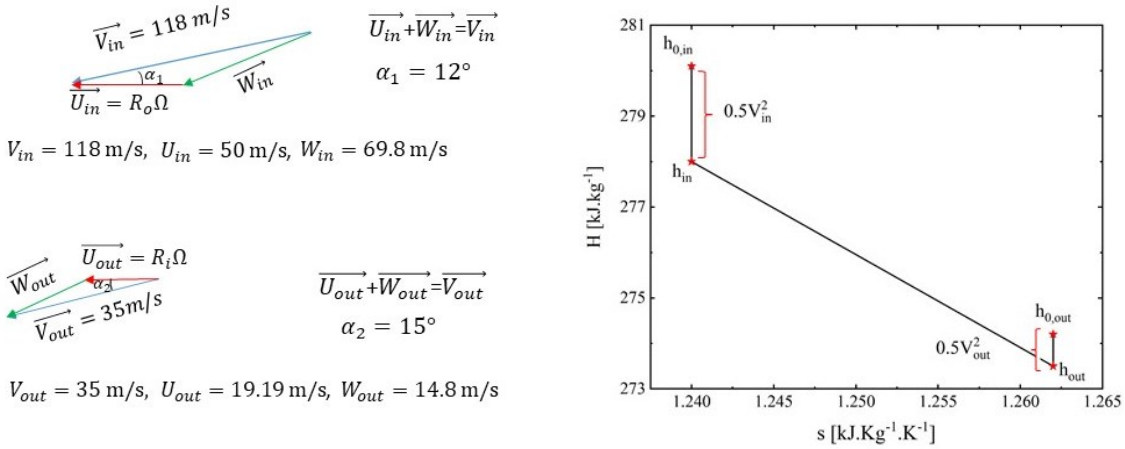

Figure 6-8. The velocity triangle and H-s diagram of the Tesla turbine.

6-5-2 The effect of rotor angular velocity on Tesla turbine exergy losses at constant inlet and outlet pressures

The effect of inlet and outlet pressures on the exergy loss of the semi-ideal and real heat pump cycles at different rotor angular velocities are indicated in Figure 6-9 and Figure 6-10, respectively. As has been indicated previously, the Tesla turbine exergy losses are divided into internal exergy losses due to entropy generation and external losses due to the velocity. It can be observed that the minimum exergy losses of semi-ideal and real cycles occur at the same operating parameter values, such as angular velocity, and turbine inlet and outlet pressures. It indicates the preponderant role of the turbine exergy losses on the total exergy losses of the overall supercritical cycle. To understand the physical causes of the influence of the inlet pressure outlet pressure and rotor angular velocity on the exergy losses will be conducted. Hence, the analysis of the impact of these parameters on the working fluid conditions such as the vapor quality and velocity at the outlet of the Tesla turbine as well as on the turbine power production will be investigated.

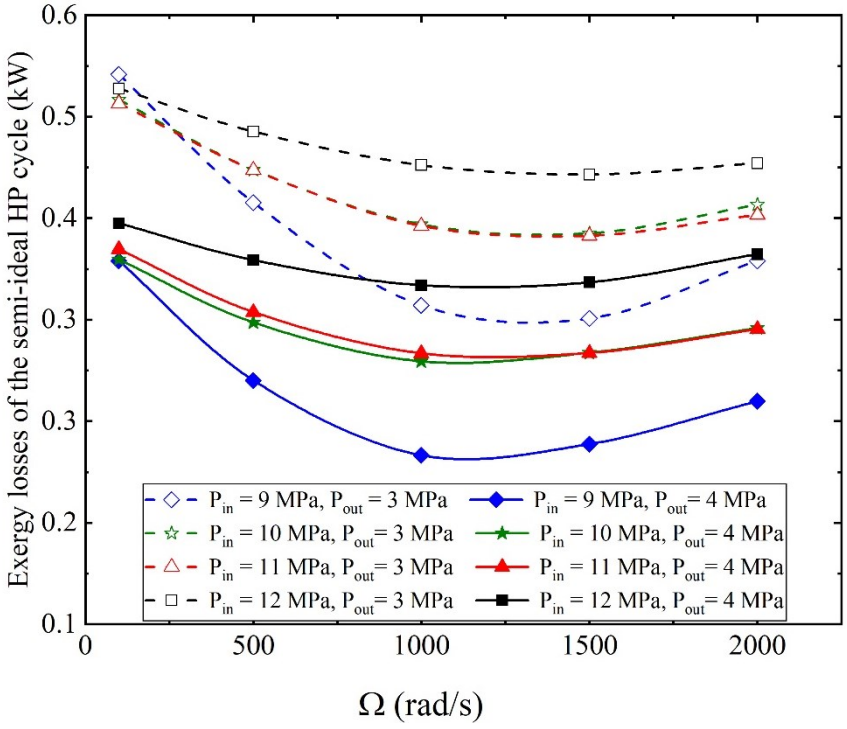

Figure 6-9. The effect of inlet and outlet pressures on exergy losses of the semi-ideal heat pump cycle at different rotor angular velocities.

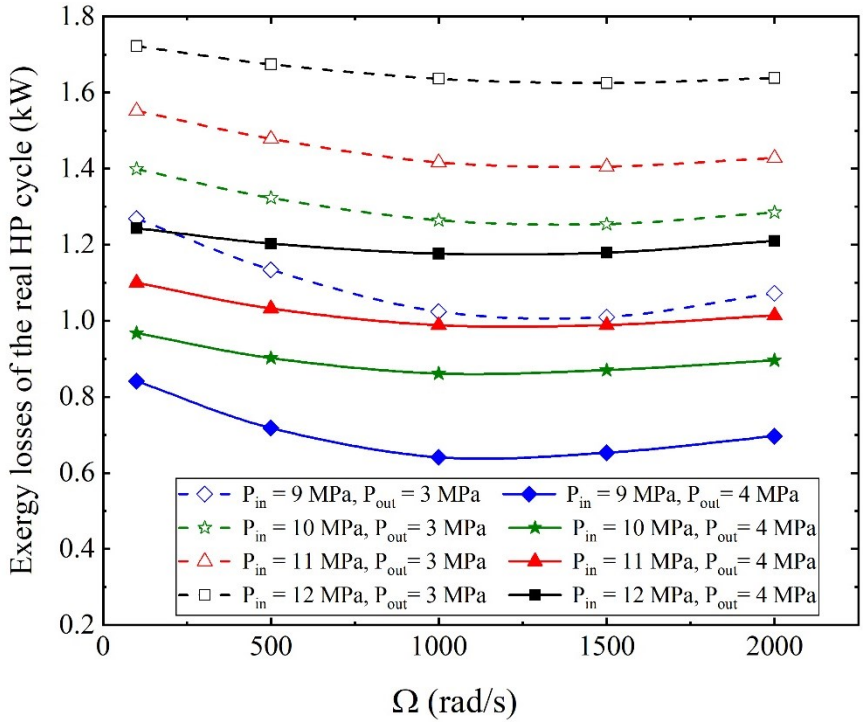

Figure 6-10. The effect of inlet and outlet pressures on exergy losses of the real heat pump cycle at different rotor angular velocities.

The turbine power can be defined either by thermodynamics or fluid dynamics. The thermodynamic definition of turbine power is based on the total enthalpy difference between the inlet and outlet of the turbine. The fluid dynamics definition of the turbine power is based on the torque (σ) multiplied by the rotor angular velocity (Ω). Therefore, the effect of the rotor angular velocity on the torque, and on the outlet vapor quality will be investigated in order to analyze the effect of rotor angular velocity on the Tesla turbine power.

The effect of rotor angular velocity on the torque is illustrated in Figure 6-11. As the rotor angular velocity increases, the torque decreases. This is due to the reduction in momentum exchange between the working fluid and the rotor disk. To clarify this fact, Figure 6-12 presents the effect of rotor angular velocity on Mach number, where the higher Mach number is associated with the lower rotor angular velocity. Therefore, the working fluid transfers more momentum to the disks at a lower angular velocity, so the velocity of the working fluid at the outlet is lower. Therefore, increasing the rotor angular velocity has both positive and negative effects on the power of the Tesla turbine. At first, the turbine power increases by increasing the

rotor angular velocity until the optimum point (1000 rad/s) and then the turbine power decreases with increasing rotor angular velocity. The effect of the rotor angular velocity on turbine power is illustrated in Figure 6-13.

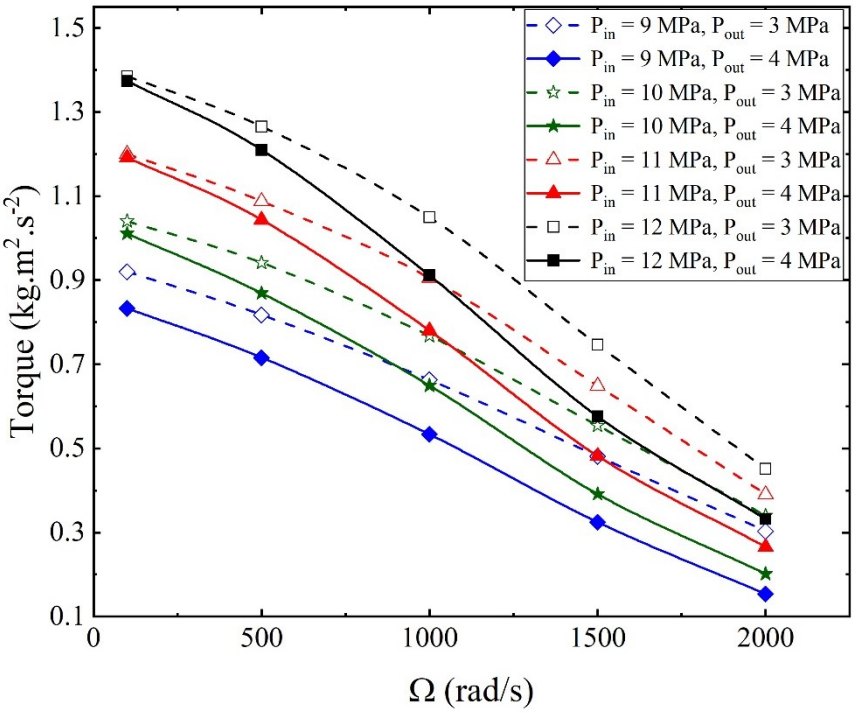

Figure 6-11. Effect of inlet and outlet pressures on torque at different rotor angular velocities.

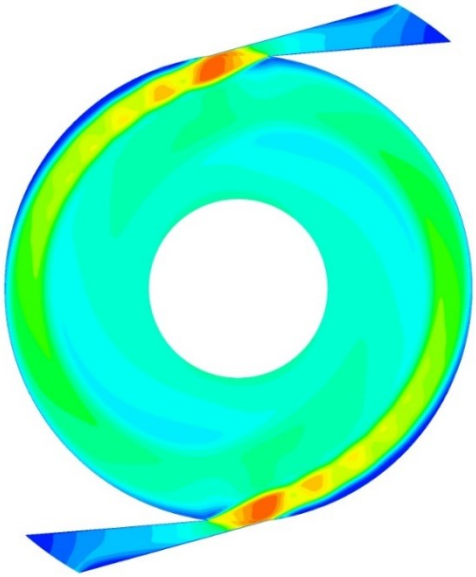

(a)

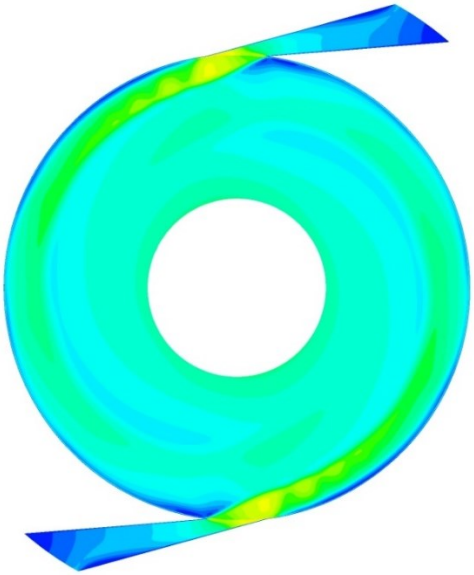

(b)

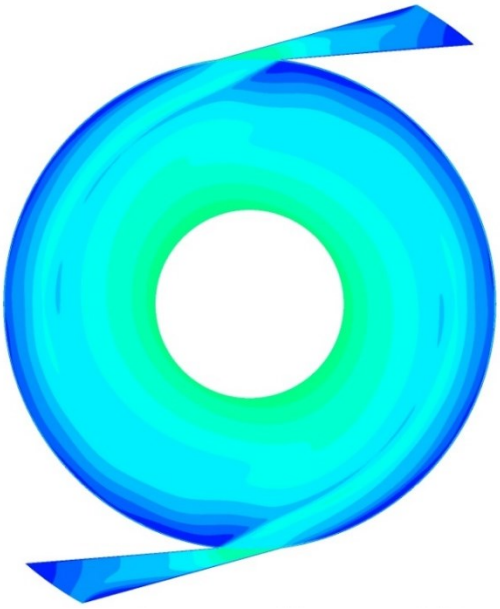

(c)

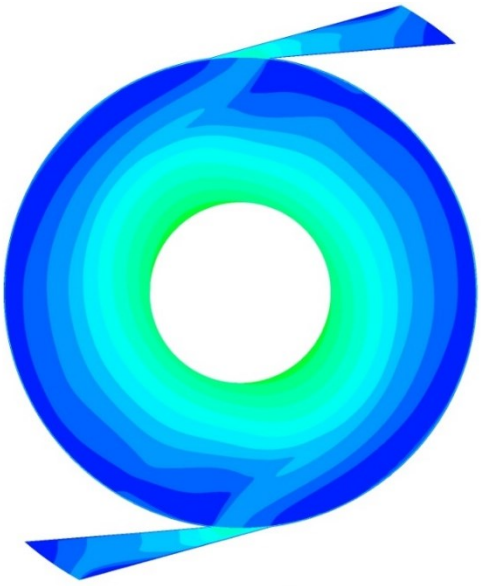

(d)

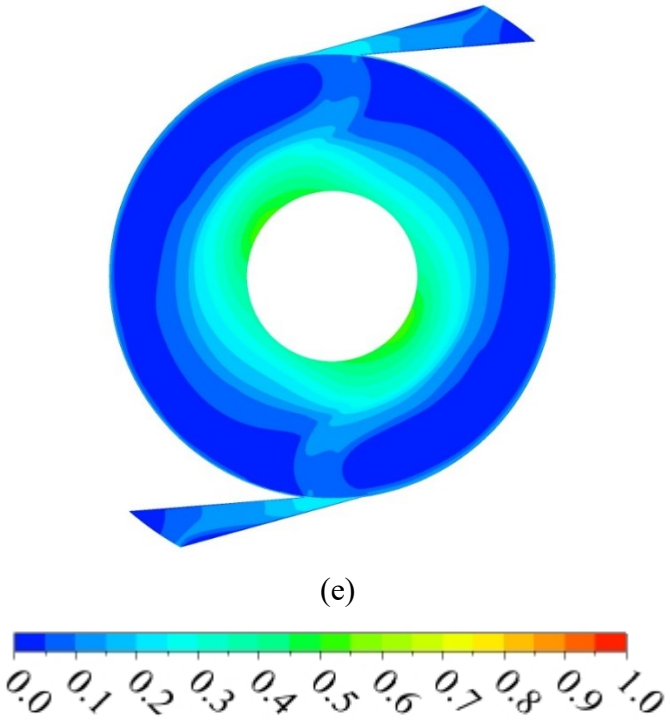

Figure 6-12. Mach number contours at the zone between disks 2 and 3 of Tesla turbine at (a)100 rad/s, (b)500 rad/s, (c)1000 rad/s, (d)1500 rad/s, and (e)2000 rad/s.

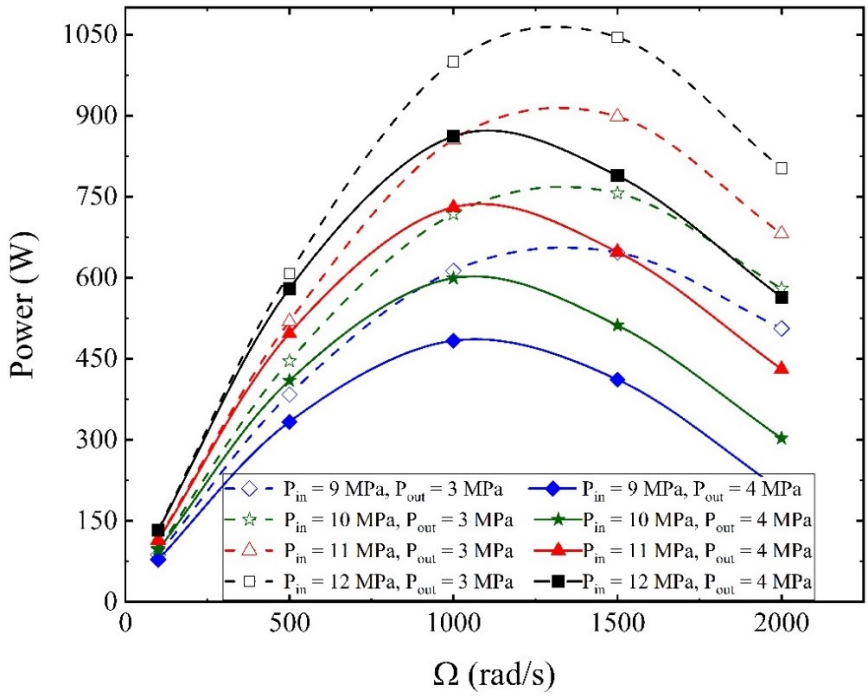

Figure 6-13. Effect of inlet and outlet pressures on Tesla turbine power at different rotor angular velocities.

Recall that the turbine power depends on the inlet and outlet static enthalpies and kinetic energies. The velocity of the working fluid at the turbine inlet is assumed to be zero, hence the inlet kinetic energy is zero. However, the velocity of the working fluid as it passes through the turbine is not negligible, and increases with rotor angular velocity. The working fluid kinetic energy of the tesla turbine outlet increases due to increasing velocity, which leads to increasing external exergy losses for the Tesla turbine. By considering constant inlet and outlet pressures, the total enthalpy at the inlet is constant for all rotor angular velocity but the static enthalpy and kinetic energy vary with rotor angular velocity. Raising the kinetic energy has a negative effect on the power of the turbine, so the static enthalpy expects to decrease in order to have a positive effect on the power of the turbine. Therefore the outlet quality of the vapor expects to decrease by increasing the rotor angular velocity, as is shown in Figure 6-14 which causes increasing the evaporator latent heat. What can be concluded is that the internal exergy losses of the Tesla turbine decrease with increasing rotor angular velocity due to the reduction of the outlet vapor quality. At $\Omega = 1000$ [rad/s], the Tesla turbine power is maximum for the outlet pressure equals to 4 MPa which varies from 450 W to 830 W.

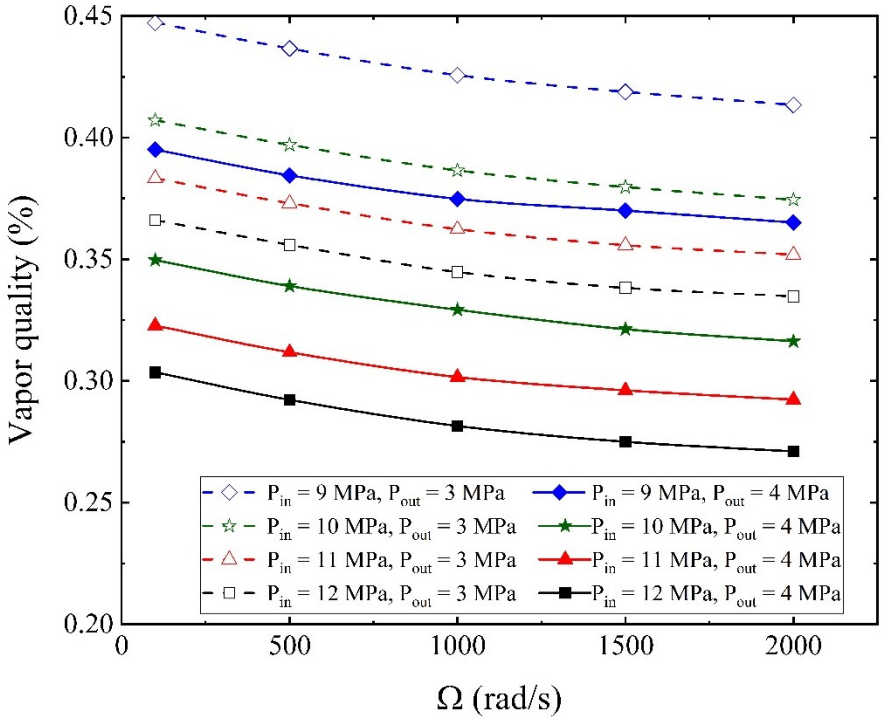

Figure 6-14. Effect of inlet and outlet pressures on outlet vapor quality at different rotor angular velocities.

The total losses of the turbine are the sum of the external and internal losses. By increasing the rotor angular velocity, the external losses increase and the internal losses decrease. For example, for an outlet pressure of 4 MPa, the optimum angular velocity is 1000 rad/s. Minimizing either the external or internal losses does not minimize the total exergy losses. It's obvious that the exergy losses of the real heat pump cycle should be higher than the exergy losses of the semi-ideal cycle due to the fact that in the semi-ideal cycle, the exergy loss of the compressor, evaporator, and gas cooler are zero. However, by comparing the two cycles, it can be seen that the minimum total exergy loss of both cycles occur at the same rotor angular velocity. The minimum exergy losses of the semi-ideal and real heat pump cycles occurs at the same inlet pressure equals to 9 MPa which are 0.27 kW and 0.65 kW, respectively.

6-5-3 The effect of inlet and outlet pressures on Tesla turbine exergy losses at constant angular velocity

This section explains the effect of the inlet and outlet pressures of the Tesla turbine on the exergy losses and it's worth mentioning that the inlet and outlet pressures of the Tesla turbine are the gas cooler and evaporator pressures, respectively.

At higher inlet pressure, the working fluid has a higher tangential velocity which the working fluid has a higher mass flow rate at constant geometry and density. The flow with higher tangential velocity and produces higher torque due to higher momentum so the torque at 12 MPa is greater than 9 MPa. In addition, the velocity is a result of the pressure drop and the pressure drop at 3 MPa is greater than 4 MPa which leads to higher velocity and higher momentum and consequently higher torque, which Figure 6-11 presents the effect of the inlet and outlet pressure as well rotor angular velocity on the torque. The working fluid outlet velocity increases by increasing the momentum, which causes the Tesla turbine external exergy loss to increase.

As was explained in section 6.5.2, the power of the turbine is expressed as the multiplication of torque and rotor angular velocity. Thus, torque is the only effective factor at constant rotor angular velocity, so increasing the inlet pressure and decreasing the outlet pressure leads to increasing the power of the Tesla turbine, as indicated in Figure 6-13. In

addition, by increasing the inlet pressure from 9 MPa to 12 MPa, the vapor quality at the exit of the Tesla turbine decreases from 0.447 to 0.366 at P_{out} = 3 MPa and rotational angular speed=100 rad/s. The reduction in pressure at the exit of the Tesla turbine from 4 MPa to 3 MPa causes an increase in the vapor quality due to the vaporizing of the liquid as the pressure drops, which is illustrated in Figure 6-14. Increasing the inlet pressure and decreasing the outlet pressure at constant rotor angular velocity leads to increasing the internal exergy loss of the turbine, due to the raising turbine pressure drop. By taking into account both internal and external exergy losses, it can be realized that at higher inlet pressure and lower outlet pressure, both internal and external exergy losses are higher so the total exergy loss of the tesla turbine is higher.

6-5-4 The effect of inlet and outlet pressures on transiting exergy efficiency of the turbine at different rotor angular velocity

The effect of the inlet and outlet pressures on the transiting exergy efficiency at different rotor angular velocities is illustrated in Figure 6-15. The specific transiting exergy e_{Tr} is independent of the inlet condition only depends on the outlet pressure. At constant inlet and outlet pressures, the specific exergy is constant and the Tesla turbine power is the only effective parameter (Equation (6-5)). As a result, the transiting exergy efficiency increases until the optimum angular velocity and beyond this optimum, the transiting exergy efficiency decreases. By decreasing the evaporator pressure, the nominator and the dominator of equation (6-5) increase, so the augmentation of the nominator overcomes the augmentation of the dominator, which leads to higher transiting exergy efficiency, except at P_{in} = 9 MPa. In addition, by increasing the inlet pressure, the nominator of equation (6-5) is constant, however, the dominator increases due to increasing the inlet exergy, which leads to lower transiting exergy efficiency. It is interesting to notice that the maximum transiting exergy efficiency occurs at the same operating condition values where the minimum total exergy losses of the Tesla turbine takes place. The maximum and transiting exergy efficiency occurs P_{in} = 9 MPa and Ω = 1000 rad/s which is 75%. The transiting exergy efficiency of ejector at Pin = 10 MPa was reported ([5]) as 59% and 5% at Pout = 3 MPa and Pout = 4 MPa which are lower than the Tesla turbine transiting exergy efficiency which proves that the Tesla turbine could be a better expansion

device.

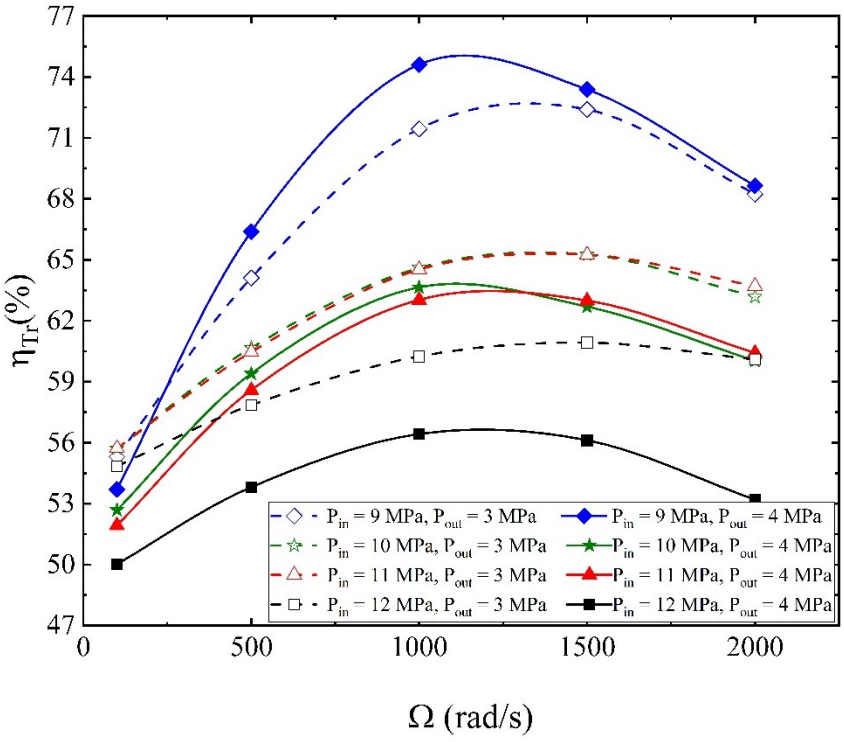

Figure 6-15. Effect of inlet and outlet pressures on Tesla turbine transiting exergy efficiency at different rotor angular velocities.

6-5-5 The effect of inlet and outlet pressures on COP of the heat pump cycle at different rotor angular velocities

The effect of the inlet and outlet pressures on the COP of the semi-ideal and real heat pump cycles at different rotor angular velocities are indicated in Figure 6-16 and Figure 6-17, respectively. The increase of the evaporator pressure leads to lower compressor work and consequently an increasing COP for the cycle. On the contrary, raising the gas cooler inlet pressure leads to higher compressor work and thus a smaller COP. Moreover, with an increase in the evaporator pressure, COP increases till the optimum rotor angular velocity (1000 rad/s) and beyond this optimum, the COP decreases due to the higher turbine power production at these points. The Maximum COP is 5.2 which occurs at Pin = 9 MPa, Pout = 4 MPa and Ω = 1000 rad/s. The COP of the semi-ideal heat pump cycle is higher than the COP of the real hat pump cycle because each component of the semi ideal heat pump cycle works at its maximum

performance (except the Tesla turbine). The maximum COP of both cycles takes place at the same optimum angular velocity, meaning that the turbine exergy losses have the most important influence on the performance of the real cycle, as measured by the COP.

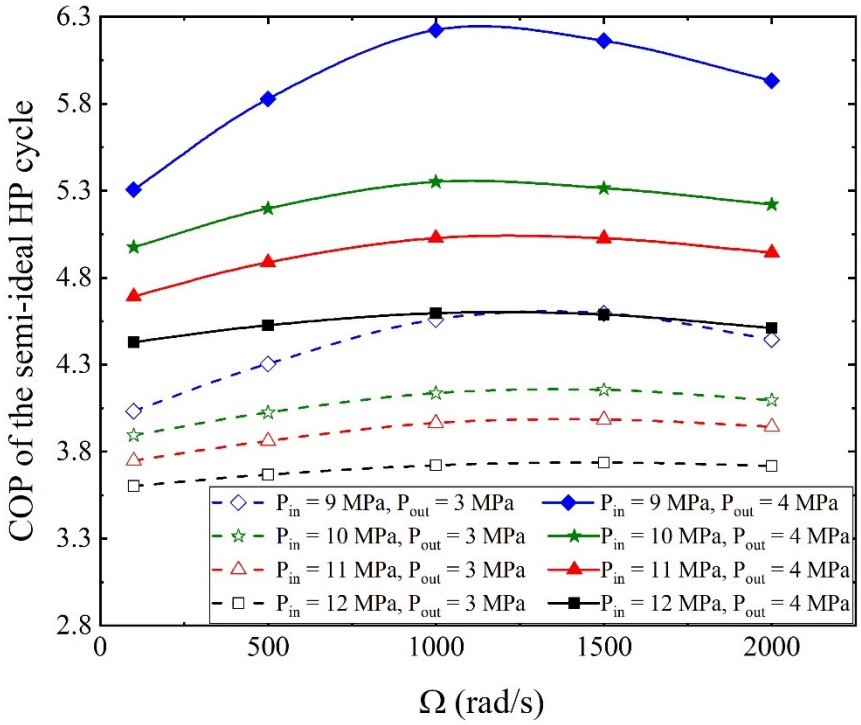

Figure 6-16. The effect of inlet and outlet pressures on COP of the semi-ideal heat pump cycle at different rotor angular velocities.

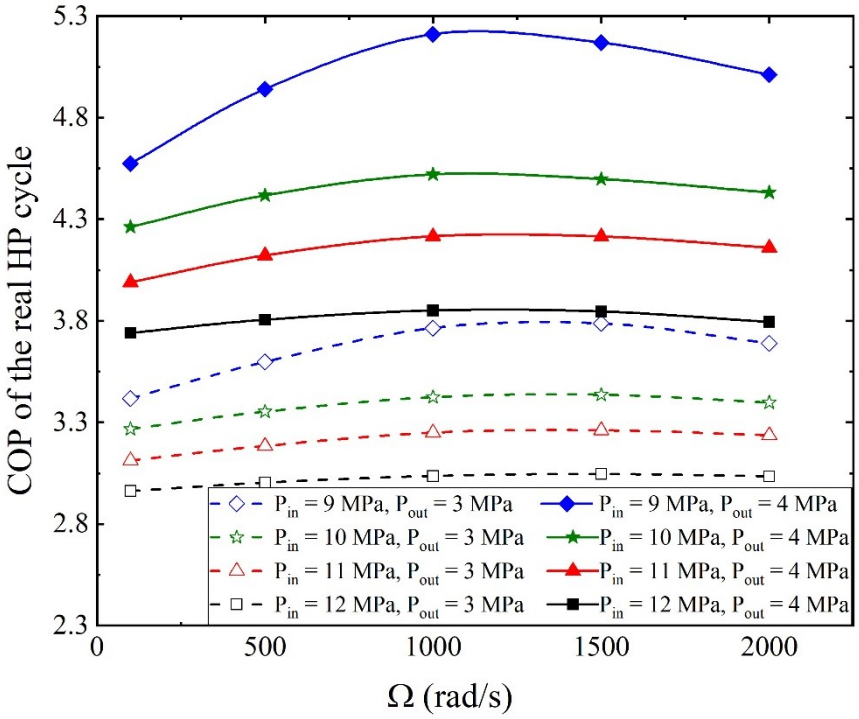

Figure 6-17. The effect of inlet and outlet pressures on COP of the real heat pump cycle at different rotor angular velocities.

6-5-6 Comparison of a cycle with an expansion valve and a cycle integrated with a Tesla turbine

Table 6-5 presents the vapor qualities at the exit of the Tesla turbine and the expansion valve. It also lists the COP for the cycle integrated with the turbine and the traditional one with the expansion valve. The values corresponding to different operating parameters of the cycles are illustrated. It can be noticed that at the optimal conditions (the angular velocity = 1000 rad/s, the inlet pressure = 9 MPa and the outlet pressure = 4 MPa) the vapor quality is 0.37. It is different from the vapor quality after the expansion valve, which is 0.40. The COP value of the cycle with the turbine under these conditions is 5.21, which is 16.3% higher than the COP=4.48 of the cycle with the expansion valve. The COP improvement of the heat pump cycle with the Tesla turbine is 16.3%, which is two times greater than the COP improvement of the heat pump cycle with ejector which is reported by [97]. In addition, the COP improvement by expander was reported as 30% because the expander efficiency was assumed as 65% [100].

Table 6-5. Vapor quality at the exits of the Tesla turbine and the expansion valve, and COP.

Inlet Pressure [MPa]	Outlet Pressure 4[MPa]					
	Vapor quality			COP		
	Tesla turbine		Expansion Valve	Heat pump integrated with Tesla turbine		Traditional heat pump
	1000 rad/s	2000 rad/s	-	1000 rad/s	2000 rad/s	-
9	0.37	0.36	0.40	5.21	5.01	4.48
10	0.33	0.32	0.36	4.52	4.43	4.22
11	0.31	0.29	0.33	4.22	4.16	3.95
12	0.28	0.27	0.31	3.85	3.79	3.72

6-6 Conclusions

In the present study, three-dimensional CFD simulation of the Tesla turbine is investigated with CO_2 as a compressible working fluid where the RGP table of CO_2 is coupled with the commercial ANSYS CFX solver to illustrate the Tesla turbine capacity as an expansion device. By employing the Tesla turbine instead of the expansion valve, the working fluid vapor quality decreases, which leads to the higher evaporator latent heat. In addition, by increasing the inlet pressure from 9 MPa to 12 MPa, the vapor quality at the exit of the Tesla turbine decreases from 0.447 to 0.366. This phenomenon, combined with the power production from the turbine, leads to an increase in the cycle COP by 16.3% compared to the classical cycle with an expansion valve. The Maximum COP is 5.2 which occurs at Pin = 9 MPa, Pout = 4 MPa and Ω = 1000 rad/s. Increasing the inlet pressure leads to increasing the Tesla turbine power and decreasing the vapor quality at the exit of the turbine. Increasing the rotor angular velocity, leads to lower vapor quality at the outlet of the turbine and decreasing the torque production. The maximum value of turbine exergy transiting exergy efficiency, as a function of rotor angular velocity, provides the maximum value of COP for the overall transcritical CO_2 cycle.

6-7 Acknowledgments

This project is a part of the Collaborative Research and Development (CRD) Grants Program at “Université de Sherbrooke”. The authors acknowledge the support of the Natural Sciences and Engineering Research Council of Canada, Hydro-Québec, Rio Tinto, Alcan and Canmet ENERGY Research Center of Natural Resources Canada (RDCPJ451917-13).

6-8 Nomenclature

A	area, m^2
COP	coefficient of performance
EoS	equation of state
ex	specific exergy, kJ kg^{-1} K^{-1}
$\dot{E}$	exergy rate, kW
h	specific enthalpy, kJ kg^{-1}
H	enthalpy, kW
HEM	homogeneous equilibrium
$\dot{I}$	exergy loss, kW
k	turbulence kinetic energy, m^2 s^{-2}
$\dot{m}$	mass flow rate, kg s^{-1}
P	pressure, MPa
$\dot{Q}$	thermal power, W
R	gas constant, J mol^{-1} K^{-1}
$\dot{S}$	entropy rate, W K^{-1}
s	specific entropy, kJ kg^{-1} K^{-1}
t	time, s
T	temperature, °C or K
u_i	fluid velocity component in xi-direction, m s^{-1}
V	velocity, m s^{-1}
$\dot{W}$	power, W
x_i	coordinates

Subscripts

D	Destruction
in	Inlet
i, j, k	Cartesian indices
l	Liquid
out	out
ph	Physical
sat	Saturate
T	Turbine
Tr	Transitive
v	Vapor
w	Work

Greek symbols

ν	specific volume, $m^3\ kg^{-1}$
η	Efficiency
ρ	density, $kg\ m^{-3}$
μ	dynamic viscosity, $kg\ m^{-1}\ s^{-1}$
Ω	rotor angular velocity, $rad\ s^{-1}$
τ	stress tensor, $N\ m^{-2}$
σ	Torque, N m
ω	specific dissipation

Chapter 7

CONCLUSION AND FUTURE VIEW

Conclusion de la thèse

L'objectif principal de cette étude était d'introduire un nouveau dispositif d'expansion pour réduire les pertes d'exergie pendant le processus d'expansion du système de pompe à chaleur transcritique au CO_2. Pour atteindre cet objectif, deux dispositifs d'extension différents, à savoir; le tube vortex et la turbine Tesla ont été choisis. La simulation CFD a été réalisée pour étudier les pertes d'exergie et les efficacités exergetiques de ces deux appareils. L'étape suivante consiste à mettre en œuvre chaque dispositif d'expansion à l'intérieur du système d'une pompe à chaleur pour évaluer l'impact de ces pertes sur le COP du système entier.

Dans le chapitre 3, la simulation CFD d'un tube vortex basse pression avec du CO_2 comme gaz de travail a été étudiée pour évaluer la capacité du tube vortex à la séparation d'énergie. Les résultats ont montré que la pression d'entrée a un effet positif sur la séparation de température à l'intérieur du tube vortex.

Au chapitre 4, la simulation CFD d'un tube vortex haute pression a été étudiée. Un tableau des propriétés des gaz réels du CO_2 (RGP) à très haute résolution est générée et couplé au solveur ANSYS CFX du logiciel CFD commercial. Les résultats ont montré que la différence de température est relativement faible lorsque la pression d'entrée est élevée.

Au chapitre 5, le tube vortex a été intégrée au système de pompe à chaleur transcritique pour récupérer partiellement les pertes d'étranglement. Le COP du nouveau système de pompe à chaleur a augmenté de 8% par rapport au système de pompe à chaleur traditionnel.

Auchapitre 6, la turbine Tesla en tant qu'un nouveau dispositif d'expansion a été introduite pour améliorer le système de pompe à chaleur en effectuant partiellement la récupération du travail. La simulation CFD de la turbine Tesla a été réalisée à différentes pressions d'entrée. Les

résultats ont indiqué que la turbine Tesla est le meilleur dispositif d'expansion dont le COP du système a été amélioré de 16,3%.

Travail futur et perspective

Dans l'étude actuelle, la turbine Tesla a été présentée comme une machine d'expansion intéressante en raison de son efficacité et de sa capacité à travailler avec des fluides biphasés. Le premier sujet de travaux futurs peut être l'étude des paramètres géométriques de la turbine Tesla tels que le nombre de buses d'entrée, le diamètre du disque rotatif, etc. pour atteindre le meilleur rendement et réduire les pertes d'expansion du système de pompe à chaleur. En outre, il peut être intéressant d'analyser expérimentalement le système de pompe à chaleur intégré à la turbine Tesla.

Le deuxième sujet de travaux futurs peut être l'analyse expérimentale du tube vortex avec un fluide de travail haute pression et l'intégrer au système de pompe à chaleur transcritique pour évaluer l'effet du tube vortex sur le COP de la pompe à chaleur.

Thesis conclusions

The main objective of this study was to introduce a novel expansion device to reduce the exergy losses during the expansion process for the transcritical CO_2 heat pump system. To achieve this purpose, two different expansion devices, namely; the vortex tube and Tesla turbine were chosen. The CFD simulation has been carried out to investigate the exergy losses and exergy efficiencies on both devices. The next step was to implement each expansion device to evaluate the COP of the heat pump system.

In chapter 3, the CFD simulation of a low-pressure vortex tube with CO_2 as a working gas was investigated to evaluate the vortex tube capability to energy separation. The results showed that the inlet pressure has a positive effect on the temperature separation inside the vortex tube.

In chapter 4, the CFD simulation of a high-pressure vortex tube was investigated. A CO_2 real gas properties (RGP) table with very-high-resolution is generated and is coupled with

commercial CFD software ANSYS CFX solver. The results showed that the temperature difference is relatively low when the inlet pressure is high.

In chapter 5, the vortex tube was integrated with the transcritical heat pump system to partially recover the throttling losses. The COP of the novel heat pump system raised 8% in comparison with the traditional heat pump system.

In chapter 6, the Tesla turbine as a new expansion device was introduced to improve the heat pump system by partially making work recovery. The CFD simulation of the Tesla turbine was carried out at different inlet pressures. The results indicated that the Tesla turbine is the best expansion device and the COP of the system was 16.3% improved.

Future work and perspective

In the current study, the Tesla turbine was introduced as an interesting expansion machine due to its efficiency and capability of working with two-phase fluids. The first subject for future work can be the investigation of geometrical parameters of the Tesla turbine such as the number of inlet nozzle, the diameter of the rotating disk, etc. to achieve the highest efficiency and reduce the expansion losses of the heat pump system. Besides, it can be beneficial to analyze the heat pump system integrated with the Tesla turbine experimentally.

The second subject for future work can be the analysis of the vortex tube with high-pressure working fluid experimentally and integrate with the transcritical heat pump system to evaluate the effect of the vortex tube on the COP of the heat pump.

The results of this Ph.D. study have been published in the following international journals and conference:

Journals

- A. Aghagoli, M. Sorin, Thermodynamic performance of a CO_2 vortex tube based on 3D CFD flow analysis, International Journal of Refrigeration. 108 (2019) 124–137, https://doi.org/10.1016/j.ijrefrig.2019.08.022.
- A. Aghagoli, M. Sorin, CFD modelling and exergy analysis of a heat pump cycle with Tesla turbine using CO_2 as a working fluid, Applied Thermal Engineering. 178 (2020) 115587. https://doi.org/10.1016/j.applthermaleng.2020.115587.
- Aghagoli, M. Sorin, 3D CFD modelling and exergy loss minimization within a high-pressure vortex tube, International Journal of Refrigeration (under review)

Conference

- A. Aghagoli, M. Sorin, S. Poncet, Thermodynamics analysis of a novel transcritical CO_2 vortex tube heat pump cycle. Sherbooke, Canada, 2019.

LIST OF REFERENCES

[1] E.A. Groll, J. Kim, Review Article : Review of Recent Advances toward Transcritical CO2 Cycle Technology, HVAC&R Res. 13 (2007).

[2] G. Myhre, D. Shindell, J. Pongratz, Anthropogenic and natural radiative forcing, Clim Chang. (2014) 659–740.

[3] X. Peng, D. Wang, G. Wang, Y. Yang, S. Xiang, Numerical investigation on the heating performance of a transcritical CO 2 vapor-injection heat pump system, Appl. Therm. Eng. 166 (2020) 114656. doi:10.1016/j.applthermaleng.2019.114656.

[4] J. Han, M. Cui, J. Chen, W. Lv, Analysis of thermal performance and economy of ground source heat pump system: a case study of the large building, Geothermics. 89 (2021) 101929. doi:10.1016/j.geothermics.2020.101929.

[5] S. Taslimi Taleghani, M. Sorin, S. Poncet, Analysis and Optimization of Exergy Flows inside a Transcritical CO 2 Ejector for Refrigeration, Air Conditioning and Heat Pump Cycles, Energies. 12 (2019).

[6] P. Maina, Z. Huan, A review of carbon dioxide as a refrigerant in refrigeration technology, S. Afr. J. Sci. 111 (2015) 1–10. doi:10.17159/sajs.2015/20140258.

[7] M.M. Rashidi, A. Aghagoli, R. Raoofi, Thermodynamic analysis of the ejector refrigeration cycle using the artificial neural network, Energy. 129 (2017). doi:10.1016/j.energy.2017.04.089.

[8] N.. Gay, Refrigerating system. U.S. Patent 1,836,318, 1931.

[9] Z. Zhang, L. Tian, Effect of Suction Nozzle Pressure Drop on the Performance of an Ejector-Expansion Transcritical CO2 Refrigeration Cycle, Entropy. 16 (2015) 4309–4321. doi:10.3390/e16084309.

[10] D. Li, E.A. Groll, Transcritical CO 2 refrigeration cycle with ejector-expansion device, Int. J. Refrig. 28 (2005) 766–773. doi:10.1016/j.ijrefrig.2004.10.008.

[11] S. Taslimi Taleghani, M. Sorin, S. Poncet, H. Nesreddine, Performance investigation of a two-phase transcritical CO 2 ejector heat pump system, Energy Convers. Manag. 185 (2019) 442–454. doi:10.1016/j.enconman.2019.02.004.

[12] Z. Aidoun, K. Ameur, M. Falsafioon, M. Badache, Current Advances in Ejector Modeling, Experimentation and Applications for Refrigeration and Heat Pumps. Part 2: Two-Phase Ejectors, Invention. 4 (2019) 1–54. doi:10.3390/inventions4010016.

[13] T. Sharma Karthikeya, G. Amba Prasad Rao, K. Madhu Murthy, Numerical Analysis of a Vortex Tube : A Review, Arch. Comput. Methods Eng. 24 (2017) 251–280. doi:10.1007/s11831-016-9166-3.

[14] N.F. Aljuwayhel, G.F. Nellis, S.A. Klein, Parametric and internal study of the vortex tube using a CFD model, Int. J. Refrig. 28 (2005) 442–450. doi:10.1016/j.ijrefrig.2004.04.004.

[15] S.E. Rafiee, M.M. Sadeghiazad, Three-dimensional and experimental investigation on the effect of cone length of throttle valve on thermal performance of a vortex tube using k-ε turbulence model, Appl. Therm. Eng. 66 (2014) 65–74. doi:10.1016/j.applthermaleng.2014.01.073.

[16] S.E. Rafiee, M.M. Sadeghiazad, Experimental and 3D CFD analysis on optimization of geometrical parameters of parallel vortex tube cyclone separator, Aerosp. Sci. Technol. 63 (2017) 110–122. doi:10.1016/j.ast.2016.12.014.

[17] J. Lagrandeur, S. Croquer, S. Poncet, M. Sorin, International Journal of Heat and Mass Transfer Exergy analysis of the flow process and exergetic optimization of counterflow vortex tubes working with air, Int. J. Heat Mass Transf. 152 (2020) 119527. doi:10.1016/j.ijheatmasstransfer.2020.119527.

[18] D. Li, J.S. Baek, E.A. Groll, P.B. Lawless, Thermodynamic analysis of vortex tube and work output expansion devices for the transcritical carbon dioxide cycle, in: Proc. 4th IIR-Gustav Lorentzen Conf. Nat. Work. Fluids, Purdue Univ., West Lafayette, IN, 2000: pp. 433–440.

[19] H.. Huff, R. Radermacher, CO2 compressor–expander analysis. Arlington, VA: Air-Conditioning and Refrigeration Technology Institute., 2003.

[20] M. Fukuta, T. Yanagisawa, M. Higashiyama, M. Fukuta, Performance of Vane-Type CO 2 Expander and Characteristics of Transcritical Expansion Process, HVAC&R Res. 15 (2009) 711–727.

[21] N. Tesla, Turbine, U.S. Patent No.1 061 206, 1913.

[22] J. Song, C. Gu, X. Li, Performance estimation of Tesla turbine applied in small scale Organic Rankine Cycle (ORC) system, Appl. Therm. Eng. 110 (2017) 318–326. doi:10.1016/j.applthermaleng.2016.08.168.

[23] C. Schosser, S. Lecheler, M. Pfitzner, Analytical and Numerical Solutions of the Rotor Flow in Tesla Turbines, Period. Polytech. Mech. Eng. 61 (2017) 12–22. doi:10.3311/PPme.9000.

[24] A. Guha, S. Sengupta, The fluid dynamics of the rotating flow in a Tesla disc turbine, Eur. J. Mech. B/Fluids. 37 (2013) 112–123. doi:10.1016/j.euromechflu.2012.08.001.

[25] A. Guha, B. Smiley, Experiment and analysis for an improved design of the inlet and nozzle in Tesla disc turbines, Proc. IMechE Part A J. Power Energy. 224 (2009) 261–277. doi:10.1243/09576509JPE818.

[26] K.J. Chua, S.K. Chou, W.M. Yang, Advances in heat pump systems : A review, Appl. Energy. 87 (2010) 3611–3624. doi:10.1016/j.apenergy.2010.06.014.

[27] G. Besagni, R. Mereu, F. Inzoli, Ejector refrigeration : A comprehensive review, Renew. Sustain. Energy Rev. 53 (2016) 373–407. doi:10.1016/j.rser.2015.08.059.

[28] K.D. Devade, A.T. Pise, Issues and prospects of energy separation in vortex tubes: Review, Heat Transf. - Asian Res. (2017) 1–31. doi:10.1002/htj.21313.

[29] T. Dutta, K.P. Sinhamahapatra, S.S. Bandyopadhyay, CFD Analysis of Energy Separation in Ranque-Hilsch Vortex Tube at Cryogenic CFD Analysis of Energy Separation in Ranque-Hilsch Vortex Tube at Cryogenic Temperature, (2013).

doi:10.1155/2013/562027.

[30] R. Hilsch, The use of the expansion of gases in a centrifugal field as cooling process, Rev. Sci. Instrum. 18 (1947) 108–113. doi:10.1063/1.1740893.

[31] B. Ahlborn, S. Groves, FLUID DYNAMICS Secondary flow in a vortex tube, Fluid Dyn. Res. 21 (1997) 73–86.

[32] B.K. Ahlborn, J.U. Keller, E. Rebhan, The heat pump in a vortex tube, J. Non-Equilibrium Thermodyn. 23 (1998) 159–165. doi:10.1515/jnet.1998.23.2.159.

[33] U. Behera, P.J. Paul, S. Kasthurirengan, R. Karunanithi, S.N. Ram, K. Dinesh, S. Jacob, CFD analysis and experimental investigations towards optimizing the parameters of Ranque-Hilsch vortex tube, Int. J. Heat Mass Transf. 48 (2005) 1961–1973. doi:10.1016/j.ijheatmasstransfer.2004.12.046.

[34] M.O. Hamdan, S.B. Al-omari, A.S. Oweimer, Experimental study of vortex tube energy separation under di ff erent tube design, Exp. Therm. Fluid Sci. 91 (2018) 306–311. doi:10.1016/j.expthermflusci.2017.10.034.

[35] A.D. Gutak, Experimental investigation and industrial application of Ranque-Hilsch vortex tube, Int. J. Refrig. 49 (2015) 93–98. doi:10.1016/j.ijrefrig.2014.09.021.

[36] Y. Xue, M. Arjomandi, R. Kelso, Experimental study of the thermal separation in a vortex tube, Exp. Therm. Fluid Sci. 46 (2013) 175–182. doi:10.1016/j.expthermflusci.2012.12.009.

[37] X. Han, N. Li, K. Wu, Z. Wang, L. Tang, G. Chen, X. Xu, The influence of working gas characteristics on energy separation of vortex tube, Appl. Therm. Eng. 61 (2013) 171–177. doi:10.1016/j.applthermaleng.2013.07.027.

[38] N. Agrawal, S.S. Naik, Y.P. Gawale, Experimental investigation of vortex tube using natural substances, Int. Commun. Heat Mass Transf. 52 (2014) 51–55. doi:10.1016/j.icheatmasstransfer.2014.01.009.

[39] H.R. Thakare, A. Monde, A.D. Parekh, Experimental, computational and optimization

studies of temperature separation and flow physics of vortex tube: A review, Renew. Sustain. Energy Rev. 52 (2015) 1043–1071. doi:10.1016/j.rser.2015.07.198.

[40] H.R. Thakare, A.D. Parekh, Computational analysis of energy separation in counter-flow vortex tube, Energy. 85 (2015) 62–77. doi:10.1016/j.energy.2015.03.058.

[41] S.E. Rafiee, M.M. Sadeghiazad, Experimental and 3D CFD investigation on heat transfer and energy separation inside a counter flow vortex tube using different shapes of hot control valves, Appl. Therm. Eng. 110 (2017) 648–664. doi:10.1016/j.applthermaleng.2016.08.166.

[42] M.R. and A.H. N. Pourmahmoud, S.E Rafiee, Numerical Energy Separation analysis on the commercial Ranque-Hilsch vortex tube on basis of application of different gases, Sci. Iran. Trans. B Mech. Eng. 20 (2013) 1528–1537.

[43] U. Behera, P.J. Paul, K. Dinesh, S. Jacob, Numerical investigations on flow behaviour and energy separation in Ranque-Hilsch vortex tube, Int. J. Heat Mass Transf. 51 (2008) 6077–6089. doi:10.1016/j.ijheatmasstransfer.2008.03.029.

[44] S. Mohammadi, F. Farhadi, Experimental and numerical study of the gas-gas separation efficiency in a Ranque-Hilsch vortex tube, Sep. Purif. Technol. 138 (2014) 177–185. doi:10.1016/j.seppur.2014.10.022.

[45] V. Kırmacı, O. Uluer, K. Dincer, An Experimental Investigation of Performance and Exergy Analysis of a Counterflow Vortex Tube Having Various Nozzle Numbers at Different Inlet Pressures of Air, Oxygen, Nitrogen, and Argon, J. Heat Transfer. 132 (2010) 121701. doi:10.1115/1.4002284.

[46] P. Grassmann, Zur allgemeinen Definition des Wirkungsgrades, Chemie Ing. Tech. 22 (1950) 77–80. doi:10.1002/cite.330220402.

[47] V.M, Brodyansky, M. Sorin, P. Legoff, The efficiency of industrial processes: energy analysis and optimization, in: Amsterdam : Elsevier Science B. V, 1994.

[48] M. Sorin, M. Khennich, Exergy Flows Inside Expansion and Compression Devices

Operating below and across Ambient Temperature, in: Energy Syst. Environ., InTech, 2018. doi:10.5772/intechopen.74041.

[49] X. Guo, B. Zhang, B. Liu, X. Xu, A critical review on the flow structure studies of Ranque – Hilsch vortex tubes Examen critique des études de structure d ' écoulement des tubes vortex de, Int. J. Refrig. 104 (2019) 51–64. doi:10.1016/j.ijrefrig.2019.04.030.

[50] G. Ranque, Experiments on expansion in a vortex with simultaneous exhaust of hot air and cold air., J Phys Radium. 4 (1933) 112–115.

[51] J.V.S. Technol, Y. Xue, M. Jafarian, A. Choudhry, M. Arjomandi, The Expansion Process in a Counter-flow Vortex Tube, J. Vor. Sci. Technol. 02 (2015) 1–6. doi:10.4172/2090-8369.1000114.

[52] F. Liang, H. Wang, X. Wu, Study on energy separation characteristics inside the vortex tube at high operating pressure, Therm. Sci. Eng. Prog. 14 (2019) 100432. doi:10.1016/j.tsep.2019.100432.

[53] V. Kirmaci, H. Kaya, Effects of working fluid , nozzle number , nozzle material and connection type on thermal performance of a Ranque – Hilsch vortex tube : A review, Int. J. Refrig. 91 (2018) 254–266. doi:10.1016/j.ijrefrig.2018.05.005.

[54] A. Aghagoli, M. Sorin, Thermodynamic performance of a CO 2 vortex tube based on 3D CFD flow analysis Performance, Int. J. Refrig. 108 (2019) 124–137. doi:10.1016/j.ijrefrig.2019.08.022.

[55] A. Ouadha, M. Baghdad, Y. Addad, Effects of variable thermophysical properties on flow and energy separation in a vortex tube, Int. J. Refrig. 36 (2013) 2426–2437. doi:10.1016/j.ijrefrig.2013.07.018.

[56] H. Kaya, O. Uluer, E. Kocao, V. Kirmaci, Experimental analysis of cooling and heating performance of serial and parallel connected counter-flow Ranquee – Hilsch vortex tube systems using carbon dioxide as a working fluid Analyse expérimentale des performances de refroidissement et de chauffage d, Int. J. Refrig. 106 (2019) 297–307. doi:10.1016/j.ijrefrig.2019.07.004.

[57] V. Kirmaci, Exergy analysis and performance of a counter flow Ranque – Hilsch vortex tube having various nozzle numbers at different inlet pressures of oxygen and air, Int. J. Refrig. 32 (2009) 1626–1633. doi:10.1016/j.ijrefrig.2009.04.007.

[58] K. Zhang, M. Liu, Y. Zhao, C. Wang, J. Yan, Entropy generation versus transition time of heat exchanger during transient processes, Energy. (2020) 117490. doi:10.1016/j.energy.2020.117490.

[59] A. Omidvar, M. Ghazikhani, S.M.R. Rezavi Modarres, Entropy analysis of a solar-driven variable geometry ejector using computational fluid dynamics, Energy Convers. Manag. 119 (2016) 435–443. doi:10.1016/j.enconman.2016.03.090.

[60] A. Khait, A. Noskov, V. Alekhin, V. Bianco, Analysis of the local entropy generation in a double-circuit vortex tube, Appl. Therm. Eng. 130 (2018) 1391–1403. doi:10.1016/j.applthermaleng.2017.11.136.

[61] A. Bejan, Entropy generation minimization : The new thermodynamics of finite-size devices and finite-time processes, J. Appl. Phys. 79 (2017) 1191–1218.

[62] Z. Wang, K.O. Suen, Numerical comparisons of the thermal behaviour of air and refrigerants in the vortex tube, Appl. Therm. Eng. 164 (2020) 114515. doi:10.1016/j.applthermaleng.2019.114515.

[63] K.I. Matveev, J. Leachman, Numerical investigation of vortex tubes with extended vortex chambers, Int. J. Refrig. 108 (2019) 145–153. doi:10.1016/j.ijrefrig.2019.08.030.

[64] L.M.. Zangana, R.R.I. Barwari, The effect of convergent-divergent tube on the cooling capacity of vortex tube : An experimental and numerical study, Alexandria Eng. J. (2020). doi:10.1016/j.aej.2019.12.036.

[65] M.A. Qyyum, A.A. Noon, F. Wei, M. Lee, Vortex tube shape optimization for hot control valves through computational fluid dynamics, Int. J. Refrig. 102 (2019) 151–158. doi:10.1016/j.ijrefrig.2019.02.014.

[66] J. Chen, R. Zeng, W. Zhang, L. Qiu, X. Zhang, Numerical analysis of energy separation

in Ranque-Hilsch vortex tube with gaseous hydrogen using real gas model, Appl. Therm. Eng. 140 (2018) 287–294. doi:10.1016/j.applthermaleng.2018.05.017.

[67] S. Syed, M. Renganathan, Numerical investigations on flow characteristics and energy separation in a Ranque Hilsch vortex tube with hydrogen as working medium, Int. J. Hydrogen Energy. 44 (2019) 27825–27842. doi:10.1016/j.ijhydene.2019.08.239.

[68] E.W. Lemmon, M.O. Mclinden, M.L. Huber, NIST Reference Fluid Thermodynamic and Transport Properties — REFPROP, (n.d.).

[69] G. SOAVE, Equilibrium constants from a modified Redkh-Kwong equation of state, Chem. Eng. Sci. 27 (1972) 1197–1203.

[70] D. Peng, D.B. Robinson, A New Two-Constant Equation of State, Ind. Eng. Chem. Fundam. 15 (1976) 59–64.

[71] Y. Fang, M. De Lorenzo, P. Lafon, S. Poncet, Y. Bartosiewicz, An Accurate and Efficient Look-up Table Equation of State for Two-phase Compressible Flow Simulations of Carbon Dioxide An Accurate and E ffi cient Look-up Table Equation of State for Two- Phase Compressible Flow Simulations of Carbon Dioxide, Ind. Eng. Chem. Res. 57 (2018) 7676−7691. doi:10.1021/acs.iecr.8b00507.

[72] A. Ameli, A. Uusitalo, T. Turunen-Saaresti, J. Backman, Numerical Sensitivity Analysis for Supercritical CO2 Radial Turbine, Energy Procedia. 129 (2017) 1117–1124. doi:10.1016/j.egypro.2017.09.233.

[73] M. Palacz, J. Smolka, A. Fic, Z. Bulinski, A.J. Nowak, K. Banasiak, A. Hafner, Application range of the HEM approach for CO2 expansion inside two-phase ejectors for supermarket refrigeration systems Michal, Int. J. Refrig. 59 (2015) 251–258. doi:10.1016/j.ijrefrig.2015.07.006.

[74] O. Poujade, M. Julien, Modelling of an Homogeneous Equilibrium Mixture Model (HEM) Modelling of an Homogeneous Equilibrium Mixture Model (HEM), (2014). doi:10.1007/s10440-013-9827-2.

[75] C. Lucas, H. Rusche, A. Schroeder, J. Koehler, Numerical investigation of a two-phase CO2 ejector, Int. J. Refrig. 43 (2014) 154–166. doi:10.1016/j.ijrefrig.2014.03.003.

[76] A. Aghagoli, M. Sorin, CFD modelling and exergy analysis of a heat pump cycle with Tesla Turbine using CO2 as a working fluid, Appl. Therm. Eng. (2020) 115587. doi:10.1016/j.applthermaleng.2020.115587.

[77] S.E. Rafiee, M.M. Sadeghiazad, Experimental and CFD analysis on thermal performance of Double-Circuit vortex tube (DCVT)-geometrical optimization, energy transfer and flow structural analysis, Appl. Therm. Eng. 128 (2018) 1223–1237. doi:10.1016/j.applthermaleng.2017.09.112.

[78] F. Kock, H. Herwig, Local entropy production in turbulent shear flows : a high-Reynolds number model with wall functions, Int. J. Heat Fluid Flow. 47 (2004) 2205–2215. doi:10.1016/j.ijheatmasstransfer.2003.11.025.

[79] F. Kock, H. Herwig, Entropy production calculation for turbulent shear flows and their implementation in cfd codes, Int. J. Heat Fluid Flow. 26 (2005) 672–680. doi:10.1016/j.ijheatfluidflow.2005.03.005.

[80] V. Kirmaci, H. Kaya, I. Cebeci, An experimental and exergy analysis of a thermal performance of a counter flow Ranque – Hilsch vortex tube with different Analyse expérimentale et exergétique de la performance thermique d ' un tube vortex de Ranque-Hilsch à contre- courant avec différent, Int. J. Refrig. 85 (2018) 240–254. doi:10.1016/j.ijrefrig.2017.10.003.

[81] N. Bej, K.P. Sinhamahapatra, Exergy analysis of a hot cascade type Ranque- Hilsch vortex tube using turbulence model, Int. J. Refrig. 45 (2014) 13–24. doi:10.1016/j.ijrefrig.2014.05.020.

[82] K. Dincer, Y. Yilmaz, A. Berber, S. Baskaya, Experimental investigation of performance of hot cascade type Ranque-Hilsch vortex tube and exergy analysis, Int. J. Refrig. 34 (2011) 1117–1124. doi:10.1016/j.ijrefrig.2011.01.017.

[83] B.T. Austin, K. Sumathy, Transcritical carbon dioxide heat pump systems: A review,

Renew. Sustain. Energy Rev. 15 (2011) 4013–4029. doi:10.1016/j.rser.2011.07.021.

[84] S. Taslimi Taleghani, M. Sorin, S. Poncet, Exergy performance of a transcritical CO 2 two- phase ejector, in: 31st Int. Conf. Effic. Cost, Optim. Simul. Environ. Impact Energy Syst., GUIMARÃES,PORTUGAL, 2018.

[85] S. Taslimi Taleghani, M. Sorin, S. Poncet, Modeling of two-phase transcritical CO 2 ejectors for on-design and off-design conditions, Int. J. Refrig. 87 (2018) 91–105. doi:10.1016/j.ijrefrig.2017.10.025.

[86] M. Mohiuddin, S. Elbel, A Fresh Look at Vortex Tubes used as Expansion Device in Vapor Compression Systems, (2014) 1–10.

[87] S. Eiamsa-ard, P. Promvonge, Review of Ranque-Hilsch effects in vortex tubes, Renew. Sustain. Energy Rev. 12 (2008) 1822–1842. doi:10.1016/j.rser.2007.03.006.

[88] L. Yingfu, G. Chunjing, J. Guangya, Vortex Tube Expansion Transcritical CO2 Heat Pump Cycle, Appl. Mech. Mater. 190–191 (2012) 1340–1344. doi:10.4028/www.scientific.net/AMM.190-191.1340.

[89] J. Zhao, J. Ning, Performance Analysis on CO2 Heat Pump Cycle with a Vortex Tube, in: 3rd Int. Conf. Smart Mater. Nanotechnol. Eng., 2016.

[90] M.M. Rashidi, O.A. Bég, A. Aghagoli, Utilization of waste heat in combined power and ejector refrigeration for a solar energy source, Int. J. Appl. Math Mech. 8 (2012) 1–16.

[91] M.M. Rashidi, A. Aghagoli, O.A. Bég, R. Gorla, optimum thermodynamic exergy analysis and design of an ejector refrigeration cycle, Int. J. Appl. Math. Mech. 20 (2014).

[92] A.S. Karakurt, V. Bashan, Y. Ust, COMPARATIVE MAXIMUM POWER DENSITY ANALYSIS OF A SUPERCRITICAL CO2 BRAYTON POWER CYCLE, J. Therm. Eng. 6 (2020) 50–57. doi:10.18186/thermal.671148.

[93] A. Aghagoli, M. Sorin, S. Poncet, Thermodynamics analysis of a novel transcritical CO2 vortex tube heat pump cycle, in: Proc. 27th CANCAM, Sherbrooke, Québec, Canada, 2019: p. 4.

[94] H. Li, H. Cong, X. Li, X. Li, X. Gao, Systematic design of the integrating heat pump into heat integrated distillation column for recovering energy, Appl. Therm. Eng. 105 (2016) 93–104. doi:10.1016/j.applthermaleng.2016.05.141.

[95] N. Brandt, T. Alpögger, W. Tegethoff, M. Bockholt, A. Möhlenkamp, J. Köhler, T.U. Braunschweig, I. Thermodynamik, H.S. Straße, Exergetic analysis of different R744 heat pump tumble dryer system topologies, Appl. Therm. Eng. 161 (2019) 114107. doi:10.1016/j.applthermaleng.2019.114107.

[96] J. Sarkar, Optimization of ejector-expansion transcritical CO 2 heat pump cycle, Energy. 33 (2008) 1399–1406. doi:10.1016/j.energy.2008.04.007.

[97] S. Elbel, P. Hrnjak, Experimental validation of a prototype ejector designed to reduce throttling losses encountered in transcritical R744 system operation, Int. J. Refrig. 31 (2008) 411–422. doi:10.1016/j.ijrefrig.2007.07.013.

[98] S. Croquer, Combined CFD and thermodynamic analysis of a supersonic ejector with liquid droplets, Université de Sherbrooke, Sherbrooke, QC, Canada, 2018.

[99] N. Ruangtrakoon, T. Thongtip, An experimental investigation to determine the optimal heat source temperature for R141b ejector operation in refrigeration cycle, Appl. Therm. Eng. 170 (2020) 114841. doi:10.1016/j.applthermaleng.2019.114841.

[100] J.L. Yang, Y.T. Ma, M.X. Li, H.Q. Guan, Exergy analysis of transcritical carbon dioxide refrigeration cycle with an expander, 30 (2005) 1162–1175. doi:10.1016/j.energy.2004.08.007.

[101] W. Rice, Tesla Turbomachinery, in: Proc. . IV Int. Nikola Tesla Symp., 1991.

[102] M.J. Traum, H.L. Weiss, Tiny Tesla Turbine Analytical Performance Validation Via Dynamic Dynamometry, in: E3S Web Conf., 2019: pp. 1–8. doi:10.1051/e3sconf/201911303024.

[103] G. Manfrida, L. Pacini, L. Talluri, An upgraded Tesla turbine concept for ORC applications, Energy. 158 (2018) 33–40. doi:10.1016/j.energy.2018.05.181.

[104] L. Talluri, D. Fiaschi, G. Neri, L. Ciappi, Design and optimization of a Tesla turbine for ORC applications, Appl. Energy. 226 (2018) 300–319. doi:10.1016/j.apenergy.2018.05.057.

[105] P. Lampart, Ł. Jędrzejewski, INVESTIGATIONS OF AERODYNAMICS OF TESLA BLADELESS MICROTURBINES, J. Theor. Appl. Mech. (2011) 477–499.

[106] R.J. Pandey, S. Pudasaini, S. Dhakal, R.B. Uprety, H.P. Neopane, Design and Computational Analysis of 1 kW Tesla, Int. J. Sci. Res. Publ. 4 (2014) 1–5.

[107] T.W. Choon, A.A. Rahman, F.S. Jer, L.E. Aik, Optimization of Tesla Turbine Using Computational Fluid Dynamics Approach, 2011 IEEE Symp. Ind. Electron. Appl. (2011) 477–480. doi:10.1109/ISIEA.2011.6108756.

[108] L. Ciappi, D. Fiaschi, P.H. Niknam, L. Talluri, Computational investigation of the fl ow inside a Tesla turbine rotor, Energy. 173 (2019) 207–217. doi:10.1016/j.energy.2019.01.158.

[109] M.M. Rashidi, A. Aghagoli, M. Ali, Thermodynamic analysis of a steam power plant with double reheat and feed water heaters, Adv. Mech. Eng. 2014 (2014). doi:10.1155/2014/940818.

[110] S. Alharbi, M.L. Elsayed, L.C. Chow, Exergoeconomic analysis and optimization of an integrated system of supercritical CO 2 Brayton cycle and multi-effect desalination, Energy. 197 (2020) 117225. doi:10.1016/j.energy.2020.117225.

[111] Z. Wu, H. Feng, L. Chen, W. Tang, J. Shi, Y. Ge, Constructal thermodynamic optimization for ocean thermal energy conversion system with dual-pressure organic Rankine cycle, Energy Convers. Manag. 210 (2020) 112727. doi:10.1016/j.enconman.2020.112727.

[112] H. Akbari, M. Sorin, B. Marcos, An equivalent temperature based approach for selection of the most appropriate working fl uids for refrigeration cycles, Energy Convers. Manag. 174 (2018) 227–238. doi:10.1016/j.enconman.2018.08.023.

[113] M.H. Saidi, M.R. Allaf Yazdi, Exergy model of a vortex tube system with experimental results, Energy. 24 (1999) 625–632. doi:10.1016/S0360-5442(98)00076-0.

[114] H. Cho, Comparative study on the performance and exergy ef fi ciency of a solar hybrid heat pump using R22 and R744, Energy. 93 (2015) 1267–1276. doi:10.1016/j.energy.2015.10.016.

[115] A. Naserbegi, M. Aghaie, A. Minuchehr, G. Alahyarizadeh, A novel exergy optimization of Bushehr nuclear power plant by gravitational search algorithm (GSA), Energy. 148 (2018) 373–385. doi:10.1016/j.energy.2018.01.119.

[116] W. Qi, Q. Deng, Y. Jiang, Q. Yuan, Z. Feng, Disc Thickness and Spacing Distance Impacts on Flow Characteristics of Multichannel Tesla Turbines, Proc IMechE Part A J Power Energy. (2019). doi:10.3390/en12010044.

[117] C. Schosser, S. Lecheler, Michael Pfitzne, A TEST RIG FOR THE INVESTIGATION OF THE PERFORMANCE AND FLOW FIELD, in: Proc. ASME Turbo Expo 2014 Turbine Tech. Conf. Expo., Düsseldorf, Germany, 16–20 June, 2014: pp. 1–11.

[118] W. Qi, Q. Deng, Z. Chi, L. Hu, Q. Yuan, Z. Feng, Influence of Disc Tip Geometry on the Aerodynamic Performance and Flow Characteristics of Multichannel Tesla Turbines, Energies. 12 (2019). doi:10.3390/en12030572.

[119] F.R. Menter, Two-Equation Eddy-Viscosity Turbulence Models for Engineering Applications, AIA A J. 32 (1994) 1598–1605. doi:10.2514/3.12149.

[120] W. Qi, Q. Deng, Y. Jiang, Z. Feng, Q. Yuan, Aerodynamic performance and flow characteristics analysis of Tesla turbines with different nozzle and outlet geometries, Proc IMechE Part A J Power Energy. 0 (2018) 1–21. doi:10.1177/0957650918785312.